Forschungszentrum Karlsruhe
in der Helmholtz-Gemeinschaft

Wissenschaftliche Berichte
FZKA 7167

Co-tunneling Current and Shot Noise in Molecules and Quantum Dots

A. Thielmann

Institut für Nanotechnologie

September 2005

Forschungszentrum Karlsruhe

in der Helmholtz-Gemeinschaft

Wissenschaftliche Berichte

FZKA 7167

Co-tunneling current and shot noise in molecules and quantum dots

Axel Thielmann

Institut für Nanotechnologie

Von der Fakultät für Physik

der Universität Karlsruhe (TH) genehmigte Dissertation

Forschungszentrum Karlsruhe GmbH, Karlsruhe

2005

Impressum der Print-Ausgabe:

Als Manuskript gedruckt

Forschungszentrum Karlsruhe GmbH
Postfach 3640, 76021 Karlsruhe

Mitglied der Hermann von Helmholtz-Gemeinschaft
Deutscher Forschungszentren (HGF)

ISSN 0947-8620

urn:nbn:de:0005-071672

Co-tunneling current and shot noise in molecules and quantum dots

---

Kotunnel- Strom und Schrotrauschen in Molekülen und Quantenpunkten

Zur Erlangung des akademischen Grades eines

DOKTORS DER NATURWISSENSCHAFTEN

von der Fakultät für Physik der

Universität Karlsruhe (TH)

genehmigte

DISSERTATION

von

Dipl.-Phys. Axel Thielmann

aus

Nürnberg

Tag der mündlichen Prüfung: 15. Juli 2005

Referent: Prof. Dr. Gerd Schön

Korreferent: Prof. Dr. Jürgen König

Abstract

The main issue of this work is to develop a theory of current and shot noise through nanoscale systems like molecules or quantum dots. Our approach follows a microscopic many-body description of the transport and relies on a diagrammatic technique on the Keldysh contour. The transport properties are expressed in terms of irreducible self-energy diagrams which are expanded order by order in the coupling of the nanoscale system to the electrodes. Our expressions derived in a first/second order expansion allow for a description of sequential/co-tunneling current and shot noise. We find non-Markovian memory effects to play a role for co-tunneling shot noise in the finite bias regime. Such effects have not been included in previous theories. We explicitly apply our theory to an experiment on a specific molecule and find that for a realistic description of transport through molecular devices a theory describing a complex energy spectrum, two-particle interaction effects and an intermediate coupling regime (co-tunneling) is necessary. We show that our theory can handle these demands. By studying single and multi-level systems in the sequential and co-tunneling regime we identify fundamental mechanisms leading to characteristic behavior of the shot noise. We explain in detail how to extract relevant information from transport measurements in order to spectroscopically characterize molecular devices or quantum dot structures.

Zusammenfassung

Ziel dieser Arbeit ist es, eine Theorie des Stromes und des Schrotrauschens bereitzustellen, welche den Transport durch nanoskalige Systeme wie Moleküle oder Quantenpunkte beschreibt. Unsere Theorie folgt einer mikroskopischen Vielteilchen-Beschreibung und basiert auf einer diagrammatischen Technik auf der Keldysh-Kontur. Transporteigenschaften werden durch irreduzible Selbstenergiediagramme ausgedrückt, die ihrerseits Ordnung für Ordnung in der Kopplung des nanoskaligen Systems zu den Elektroden entwickelt werden. Unsere Formeln, welche bis zu erster bzw. zweiter Ordnung entwickelt werden, ermöglichen eine Beschreibung des sequentiellen bzw. Kotunnel-Stromes und des Schrotrauschens. Unsere Theorie zeigt, dass nicht-Markovsche 'Memory-Effekte' für das Kotunnel-Schrotrauschen bei endlicher Spannung relevant sind. Solche Effekte wurden in früheren Theorien nicht berücksichtigt. Wir wenden unsere Theorie auf ein spezielles Molekülexperiment an, und zeigen, dass eine realistische Beschreibung des Transportes durch Moleküle nur möglich ist, wenn ein komplexes Energiespektrum, Wechselwirkungseffekte sowie ein mittelstarker Kopplungsbereich (Kotunneln) theoretisch beschrieben werden. Unsere Theorie wird diesen Ansprüchen gerecht. Indem wir Systeme mit einem bzw. mehreren Energieniveaus untersuchen, identifizieren wir Transportmechanismen, die zu charakteristischem Verhalten des Schrotrauschens führen. Es wird im Detail erklärt, wie relevante Informationen aus Transportmessungen gewonnen werden können, um Moleküle und Quantenpunkte spektroskopisch zu charakterisieren.

Deutsche Zusammenfassung

Derzeit haben Bauelemente handelsüblicher integrierter Schaltkreise typische Abmessungen von etwa 100 Nanometern. Unter der Annahme, dass die Geschwindigkeit, mit der die Miniaturisierung von Bauelementen voranschreitet, auch in Zukunft beibehalten werden kann, werden in ca. 12 Jahren Abmessungen von nur noch 10 Nanometern erreicht sein. Bei solch kleinen Skalen beginnen Quanteneffekte zunehmends wichtig zu werden, weshalb herkömmliche, auf der Silizium Halbleitertechnologie basierende Konzepte, durch völlig neue Konzepte ersetzt werden müssen.

Zu den vielversprechenden möglichen Konzepten zählen Quantencomputer, Spinelektronik oder quanten zelluläre Automaten, welche z.B. unter Verwendung von ***Quantenpunkten*** realisiert werden können. Quantenpunkte können durch lithographisch definierte Regionen in einem zwei-dimensionalen Elektronengas (2DEG) einer Halbleiterheterostruktur (laterale Quantenpunkte) oder durch geschichtete Halbleiterstrukturen kleiner Abmessung (vertikale Quantenpunkte) hergestellt werden.

Das Forschungsgebiet der ***molekularen Elektronik*** beschäftigt sich mit einem weiteren interessanten Konzept, welches einzelne Moleküle, Molekülketten oder Molekülcluster als Bestandteile aktiver elektronischer Bauelemente vorsieht. Das Potenzial der molekularen Elektronik liegt in der Vielzahl von chemisch realisierbaren Molekülen, welche nahezu unbegrenzte Möglichkeiten zum technologischen Design elektronischer Bauteile anbieten.

Um Transistoren in der Grösse von wenigen Nanometern herstellen und zudem kontrollieren zu können, müssen allerdings die auftretenden Quanten-Effekte grundlegend verstanden sein. Besonders für Moleküle stellt die kaum verstandene ***Kopplung*** der vergleichsweise grossen metallischen Elektroden an ein Nanometer grosses Objekt, mit einer möglicherweise komplexen elektronischen Struktur, ein enormes Problem dar. Diese unterschiedlichen Komponenten wechselwirken auf komplizierte Art und Weise miteinander, so dass Abschirmungseffekte, dielektrische Effekte, Vibrationen, Relaxations-Effekte über elektromagnetische Strahlung, etc. von Bedeutung sein könnten. Eine solch grosse Anzahl von 'Freiheitsgraden' führt zu nahezu unkontrollierbaren Molekül-Elektroden Kopplungsparametern, ganz im Gegensatz zu den Quantenpunkten, für die die Kopplungsparameter in der Regel gut kontrollierbar sind. Es ist daher leicht einzusehen, dass Molekülmessungen in Experimenten nur mit Hilfe geeigneter theoretischer Werkzeuge verlässlich interpretiert werden können.

Ziel dieser Arbeit ist es daher, eine ***Transporttheorie durch nanoskalige Systeme wie Moleküle oder Quantenpunkte*** bereitzustellen, welche ***Zugang zu Informationen über transportbestimmende Parameter wie Energiespektren, Wechselwirkungen oder Kopplungen*** erlaubt.

Zum Zwecke experimenteller Studien dieser Systeme werden in der Regel ***Strom-Spannungs Kennlinien*** $I(V_b)$ und deren Ableitung nach der Spannung V_b, der Leitwert $G(V_b) = \partial I(V_b)/\partial V_b$, betrachtet. Anhand eines Vergleiches unserer Theorie mit einem konkreten Experiment mit einem Terphenylmolekül zeigen wir, dass der Strom nur begrenzte Information über die Parameter, an denen wir interessiert sind, liefern kann. Ein Fit der theoretischen Kurven an die experimentellen Daten zeigt, dass zur realistischen Beschreibung des Transportes durch Moleküle ein komplexes Energiespektrum, eine starke Coulomb Wechselwirkung U sowie ein mittelstarker Kopplungsbereich gegeben sein müssen (mittelstarke Kopplung definiert eine Kopplungsstärke, die nicht klein gegenüber anderen Energieparametern des Systemes oder der Temperatur T ist). Neben diesen qualitativen Aussagen lassen sich allerdings keine klaren quantitativen Aussagen machen (z.B. über Asymmetrie der Kopplungen), was verdeutlicht, dass zusätzliche 'spektroskopische' Information nötig ist, um Fragen über den Transport durch mesoskopische Systeme eindeutig zu beantworten.

Zusätzliche Information liesse sich aus dem Strom gewinnen, würde man in Molekülexperimenten neben den beiden Kontaktelektroden darüberhinaus eine dritte (Gate-) Elektrode anbringen. Dies hat sich jedoch als schwierig erwiesen und kann nur in wenigen Experimenten realisiert werden. Ein vielversprechender Kandidat für ein 'spektroskopisches' Werkzeug ist das ***Schrotrauschen*** $S(V_b)$, welches eng mit der Strom-Strom Korrelationsfunktion zusammenhängt. Während der Strom nur Information über die mittlere Wahrscheinlichkeit des Elektronentransfers durch die Systeme beinhaltet, gibt das Schrotrauschen zusätzlichen Aufschluss über die Dynamik der Elektrontransferprozesse. Natürlich würden höhere Korrelationsfunktionen als der zweite Stromkorrelator das Verständnis des Elektronentransportes weiter vervollständigen. Diese sind aber experimentell schwierig zu messen und die theoretischen Zugänge (z.B. Full Counting Statistics) sind immer noch auf die einfachsten Modellsysteme beschränkt. Eine Theorie des Schrotrauschens ist daher den obengenannten Alternativen derzeit vorzuziehen. Schrotrauschen resultiert aus der Quantisierung der Elektronenladung und führt zu zeitabhängigen Fluktuationen des Stromes, welche insbesonders in nanoskaligen elektronischen Schaltkreisen stark auftreten, da nur wenige Elektronen am Transport beteiligt sind. Es zeigt sich, dass besonders Elektron-Elektron-Wechselwirkungen zu starken Korrelationen in dem System führen können und das Verhalten des Schrotrauschens charakteristisch beeinflussen. Schrotrauschen zeigt sich daher empfindlich gegenüber zwei Energieskalen: der elektronischen Struktur des Systems, die Elektron-Elektron Wechselwirkung inbegriffen, und der Kopplungsenergie des Systems an die Elektroden. Dies sind aber genau die Energieparameter, welche wir als wichtige, den Transport bestimmende Parameter identifiziert haben.

Derzeit gibt es keinen theoretischen Zugang zum Schrotrauschen, welcher alle diese Parameter exakt beschreibt. Bislang beschränkt man sich entweder auf starke oder schwache Kopplungssituationen zwischen Molekülen und Elektroden.

Für den Fall ***starker Kopplung*** wird der Transport durch die Kontaktregionen dominiert und das Molekül oder der Quantenpunkt verhalten sich wie ein Streuzentrum, an dem kohärente Quentenzustände gestreut werden. Ein theoretischer Zugang, welcher alle Transporteigenschaften einer Streumatrix zuordnet, ist durch die Landauer-Büttiker Theorie gegeben. Diese Theorie ist in Situationen des ballistischen Transportes, in welchen Wechselwirkungseffekte vernachlässigbar sind, gut anwendbar. Physikalisch interessanter ist der Fall ***schwacher Kopplung***, da die Elektronen im Transport eine lange Zeit auf dem Molekül verbringen und Wechselwirkungseffekte daher relevant oder gar dominant sein werden. Der Transport wird in diesem Fall durch eine Sequenz inkohärenter Hüpfprozesse (***sequentielles Tunneln***) zwischen Molekül (bzw. Quantenpunkt) und Elektroden beschrieben. Dieser Einzelelektronen-Transport, bekannt als 'orthodoxe Theorie', wird theoretisch durch eine Störungsentwicklung in erster Ordnung in der Kopplung beschrieben und ist gültig, solange die Kopplung klein gegenüber der Temperatur ist. Das Bild des sequentiellen Transportes muss jedoch im Coulomb-Blockadebereich (ein Bereich in dem die Spannung klein gegenüber der Energie ist, welche das System benötigt um be/entladen zu werden) erweitert werden, da der Transport hier exponentiell unterdrückt ist. ***Kotunnelprozesse***, welche durch eine Störungsentwicklung zur zweiten Ordnung in der Kopplung beschrieben werden, dominieren in diesem Fall, selbst bei (algebraisch) schwacher Kopplung. Sie ermöglichen das Tunneln mittels virtueller Zwischenprozesse durch das System ohne den Ladungszustand zu ändern. Eine Transportbeschreibung durch eine Theorie erster Ordnung kann aber auch bei grossen Spannungen zusammenbrechen, falls die Stärke der sequentiellen Tunnelprozesse unter die der Kotunnelprozesse unterdrückt ist, was z.B. bei stark asymmetrischen Kopplungsparametern möglich ist. Kotunnelprozesse sind also wichtig, um das Bild des sequentiellen Transportes für den gesamten Spannungsbereich konsistent zu erweitern, und natürlich notwendig um einen mittelstarken Kopplungsbereich (in dem Wechselwirkungseffekte noch relevant sind) zu beschreiben.

Ein wichtiges Ergebnis der vorliegenden Arbeit ist es daher, eine ***Theorie des Stromes und des Schrotrauschens*** basierend auf einer mikroskopischen Vielteilchen-Beschreibung bereitzustellen, welche eine Beschreibung komplexer Energiespektren, beliebiger Wechselwirkungseffekte, Spannungen und eines mittelstarken Kopplungsbereiches (Kotunneln) ermöglicht. Unsere Theorie bedient sich einer diagrammatischen Technik auf der Keldysh-Kontur und erlaubt es alle Transporteigenschaften durch irreduzible Selbstenergie-Diagramme auszudrücken, welche ihrerseits Ordnung für Ordnung in der Kopplung des nanoskaligen Systems zu den Elektroden entwickelt werden. Zudem zeigen wir, dass eine Beschreibung höherer Korrelatoren, sowie frequenzabhängiges Rauschen und die Berücksichtigung von Kohärenz-Effekten möglich ist, was unseren theoretischen Zugang auch für zukünftige weitere Anwendungen attraktiv macht. Für das Schrotrauschen zeigt unsere Theorie, dass ***nicht-Markovsche Effekte*** bei Prozessen höherer Ordnung (beginnend mit Kotunnelprozessen) den Transport mitbestimmen.

Um den ***Transport durch Moleküle und Quantenpunkte*** realistisch zu beschreiben und zudem die den Transport bestimmenden Parameter verlässlich bestimmen zu können, wenden wir unsere Theorie des sequentiellen sowie des Kotunnel-Stromes und Schrotrauschens zunächst auf einfache Modellsysteme an, die uns erlauben, fundamentale Transportmechanismen zu identifizieren, welche auch in komplexeren Systemen relevant sein werden.

Für eine Analyse der Transporteigenschaften erweist sich das Rausch-zu-Signal-Verhältnis $F(V_b) = S(V_b)/2eI(V_b)$, der sogenannte ***Fano-Faktor*** als nützlich, da er charakteristische Informationen des Schrotrauschens über Korrelationen der Elektronen oft besser visualisiert. So ergibt sich im Falle unkorrelierter Elektronen (der Transport wird durch Poissonstatistik beschrieben) ein Fano-Faktor von $F = 1$. Abweichungen von diesem Wert ergeben sich, wenn ein sogenanntes 'Anti-Bunching' oder 'Bunching' (Bündelung) der Elektronen zu Korrelationen führt, z.B. aufgrund spezieller Kopplungssituationen, Wechselwirkungen, etc. Für den Fano-Faktor ergeben sich dann sub-Poissonsche ($F < 1$) oder super-Poissonsche ($F > 1$) Werte. Im Fall schwacher Kopplung sind Werte zwischen $F = 1/2$ (symmetrische Kopplungen an beiden Elektroden) und $F = 1$ (stark asymmetrische Kopplung) typisch, was wir an einem Experiment zum Schrotrauschen an selbsorganisierten InAs Quantenpunkten belegen. Super-Poissonsche Werte lassen sich in bestimmten Situationen beobachten, wenn die Symmetrie das Systemes gebrochen ist, z.B. durch asymmetrische Kopplungsparameter (für lokalisierte Systeme mit mehreren Energieniveaus oder spinabhängiger Kopplung) oder durch starke Wechselwirkungseffekte (für delokalisierte Systeme). Dynamisches Bunching oder Blockade-Effekte der Elektronen führen in diesen Fällen zu einem Wettbewerb verschiedener Transportkanäle. Oftmals wird ein negativer differentieller Leitwert und ein stark unterdrücktes (oder auch verstärktes) Schrotrauschen beobachtet. Relaxations- oder Kotunnelprozesse können ein solches Verhalten in manchen Fällen wieder zerstören.

Wir besprechen detailliert, wie Information über Energieniveaus, Kopplungsparameter, Stärke von Wechselwirkungen, magnetische Felder, Temperatur, etc. in sequentiellen bzw. durch Kotunneln dominierten Spannungsbereichen (sowie Bereichen, in welchen beide gleich wichtig sind) aus der kombinierten Betrachtung des Stromes, des Schrotrauschens sowie des Fano-Faktors gewonnen werden kann. Nur eine unabhängige Untersuchung des Einflusses verschiedenster Effekte kann im Falle ihres Zusammenspieles helfen, die physikalischen Vorgänge in solch komplexen Systemen wie Molekülen zu verstehen. Theoretische Vorhersagen über charakteristisches Verhalten des Schrotrauschens könnten anhand der bekannten Kopplungsparameter bei Experimenten mit Quantenpunkten überprüft werden, um in Experimenten mit Molekülen als spektroskopisches Werkzeug zu dienen und unbekannte Parameter möglicherweise selbst-konsistent zu bestimmen. Dies könnte zukünftig eine Kontrolle und Design molekularer Schaltkreise ermöglichen.

Contents

1 Introduction

Commercially manufactured integrated circuits have currently typical feature dimensions of about 100 nanometers. Assuming that the current rate of miniaturization continues in the future, circuit feature dimensions of only 10 nanometers will be reached in about 12 years. At these nanoscale dimensions *quantum effects* will become increasingly important and current circuit designs will run into fundamental difficulties. Present day device designs will therefore have to be replaced by entirely new concepts. There are several nanoscale concepts which could take over from here.

Concepts like quantum computing, spintronics or quantum cellular automata can be realized e.g. by the use of ***quantum dots*** (QDs) [1, 2]. QDs can be formed by lithographically defined regions in a two-dimensional electron gas (2DEG) of a semiconductor heterostructure (lateral QDs) or in layered semiconductor structures with small diameter (vertical QDs).

Molecular electronics is another promising concept. Here, single molecules, chains or clusters of molecules are supposed to act as wires and active electronic devices [3, 4]. The research field of molecular electronics has rapidly advanced in recent years as nanofabrication techniques have made it possible to manipulate and explore the electronic transport through individual atoms and molecules. The potential in molecular electronics lies in the huge variety of available molecules that allows one to design an almost unlimited number of distinct molecular electronic devices.

These concepts provide interesting fields for experimental and theoretical investigation with a potential of a rich variety of applications. However, the realization and control of nanosize transistors demands a fundamental understanding of the numerous new physical effects in these systems. In particular, for molecular devices a major problem consists in the poorly understood ***coupling*** of a nanosize 'island' (with a possibly complex electronic structure) to the metallic reservoirs of much larger cross section that form the source and drain electrodes of the device. The various device components interact with each other in a complex way which may give rise e.g. to field effects, screening, dielectric effects, vibrations, electro-mechanical effects or relaxation effects via electromagnetic radiation. This results in more 'degrees of freedom' in the molecular devices in contrast to the typically better defined quantum dots. Whereas the coupling parameters of quantum dots can be tuned very well, we have to deal with almost uncontrollable molecule-electrode couplings. However, devices involving many degrees of freedom provide also more possibilities for technological designs, which is an important reason for the particular interest in molecular electronics. The complexity of the coupled molecule-electrode system reflects directly on the difficulties in the interpretation of experiments. Therefore reliable theoretical tools are needed to guide experimental observations.

To characterize the transport through molecules and quantum dots one usually studies the ***current-voltage characteristics*** $I(V_b)$ and its derivative with respect to the bias voltage V_b, the conductance $G(V_b) = \partial I(V_b)/\partial V_b$. However, the current provides information only about certain combinations of the molecule-electrode coupling parameters as one basically measures a series of resistors. No definite predictions can be made about asymmetries of the coupling parameters, number of relevant transport channels, etc. by the consideration of the current alone. This is illustrated in ***chapter 2.2.2*** where we apply our theory to a specific experiment on a terphenyl-type molecule. A comparison of experimentally measured and theoretically fitted current and conductance curves shows that more than one transport channel, a finite ***Coulomb-interaction*** U and an ***intermediate coupling*** regime ('intermediate coupling' means a coupling that is not small compared to other energy parameters of the system or the ***finite temperature*** T) are necessary to consistently explain the experimental data. While this qualitative information is important, quantitative predictions, especially about asymmetries of the coupling parameters, are difficult. This leads us to the conclusion that more detailed answers to the questions in mesoscopic transport can be given only if additional 'spectroscopic' tools are available.

More information could be gained from the current alone, if instead of a two-terminal measurement (only source and drain electrodes) via inclusion of a gate electrode a three-terminal measurement were realized. However, contacting a molecule with a gate electrode is very difficult and can be realized only in a limited variety of experimental setups. A promising candidate to serve as a further spectroscopic tool is the ***shot noise*** $S(V_b)$ which is intimately related to the current-current correlation function [5]. Whereas the current contains information on the average probability for the transmission of electrons through the device, the shot noise provides additional information on the dynamics of the electron transfer process. Of course, higher correlators than the second current correlator would further complete a picture of transport, but are very difficult to measure in experiment, and present theories to compute the higher current correlators (e.g. full counting statistics) are still restricted to the simplest model systems (a small number of system states). In ***chapter 3.7*** we show that our theory can describe higher correlators while addressing more complex systems. However, the shot noise is much easier accessible both theoretically and experimentally (although still far from trivial). Shot noise is due to the discreteness of the electron charge that leads to time-dependent fluctuations in the measured current. Such statistical fluctuations show up much stronger in the nanosize electronic devices compared to macroscopic classical devices due to the 'small' number of electrons participating in transport. Interaction effects (like the Coulomb-interaction between electrons) may lead to strong correlations in the system resulting in characteristic features in the shot noise. Shot noise therefore turns out to be sensitive to two classes of energy scales: the system inherent electronic structure, including the electron-electron interaction, and the coupling strength(s) of

the system to the electrodes. These are exactly the energy parameters that we know to be of fundamental importance to the transport. Depending on the applied bias voltage, they determine if and how transport can occur.

Often the ***Fano factor***, being the noise to current ratio ($F(V_b) = S(V_b)/2eI(V_b)$), turns out to provide a better access to the information contained in the noise. We consider this special combination of current and shot noise as it allows easy extraction of information about electron correlations in the system. For uncorrelated, independent transport a Fano factor with a value $F = 1$ can be found, as the transport is described by Poissonian statistics. Deviations from $F = 1$ due to anti-bunching or bunching of electrons are then due to correlations arising from special coupling situations, interaction effects, etc. and lead to a sub- ($F < 1$) or super-Poissonain ($F > 1$) behavior of the Fano factor. Most of our discussion in ***chapter 4*** is concerned with the identification of the fundamental mechanisms leading to such correlated transport behavior. Indeed, the combined study of current, shot noise and Fano factor provides the deepest insights into the mesoscopic transport properties. A side-by-side comparison of all quantities in the various bias regimes does allow for a considerable increase of knowledge about transport parameters, possibly even for a self-consistent determination of these parameters.

In the case of controllable quantum dot structures, the investigation of shot noise may serve as a playground to study transport physics. The easily determined parameters allow us to focus on fundamental transport mechanisms and to test the predictions made from theory. In ***chapter 2.2.1*** we compare with shot noise measurements on self-assembled InAs quantum dots. Such knowledge is the feedback experimentalists need to achieve better control and design reliable technological devices.

The experimental challenge to measure shot noise consists of the elimination of ***other sources of noise***, such as low frequency $1/f$-noise or random telegraph noise (RTN). These kinds of noise originate from fluctuations of the charge carriers in the environment (e.g. the metallic electrodes). This is different to the fluctuations of the carriers crossing the nanoscopic system itself. Thus only the shot noise carries the information about system inherent properties (electronic structure, energy barriers, etc.). A distinguishing feature of the shot noise is its frequency independence (white noise) over a wide region, in contrast to the other kinds of noise mentioned above, which vanish for sufficiently large frequencies. For quantum dots $1/f$-noise has vanished typically at frequencies above 100kHz, whereas for molecules frequencies of several MHz are certainly needed to sufficiently suppress $1/f$-type noise.

Having elucidated the relevance of current and shot noise measurements to characterize technologically interesting quantum dot systems and molecular devices, the question for an appropriate theoretical description arises. Up to date there is no technique available that is able to describe shot noise through complex electronic structures, while

taking into account two-particle interaction effects and arbitrarily strong coupling to an environment as would be crucial to fully describe the systems we are interested in. Available theories focus on either a strong or a weak coupling situation between molecule and electrodes.

In the case of a ***strong coupling*** to the reservoirs, electrons tunneling through the device will spend much more time in the large reservoirs compared to the nanoscale object in between. The transport in this regime is dominated by the contact and happens via scattering states that are coherent quantum states over the entire system. The molecule or quantum dot acts like a scatterer, similar to a metallic constriction, where interaction effects are less important. This reflects a situation of ballistic transport, where the so called Landauer-Büttiker approach (relating all transport properties to the scattering matrix) can be applied. Theories like density functional theory (DFT), Hartree-Fock or mean field approaches are typically used to describe the conductance, current and noise in an effectively non-interacting system.

A physically and technologically more interesting situation is the ***weak coupling*** regime. Since electrons tunneling through the devices will spend a lot of time on the molecule, interaction effects are relevant and sometimes dominant. This is the regime where single-electron tunneling is observed, as the charging energy $E_C = e^2/2C$ (being the relevant energy-scale for charging effects) is relatively high compared to the coupling energy Γ. For quantum dots typical capacitances are in the range of $C = 10^{-15}F$ ($E_C \sim 10^{-4}$eV) corresponding to a temperature of $E_C/k_\mathrm{B} \sim 1K$. For molecules capacitances of about $C = 10^{-18}F$ ($E_C \sim 0.1$eV) should make single-electron tunneling observable even at room temperature. The transport in this regime is described as a sequence of incoherent hops of single-electrons on and off the molecule or quantum dot. These kinds of processes are called ***sequential tunneling*** processes and are described theoretically by a first order perturbation expansion in the coupling strength Γ, equivalent to a golden rule approximation. The 'orthodox' theory describing such a sequential tunneling based transport is valid, if the coupling Γ between island and electrodes is much smaller compared to the temperature ($\Gamma << k_\mathrm{B}T$).

However, there are situations where this picture of transport breaks down, as in the case of the Coulomb-blockade, where single-electron tunneling is suppressed and coherent ***co-tunneling*** processes become dominant. Such processes are described by a second order perturbation expansion in the coupling Γ. The Coulomb blockade defines a regime where the bias voltage is small compared to the charging energy, leading to exponentially suppressed transport since a charging and un-charging of the system via sequential tunneling processes is only possible after thermal activation of excited states. However, processes allowing for tunneling through the island via an intermediate virtual state without changing the island charge are possible without thermal excitation. A first order description may also fail in the finite transport regime (at larger bias) whenever sequential tunneling processes are suppressed below co-tunneling

processes, e.g. due to strongly asymmetric couplings. Obviously higher order tunneling processes (described by higher than first order expansions in Γ) need to be included when stronger (intermediate) coupling situations are present in experiment. Therefore, for current and shot noise in molecules and quantum dots the need for a valid theory in such an ***intermediate coupling regime*** is twofold. 1) In experiments with molecules the extreme situations of weak or strong coupling are not necessarily realized. An intermediate situation is more likely to be present in general, where however a correct treatment of interaction effects is still required. An adequate theoretical description allowing for an understanding of the physically relevant transport mechanisms is thus given only, if higher than first order tunneling processes are considered. 2) For experiments with molecules or quantum dots co-tunneling effects are important whenever the sequential tunneling picture fails, which may happen even in an assumed small coupling situation (Coulomb-blockade or blocked transport due to asymmetric coupling). Then, only the combination of lowest and higher order transport processes provide a complete picture.

The aim of this thesis is therefore to provide a theory of transport of interacting electrons which allows to push to an intermediate coupling regime by taking into account co-tunneling processes. This will allow for a study of ***co-tunneling current and shot noise in molecules and quantum dots***.

The thesis is partly based on previous and forthcoming publications [6, 7, 8, 9, 10, 11, 12, 13] and is organized as follows: In ***chapter 2*** we give a more detailed introduction to shot noise in nanoscopic systems like molecules or quantum dots. We discuss different sources of noise and how they differ from shot noise, which allows for their elimination in experiment. We discuss in detail why especially the shot noise is the relevant tool to analyze transport. Basic features of the noise and the Fano factor are discussed in order to prepare the reader for the discussion of our results presented later in this work. Two particular current or shot noise measurements are considered in detail, to show the applicability of our theory and relate to experimental observations. The comparison of our theory to a specific current measurement on a molecule emphasizes the incomplete information about transport properties and stresses the need of further spectroscopic tools like shot noise.

Our theory to describe current and shot noise in nanoscopic systems is presented in ***chapter 3***. We provide an overview over various approaches and their physical limitations, and contrast a regime of strong electrode-molecule (electrode-quantum dot) coupling with the opposite weak coupling regime. The development of a theory for current and shot noise, being able to describe also an intermediate coupling regime (by taking into account higher order co-tunneling processes) is the main theoretical achievement of the present work [9, 10]. Our theoretical approach relies in a diagrammatic technique formulated on the Keldysh contour which enables a description of all transport properties in terms of transition rates which we expand order by order in

the coupling strength. Tools which are needed for the calculations are discussed in the appendices A,B and C, which reduces the technical discussion in this chapter. We relate the current and shot noise to so called irreducible blocks (self-energies, transition rates), which can be calculated in a straightforward way. The range of validity of our theory and several extensions to address frequency dependent noise, coherence effects or higher order current correlators are discussed at the end of this chapter.

In ***chapter 4*** we discuss results for single [6] as well as multi-level systems (taking into account relaxation effects) [7, 8] in the sequential (first order in the coupling strength) and the co-tunneling regime (second order) [9]. Since our theory is applicable to a large variety of systems we can also describe ***spin-dependent transport*** relevant for spintronics by considering magnetically polarized leads [10, 11]. We summarize the main features of first order transport and explain the physical mechanisms that lead to interesting transport behavior, which will be relevant also in more complex systems. Together with the co-tunneling transport picture, we show that a complete understanding of current, shot noise and Fano factor in the entire bias regime is possible now. The chapter closes with an outlook towards a description of transport through real molecular devices [12, 13].

Finally, in ***chapter 5*** we summarize again the main ideas and results of the thesis and discuss possible future projects, both from an experimental and a theoretical point of view.

Special tools, formulas, etc. that are not needed to understand the general ideas and results of this work are presented in the ***appendices A,B,C***. They are only relevant to those readers, who want to apply the diagrammatic technique presented in chapter 3.

Depending on the interests and demands of the reader, it is thus possible to read any single chapter of this work by itself.

2 Motivation

Noise is an unavoidable quantity inherent in every measurement. Experimentalists normally want to reduce the noise as much as possible. It is due to statistical fluctuations in electronic devices. Depending on the system (size, material, geometry, etc.) and the conditions under which it is observed (temperature, bias voltage, frequency, etc.) different types of noise can occur. In this chapter we want to show, that noise does not necessarily have a disturbing presence but can also be used to obtain additional information about fundamental system parameters. In particular this is the case for the shot noise. Other sources of noise have to be filtered out before the shot noise we are interested in can be studied. We therefore have to know the properties of these sources and the conditions under which they are absent in nanoscale systems like molecules or quantum dots. We thus begin with a brief discussion of such noise sources. Then we introduce the classical shot noise as discovered by Walter Schottky in an ideal vacuum tube. Basic properties are studied in order to prepare the reader for the discussions of our results in chapter 4. For this purpose the shot noise in mesoscopic systems and the importance, but also difficulties of finite interaction effects are discussed in some detail. In the second part of this chapter experiments on quantum dot structures and molecules as far as they exist are discussed. This will show, that a comparison between theoretical predictions and experimental results is possible and indeed additional information can be extracted by the consideration of the shot noise. Some arguments, why we are interested in a description of an intermediate coupling regime will be given as well, and are further deepened in the next chapter.

2.1 Shot noise: basic properties

In electrical conductors in general many sources contribute to the noise. We want to discuss the four most important ones that experimentalists are confronted with: *generation-recombination noise* relevant in semiconductors, $1/f$ *or modulation noise*, *thermal or Johnson-Nyquist noise* and *shot or non-equilibrium noise*. The origin and possible elimination of the first two of them is discussed in the following, whereas the last ones are not separable and thus will be discussed together afterwards. The main properties of shot noise in non-interacting systems are studied, leading to a discussion of universal behavior in some systems, which however is absent for interacting conductors. This makes the shot noise to an interesting spectroscopic tool in interacting mesoscopic systems that allows us to answer fundamental physical questions.

2.1.1 Other sources of noise

Generation-recombination noise can be understood by considering a semiconductor with a number of traps. The continuous trapping and de-trapping of the charge carriers causes a fluctuation in the number of carriers in the conduction and valence bands (electron-hole pair creation). The time-scale on which these processes occur is characterized by τ (lifetime of electrons in the conduction band). These fluctuations of stochastical nature show up in a Lorentzian like form of the noise spectral density [14]

$$S(\omega) \sim \frac{\tau}{1+\omega^2\tau^2}. \tag{2.1}$$

Since the generation-recombination noise additionally scales with the number around which the electrons are fluctuating, this effect will be reduced in smaller semiconductor devices. In order to eliminate this source of noise in quantum dots (or molecules), it is sufficient to consider the noise at a certain finite frequency ω. For quantum dots this is achieved typically at frequencies smaller than 100 kHz (see Ref. [15]) A more general name for this kind of noise, which is due to the switching of the electron number between discrete values at random times, is *random telegraph noise (RTN).* Other expressions like burst-, bistable- or popcorn-noise have been used as well.

$1/f$*, modulation or flicker noise* is a low frequency noise, since a dominant noise increase as an inverse power of the frequency is observed:

$$S(\omega) \sim \frac{1}{\omega^a}. \tag{2.2}$$

The exponent is often close to unity ($a \sim 1$) which is why this noise is called $1/f$-noise. The origin is due to slow variations of the resistance at constant current, which leads to slow voltage fluctuations. A possible explanation could be that the conductance jumps between two or more locally stable values, which could be due to either the motion of a scatterer between two locally stable positions or to the ionization and deionization of an impurity (e.g., a donor or acceptor in a semiconducting system). $1/f$ noise then follows if many such activated centers exist [16]. However, this kind of noise has been found in a huge variety of systems with obviously different physical origin. An established theory which explains this phenomenon in general thus still does not exist. Again, because of the special kind of frequency dependence (very different from white noise), $1/f$ noise can be eliminated since it vanishes at higher frequencies (it exists to higher frequencies than RTN). This allows the extraction of shot noise, which is frequency independent up to very high frequencies, as we will see in the following. Filtering out the unwanted sources of noise is easier in experiments with quantum dot structures embedded in a two-dimensional electron gas compared to the molecules captured between metallic gold electrodes, as the electrodes define a less stable environment.

2.1.2 Classical shot noise

Shot noise is a non-equilibrium phenomenon and due to the granularity of the charge. Compared to the other noise sources it has caused an immense interest and has been developed into a fast growing subfield of mesoscopic physics (for reviews see Ref. [5, 16, 17]). It can be used to obtain information on a system which is not available through plain current measurements. In particular, shot noise experiments can determine the charge and statistics of the quasi-particles relevant for transport, and reveal information on internal energy scales of mesoscopic systems. A high sensitivity to the effects of electron-electron interactions or the coupling of the system to the environment makes the shot noise an interesting spectroscopic tool.

In 1918 shot noise was discovered in a classical device, when Schottky calculated the noise in an ideal vacuum tube where all sources of spurious noise had been eliminated [18]. Two types of noise remained, described by him as the *Wärmeeffekt* and the *Schroteffekt*.

The first type of noise became known as *Johnson-Nyquist noise* (due to the experimentalist and theorist who investigated it), or simply *thermal noise*. It is frequency independent (white noise) and due to the thermal fluctuations of occupation numbers in the reservoirs. At temperatures $T \neq 0$ thermal noise is always present in any conductor. The thermal motion of particles gives rise to equilibrium current fluctuations in the external circuit, which are via the fluctuation-dissipation theorem related to the conductance of the system.

The second type of noise, the *shot noise*, is caused by the discreteness of the carriers charge of the electric current and a non-equilibrium (transport) phenomenon. For a better understanding of what this phenomenon is due to, we consider the simplest example, where shot noise can be observed, a single barrier with transmission probability $\mathcal{T}$. We assume, that we initially have n charge quanta q coming from the left side of the barrier per unit time τ. The probability distribution $p_n(n_\mathcal{T})$ of the number of particles $n_\mathcal{T}$ which are transmitted to the right side is then binomial:

$$p_n(n_\mathcal{T}) = \left(\begin{array}{c} n \\ n_\mathcal{T} \end{array} \right) \mathcal{T}^{n_\mathcal{T}} (1-\mathcal{T})^{n-n_\mathcal{T}} \tag{2.3}$$

Averaging the binomial distribution gives $\langle n_\mathcal{T} \rangle = n\mathcal{T}$ for the mean value and $\langle \delta n_\mathcal{T}^2 \rangle = \langle n_\mathcal{T}^2 \rangle - \langle n_\mathcal{T} \rangle^2 = \langle n_\mathcal{T} \rangle (1-\mathcal{T}) = n\mathcal{T}(1-\mathcal{T})$ for the variance, where we used the definition $\delta n_\mathcal{T} = n_\mathcal{T} - \langle n_\mathcal{T} \rangle$. These expressions can be directly derived from the characteristic function [19]. For perfect transmission (when there is no barrier) the variance vanishes. The current is given by $I = q n_\mathcal{T}/\tau$ and its variance therefore is found to be $\langle \delta I^2 \rangle = q\langle I \rangle (1-\mathcal{T})/\tau$. We further simplify this result by assuming, that the particles cross the barrier independent from each other, which leads to uncorrelated events in time and

the distribution Eq. 2.3 can be approximated by the Poissonian distribution

$$p(n_{\mathcal{T}}) = e^{-\lambda}\frac{\lambda^{n_{\mathcal{T}}}}{n_{\mathcal{T}}!} \tag{2.4}$$

with $\lambda = n\mathcal{T}$ ($n >> 1, \mathcal{T} << 1$). This describes the regime of low transmission.

If we want to relate the variance of the current to the noise, we will have to make use of the so called Wiener-Khintchine theorem, which states, that the noise is the Fourier transform of the autocorrelation function. The finite frequency noise thus takes the form

$$S(\omega) = \int_{-\infty}^{\infty} dt e^{i\omega t} \left\langle \delta I(t)\delta I(0) + \delta I(0)\delta I(t) \right\rangle, \tag{2.5}$$

(with $\delta I(t) = I(t) - \langle I \rangle$). We note, that only the time difference t in the current-current correlation enters.

Since the particles arrive at random times, uncorrelated pulses in the current show up in terms of a Delta-function. Integrating out Eq. 2.5 then yields $S(0) = 2q\langle I \rangle$ for the zero frequency noise. If the charge would not be quantized, shot noise would be absent since $S \to 0$ for $q \to 0$. In Schottky's case, the granularity of the current was the elementary charge $q = e$, but this does not always have to be so. Values of $q = 2e$ in superconductors (due to cooper-pairs) or $q = e/(2m+1)$ with an integer m in the fractional quantum Hall effect have been observed. This shows, that the shot noise allows to measure the effective charge transferred in electric devices.

Ugo Fano (1947) considered the ratio $F = S/2e\langle I \rangle$ in order to get a dimensionless parameter, that takes the value 1 in the case of the vacuum tube, where

$$S = S_{Poisson} = 2e\langle I \rangle. \tag{2.6}$$

For the derivation of the Poissonian shot noise, we assumed events to be uncorrelated in time and hence approximated the binomial distribution Eq. 2.3. In general we find $S = S_{Poisson}(1-\mathcal{T})$ and therefore $F = (1-\mathcal{T})$ for the Fano-factor. Since the current is proportional to $\mathcal{T}$, we immediately see, that in both cases, $\mathcal{T} = 0$ and $\mathcal{T} = 1$ the shot noise vanishes, whereas the Fano-factor can have values between 0 (ballistic conductor, $\mathcal{T} = 1$) and 1 (single tunnel-barrier with $\mathcal{T} << 1$). For $\mathcal{T} = 1/2$ the partition noise, due to the fact, that the scatterer divides the initial carrier stream into two streams, is maximal. In Fig. 2.1 an example for a barrier with $\mathcal{T} = 3/7$ is sketched, to illustrate this partitioning. A number of n (here 7) electrons arrives at a barrier, where a part is reflected and the rest passes the barrier ($n_{\mathcal{T}} = 3$ in our example). For a large number of electrons the transmission probability $\mathcal{T} = \langle n_{\mathcal{T}} \rangle / n$ is defined by the average of transmitted electrons. This classical picture of course fails in the case of only a

few arriving electrons as in our example. As we will discuss in the following, even in the regime, where a quantum mechanical treatment becomes relevant, the above expressions hold for the simple single-barrier example.

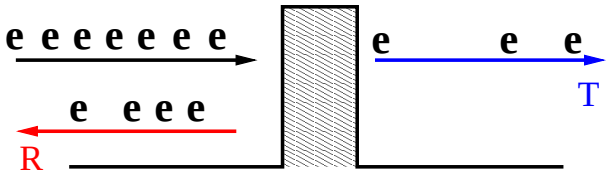

Figure 2.1: *Example for the partitioning of an initial carrier stream into two streams of transmitted and reflected carriers with probabilities* $\mathcal{T}$ *and* $\mathcal{R} = 1 - \mathcal{T}$.

Deviations from $F = 1$ have been shown to be due to statistical anti-bunching or bunching which leads to negative or positive correlations [20]. In fermionic systems usually the Pauli principle correlates the electrons such that anti-bunching effects lead to *sub-Poissonian* values of the Fano-factor with $F < 1$, whereas in bosonic systems bunching leads to *super-Poissonian* values with $F > 1$. However, this statement is based on a series of assumptions (e.g. zero-impedance external circuits, spin independent transport, normal thermal leads). If these conditions are not met, positive correlations could be found in fermionic systems, for example. Besides the Pauli principle, the Coulomb repulsion could be another source of correlations in an electronic conductor. In a vacuum tube the mean occupation of a state is so small, that the Pauli principle is inoperative, and for uncorrelated events Coulomb repulsion does not play any role.

We want to emphasize here that the shot noise in a vacuum tube or a tunnel junction is a statistical effect and a classical phenomenon, as we have seen by deriving the formula Eq. 2.6, although we have written the statistical averages in brackets (as used for expectation values in quantum mechanics). Shot noise can be present in any type of conductor, but may be smeared out, as in macroscopic metallic wires, due to inelastic scattering of the electrons with the environment. Special interest lies in studying shot noise in mesoscopic devices, where the granularity in the charge flow can still be observed and may hopefully lead to non-universal behavior of the Fano-factor. Factors of 1/3 (in diffusive wires), 1/4 (in chaotic wires) or 1/2 (in a symmetric double-barrier) have been observed, among others. Such factors provide only very restricted information and thus, changes of this factor in dependence of Temperature, barrier heights, an applied bias voltage (in transport measurements), etc. would be favorable in order to characterize the system under investigation as well as possible. Information about electronic structure, coupling of a system to its environment, etc. may be extracted from the shot noise, information which is not contained in the current.

2.1.3 Shot noise in mesoscopic systems

In order to describe the transport properties in mesoscopic systems a quantum mechanical treatment of the problem is required [5, 21, 22, 23, 24]. We want to present and discuss briefly, the well established formulas for current and shot noise which have been derived within the scattering or Landauer-Büttiker approach [5, 21]. The idea of this approach is to relate transport properties of the system to its scattering properties, which are assumed to be known from a quantum mechanical calculation.

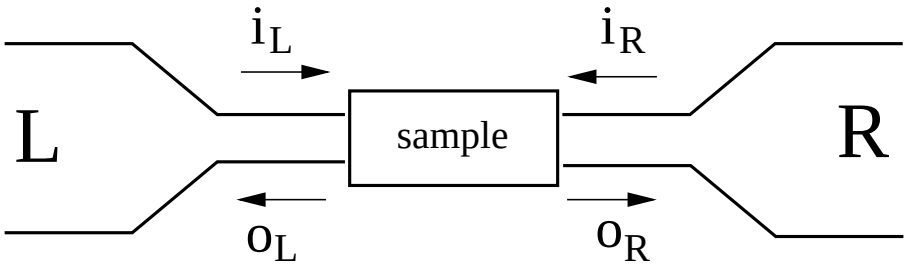

Figure 2.2: *Sketch of the scattering problem, where operators $i_{\rm L}, i_{\rm R}$ and $o_{\rm L}, o_{\rm R}$ describe electrons in the incoming and outgoing states. A mesoscopic conductor (sample) is connected to the left L and right R reservoirs.*

The conductor is considered as a scattering region, connected to electron reservoirs (left L and right R), which are described by thermally equilibrated electrons. Incoming states are occupied according to the Fermi-Dirac distribution function and scattered into outgoing states. For N modes or channels, a $2N \otimes 2N$ scattering matrix (because of two reservoirs) relates these states to each other via:

$$\begin{pmatrix} o_{\rm L} \\ o_{\rm R} \end{pmatrix} = \mathbf{S} \begin{pmatrix} i_{\rm L} \\ i_{\rm R} \end{pmatrix} \tag{2.7}$$

with the unitary matrix

$$\mathbf{S} = \begin{pmatrix} r_{\rm LL} & t_{\rm LR} \\ t_{\rm RL} & r_{\rm RR} \end{pmatrix} \tag{2.8}$$

consisting of 4 $N \otimes N$ blocks. The $N \otimes N$ blocks defining the scattering matrix are due to reflection coefficients back into leads L, R or transmission through the sample (see Fig. 2.2). Since in the presence of time-reversal symmetry the scattering matrix is symmetric, its transmission coefficients $t_{\rm LR} = t_{\rm RL} = t$ can be related to the current and shot noise via a matrix $t^\dagger(E)t(E)$. It has a real set of eigenvalues $T_n(E)$ interpreted as transmission probabilities (transverse quantum channels) which in general are energy-dependent.

For the symmetrized current $I = (\langle I_{\rm R}\rangle - \langle I_{\rm L}\rangle)/2$ the expression

$$I = \frac{e}{2\pi\hbar} \sum_n \int dE\; T_n(E)[f_{\rm L}(E) - f_{\rm R}(E)] \tag{2.9}$$

can be found, where the Fermi functions are defined as $f_{\mathrm{r}}(E) = [e^{(E-\mu_{\mathrm{r}})/k_{\mathrm{b}}T}+1]^{-1}$, with $r = \mathrm{L}, \mathrm{R}$. The chemical potentials are mostly chosen in the form $eV_b/2 = \mu_{\mathrm{L}} = -\mu_{\mathrm{R}}$ such that the bias V_b is applied symmetrically. This expression for the current is a result for a non-interacting system, where the reservoirs have been assumed to be large compared to the sample size and thus inelastic processes have been neglected. This assumption is justified in case of ballistic transport, where the sum over the eigenchannels $T_n(E)$ has to be large in the sense, that either for some n, the $T_n(E)$ have to be near unity, or for small $T_n(E)$, many channels n exist, such that the conductor is transparent. For small applied bias in the zero-temperature limit the conductance can be approximated as

$$G = \frac{e^2}{2\pi\hbar}\sum_n T_n(E). \tag{2.10}$$

Assuming the transmission probabilities to be energy-independent, $T_n(E) = T_n$, the conductance can be related to the current even for larger bias as $I = GV_b$. Eq. 2.10 is known as the Landauer formula, for the case of many channels.

Taking the definition Eq. 2.5 for the noise, an expression for the zero-frequency shot noise can be derived as well within a scattering approach. For a non-interacting system

$$S = \frac{e^2}{\pi\hbar}\sum_n \int dE \,\{T_n(E)\left[f_{\mathrm{L}}(E)\left(1-f_{\mathrm{L}}(E)\right)+f_{\mathrm{R}}(E)\left(1-f_{\mathrm{R}}(E)\right)\right] + T_n(E)(1-T_n(E))\left[f_{\mathrm{L}}(E)-f_{\mathrm{R}}(E)\right]^2\} \tag{2.11}$$

is found, where the definition of the symmetrized current has been used. Current conservation assures, that $S = S_{\mathrm{LL}} = S_{\mathrm{RR}} = -S_{\mathrm{LR}} = -S_{\mathrm{RL}}$. It is easily seen, that for zero bias (equilibrium situation) terms of the kind $f_{\mathrm{L}}(E) - f_{\mathrm{R}}(E)$ vanish. This leads to a vanishing current, as well as a vanishing second part of the noise expression. The surviving term is the thermal noise and can be related to the conductance. This relation is called the fluctuation-dissipation theorem (FDT) and leads for the Fano-factor $F = S/2eI$ to a cotangent hyperbolic behavior in $(eV_b/k_{\mathrm{B}}T)$. In the zero temperature limit in turn, contributions involving $f_{\mathrm{r}}(E)(1-f_{\mathrm{r}}(E))$ vanish, such that a simple relation of the (non-equilibrium) shot noise to the conductance is not possible anymore. For energy-independent transmission probabilities Eq. 2.11 can be approximated as

$$S = eV_b\frac{e^2}{\pi\hbar}\sum_n T_n(1-T_n), \tag{2.12}$$

which leads to a Fano factor

$$F = \frac{\sum_n T_n(1-T_n)}{\sum_n T_n}. \tag{2.13}$$

In the case of one channel ($n = 1$), we recover the same result as calculated in the last section for the case of a single-barrier.

A finite frequency formula for the shot noise has been derived for energy-independent transmission probabilities by Khlus [23] within a scattering approach assuming the scattering matrix to be diagonal, and Yang [25], within a description of a quantum point contact. The integrals as present in Eqs. 2.9 and 2.11 can be taken out, resulting in an expression being valid for frequencies $\omega < \omega_c$ below the collective response ω_c of the structure. The shot noise then reads

$$\begin{aligned} S(\omega, V_b, T) = \frac{e^2}{2\pi\hbar} \Bigg\{ & 2\hbar\omega \coth\left(\frac{\hbar\omega}{2k_B T}\right) \sum_n T_n^2 \\ & + (\hbar\omega + eV_b) \coth\left(\frac{\hbar\omega + eV_b}{2k_B T}\right) \sum_n T_n(1 - T_n) \\ & + (\hbar\omega - eV_b) \coth\left(\frac{\hbar\omega - eV_b}{2k_B T}\right) \sum_n T_n(1 - T_n) \Bigg\}, \end{aligned} \tag{2.14}$$

with arbitrary frequencies, voltages and temperatures. In the zero-frequency limit Eq. 2.11 is recovered for energy-independent transmission probabilities, when expanding in the coefficients T_n, such that terms of order T_n^2 are neglected. In this regime of low transparency corresponding to the Poissonian statistics we can consider the following three extreme situations:

(I) In the zero frequency ($\omega = 0$) and zero bias ($V_b = 0$) regime the thermal noise is found to be

$$S(0, 0, T) = 4k_{\mathrm{B}} T G, \tag{2.15}$$

which we discussed before and relates to the fluctuation-dissipation theorem. For finite temperature the noise still has a finite value due to a finite conductance G.

(II) If we consider the zero frequency ($\omega = 0$) and zero temperature ($T = 0$) regime, we find

$$S(0, V_b, 0) = 2eV_b G = 2eI, \tag{2.16}$$

which we discussed in the last section to be the Poissonian (non-equilibrium) shot noise.

(III) The excitation noise, due to non-vanishing frequency ω, but zero bias ($V_b = 0$) and zero temperature ($T = 0$) is found to be

$$S(\omega, 0, 0) = 2\hbar\omega G, \tag{2.17}$$

and accounts for vacuum-polarization effects that are important at high enough frequencies. The comparison of these three regimes allows an easy estimation of the different noise sources, since all of them are expressed in terms of the conductance. At the beginning of this chapter we discussed other frequency dependent sources of noise, which can be eliminated, when considering frequencies above $\sim$ 100 kHz (for quantum dots) or $\sim$ 100 MHz (for molecules). This corresponds to an energy scale of $\hbar\omega \sim 10^{-12}$eV (or $\hbar\omega \sim 10^{-9}$eV respectively). On the other hand, temperatures in experiment will be in the regime of about $1K$ or room temperature, which defines an energy scale of $k_{\mathrm{B}}T \sim \mu$eV ($k_{\mathrm{B}}T \sim$ meV). The bias region in which the noise is measured corresponds to a scale $\sim$ meV ($\sim$ eV). For both, quantum dots and molecules, the frequencies needed to eliminate other sources of noise are still so small ($\hbar\omega << k_{\mathrm{B}}T <<$ eV), such that the shot noise can be viewed as white noise.

We summarize the main properties of the shot noise as a non-equilibrium frequency-independent phenomenon as follows: If transport is due to uncorrelated events in time, Poissonian behavior with a Fano factor equal to one is observed. For fermionic systems that we want to describe such a behavior arises in the case of a single barrier structure, if the transparency of the junctions the electrons are tunneling through is very low. The same behavior can be observed for a double barrier with extremely asymmetric barrier heights, since the less transparent side will be the bottleneck for the tunneling events. For symmetric situations in a finite bias regime the Fano factor will have a value of 1/2, since half of the time the junction is open for electrons to tunnel through, whereas else tunneling is blocked. In case of a quantum mechanical description this blocking which leads to a sub-Poissonian $F < 1$ noise is explained by anti-bunching due to the Pauli exclusion principle. For high transparencies the Fano-factor can be reduced even down to zero. The shot noise itself turns out to be the strongest at intermediate transparency. These three values of the Fano factor reflect a universal behavior of the shot noise that is observable in many systems. However, for the use of the current-current fluctuations as a tool which should provide additional information about system parameters, we are interested to find non-universal behavior, allowing to characterize special values, non-monotonicities, etc. as being due to the specificities of the considered system.

It is obvious, that systems involving more degrees of freedom offer more possibilities to show interesting behavior in the noise, when symmetries are broken by electronic-, coupling- or other parameters. It has been shown, that the inclusion of interaction effects in mesoscopic systems has a special importance for the shot noise. Additional correlations between tunneling events will show up, making their consideration not just a simple generalization as was the case of a multi-channel model compared to a single channel model. The system, in the presence of interactions, will remember information about previous states, leading to a much more complex behavior of the shot noise and the Fano factor.

A theory taking into account such effects would help to characterize and additionally understand the physics of mesoscopic systems in more detail. This is the central concern of this thesis. A discussion of theories trying to deal with shot noise in mesoscopic devices will be presented in the next chapter, followed by our own approach, for which we demonstrate that we are able to include the desired interaction effects. Up to now a formula taking into account two particle interaction effects as well as the coupling of a system to its environment has been presented only for the current [22]. So far all theories do perturbation expansions in either interaction or coupling parameters [26, 27, 28, 29, 30]. For an intermediate coupling regime (higher order in the transmission parameter) only few work has been done while additionally focusing on restricted physical situations.

We want to end this section with the current and shot noise formulas wich we refer to when talking about non-interacting results in chapter 4. Within the Landauer-Büttiker approach, Eqs. 2.9 and 2.11 have been derived for a two-terminal, non-interacting, multi-channel system. We want to specify these results in order to discuss resonant tunneling barrier structures, which we will consider in the next chapters. Resonant tunneling arises from the wave nature of electrons, giving rise to energy quantization, and is thus observable only in sufficiently short (compared to temperature) samples. We rewrite Eq. 2.9 for the current (describing non-interacting systems $U = 0$) in the form

$$I_{U=0} = \frac{e}{2\pi\hbar} \int dE \sum_{\sigma} \tau_{\sigma}(E)[f_{\mathrm{L}}(E) - f_{\mathrm{R}}(E)], \tag{2.18}$$

and Eq. 2.11 for the shot noise as

$$S_{U=0} = \frac{e^2}{\pi\hbar} \int dE \sum_{\sigma} \{\tau_{\sigma}(E)[f_{\mathrm{L}}(E)(1 - f_{\mathrm{L}}(E) + f_{\mathrm{R}}(E)(1 - f_{\mathrm{R}}(E))] \\ + \tau_{\sigma}(E)(1 - \tau_{\sigma}(E))[f_{\mathrm{L}}(E) - f_{\mathrm{R}}(E)]^2\}, \tag{2.19}$$

where we use the Breit-Wigner formula for the transmission function

$$\tau_{\sigma}(E) = \frac{4\Gamma_{\mathrm{L}}\Gamma_{\mathrm{R}}}{\Gamma^2} \frac{(\Gamma/2)^2}{[(E - \varepsilon_{\sigma})^2 + (\Gamma/2)^2]}. \tag{2.20}$$

The energy-dependence of the coupling parameters $\Gamma_{\mathrm{L}}, \Gamma_{\mathrm{R}}$ (with a total linewidth $\Gamma = \Gamma_{\mathrm{L}} + \Gamma_{\mathrm{R}}$) has been neglected. We specified the n different channels as two spin states $\sigma = \uparrow, \downarrow$ with energies ε_{σ}. Together with the empty state, three different states are relevant in structures, described by these formulas. A non-interacting single level quantum dot connected to two electron reservoirs would be the perfect system to be studied with these formulas. Since Eqs. 2.18 and 2.19 are exact in the linewidth or coupling strength Γ associated with the transparency of the barriers, an expansion in

this parameter can be done order by order. In our results in chapter 4 an expansion in exactly this parameter to first and second order will be presented for more complicated systems and considering interaction effects. Eqs. 2.18 and 2.19 will serve as limiting cases, allowing to test the consistency of our theory.

We finally want to discuss two approximations for these equations explicitely, which are significant and have been verified in many theoretical as well as experimental works. First, in the case of small coupling Γ, an expansion up to lowest (first) order of above equations is justified, which leads to a Fano factor

$$F^{(1)} = \frac{\Gamma_{\mathrm{L}}^2 + \Gamma_{\mathrm{R}}^2}{(\Gamma_{\mathrm{L}} + \Gamma_{\mathrm{R}})^2}. \tag{2.21}$$

This result is valid for bias voltages above the lowest of the energies ε_σ (finite transport) and small temperatures. It is found that for current and shot noise, several channels provide additive contributions and thus always lead to the same Fano factor. Values between 1 (strongly asymmetric coupling) and 1/2 (symmetric coupling) are possible.

For bias voltages below the excitation energies ε_σ no transport is possible (given that the temperature is small), unless stronger coupling is considered. In the small bias regime we can therefore expand the above expressions up to second order, which leads to a Fano factor

$$F^{(2)} = \coth\left(\frac{eV_b}{2k_{\mathrm{B}}T}\right). \tag{2.22}$$

The first order contributions can be neglected in this case since they are exponentially small. The crossover from thermal noise to the Poissonian shot noise is described by this formula, which turns out to be independent of the values of coupling parameters.

We keep in mind the main results for the non-interacting system as given in Eqs. 2.18-2.22 together with the statement, that interaction effects may lead to values of the Fano factor, others than $F \leq 1$.

2.2 Experiments

Electronic devices for future technological applications may be realized in manifold ways. The only condition all of them have to obey is that electrons, by scaling down the device dimension, have to offer their real quantum nature, resulting in new physical effects, which cannot be observed in conventional transistors. In the extreme, only a few or even single electrons tunnel through structures, which are confined to less than three dimensions. Whereas a bulk semiconductor as the 'Esaki' diode describes a three dimensional electron gas (3DEG), a confinement to two dimensional electron gases (2DEG) is achieved for quantum wells, such as resonant tunneling diodes. When reducing the electrons mobility by a further degree of freedom, a 1DEG is performed, which has the structure of a quantum wire (examples are carbon nanotubes). Single-electron tunneling, exhibiting effects like Coulomb-blockade, is typical for zero dimensional (0D) quantum dot structures. Here, besides the shrinking to sizes in the order of several nanometers, all degrees of freedom (with respect to the electron mobility) have been removed, and bound or resonant states are formed. The band structure has been broken up into a set of single-particle levels, separated by a finite level spacing. Besides the semiconductor quantum dots, molecules (e.g. the fullerene molecules) can be viewed as such zero dimensional systems as well, since the molecular orbitals define the electronic level-structure in this case. The same considerations hold for sufficiently short carbon nanotubes.

From a theoretical point of view, quantum dots can be understood as localized separated levels, whereas the more complex molecules are better described by delocalized coupled orbitals, similar to several coupled quantum dots. The names 'artificial atoms' and 'artificial molecules' have been established for single and coupled quantum dots in the last years. These are the kind of systems, for which we develop a theory of current and shot noise.

Shot noise measurements have been presented for many different systems in the last years. The sub-Poissonian partition noise as discussed in the last section has been observed in a quantum mechanical system [31] as well as the anti-bunching effect within a fermionic Hanbury Brown and Twiss Experiment [32, 33] (in analogy to the bosonic Experiment). Sub-Poissonian noise with values of the Fano-factor between 1 and 1/2 has been seen in experiments using a scanning-tunneling microscope (STM) [34], in quantum wells [35, 36], where even stronger suppression for longer samples is found when a ballistic transport situation is reached. Such strong suppressions as for ballistic systems [37, 38] are present also in diffusive wires [39, 40] (suppression to $F = 1/3$) and metallic resistors [41], where a dependence of the Fano-factor on the sample length has been discussed. The strong reduction of the noise in all these systems can be explained with a large number of electron paths through the setups. This causes a good transparency.

However, also super-Poissonian behavior of the Fano-factor has been observed, as in the case of resonant tunneling diodes [42, 43, 44], when a negative differential conductance (NDC) occurs. Here, electrons tunneling into the well increase the density of states, which allows for more tunneling events in time, resulting in positively correlated transport. Super-Poissonian noise thus arises due to charge accumulation. In a metal-semiconductor field effect transistor an enhanced shot noise has been explained by two interacting impurities carrying the current in a correlated way [45], which emphasizes that possibly interesting behavior in even smaller (nanosize) systems could be found due to finite interaction effects.

For *carbon nanotubes* all degrees of freedom for electron motion up to one have been removed, which further approaches the zero dimensional molecule and quantum dot structures. Shot noise measurements showed a suppressed Fano factor [46, 47] $F = g(1-T)$ with $g = [0.2, 0.3]$, which is in agreement with theoretical calculations for Luttinger-liquid models. Ballistic transport as well as electron-electron interactions further negatively correlating the carriers explain this behavior here. For very short nanotubes the band structure, which was present for nanotubes of length $\sim \mu m$, is split into discrete energy states, and a zero dimensional system is achieved, in principle [48]. For such structures only current measurements have been presented, focusing on the Kondo regime [49, 50].

Molecules and quantum dots are structures of nanosize with respect to all spacial dimensions. They have a very limited charge capacity (molecules: $C = 10^{-18}F$, QDs: $C = 10^{-15}F$), and thus only a few electrons confined to a small volume. The de Broglie wavelength of these electrons is comparable to the size of the dot and the electrons occupy discrete quantum levels (comparable to atomic orbitals in atoms) and have a discrete excitation spectrum. This is a regime where single-electron tunneling leads to interesting quantum mechanical effects, very different to those appearing in classical devices. Charging and Coulomb-interaction determine the transport in a situation, where the discreteness of the charge plays an important role. As we discussed in the last section, this is the regime where shot noise is expected to show an interesting, non-trivial behavior. Since both, molecules and quantum dots are candidates for future technological applications due to their small size, one has to fully understand the transport properties of these kinds of devices, which makes shot noise measurements a promising venture. Whereas quantum dots can in principle be produced in a controlled way, where the coupling to the environment they are embedded in is tunable to a large degree, this is not the case for molecules. On the other hand, the variety of system parameters in setups with molecules enables many possibilities of device designs, which is the major reason, making molecular electronics so attractive.

In the following we thus want to discuss experiments on current and shot noise in quantum dots and molecules, after briefly characterizing these structures. Our special interest lies in the weak (sequential tunneling), but also intermediate (co-tunneling),

coupling regime, where interesting behavior of the Fano-factor can be expected, due to relevant interaction effects.

2.2.1 Quantum dots

We want to distinguish between two principle quantum dot structures, the *lateral (planar) and* the *vertical QD* [1, 2]:

1) A *lateral QD* is created by patterning several metal electrodes, or gates, on the surface of a two-dimensional electron gas (2DEG) heterostructure (usually of GaAs). A schematic picture is given in Fig. 2.3. A negative voltage (V_{G}) applied to a gate raises

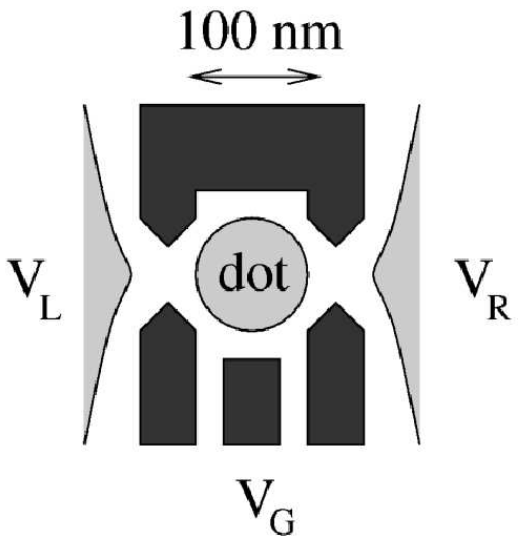

Figure 2.3: *Schematic picture of a lateral QD structure. Metallic gates define the dot in the 2DEG underneath.*

the electrostatic potential in its neighborhood and depletes the underlying 2DEG in the vicinity of the gate. The total charge on the dot structure and the barrier height, which defines the transparency of tunneling, are determined by the metallic fingers, being tuned by the applied gate voltage V_{G}. In experiments current and shot noise have to be measured by applying a finite source-drain voltage $V_{\mathrm{SD}} = V_{\mathrm{L}} - V_{\mathrm{R}}$ ($V_{\mathrm{SD}} = V_b$), which typically is of the order of ten to hundreds of mV. At low bias, the conductance $G = \partial I/\partial V_{\mathrm{SD}}$ turns out to oscillate in dependence of the gate voltage, known as Coulomb-oscillations. Peaks in the conductance are observed at the degeneracy points of adjacent charge states. In between the current is suppressed (Coulomb blockade), since the available energy for single-electron hops through the dot structure is smaller than the energy needed to charge the system. The possibility to switch the current on and off by applying a gate voltage justifies the name single-electron-transistor (SET) [51]. Only

thermal occupation at higher temperature or higher transparency may destroy this effect again. Typical temperatures in experiments are about 0.1 to $1K$ (corresponding to an energy scale of about $\sim 10 - 100$ μeV), which is small compared to a charging energy of about $10 - 100$ meV, e.g. Having barrier heights in the order of meV an estimation for the coupling strength to the dot can be made, from a WKB calculation, where the barrier length, density of states etc. enter. Typical values of a coupling Γ are in the order of 10 μeV.

2) *Vertical QDs* provide a different approach to realize single-electron tunneling. Here the current flows vertically with respect to the heterostructure layers, relying on AlAs, or other large-gap materials, to form tunnel barriers. The electrons are confined by the combination of the heterostructure layers providing vertical confinement and lithography providing in-plane confinement. Since here no in-plane tunneling is required, strong lateral confinement can be achieved by eliminating all but a narrow pillar in a double-barrier heterostructure. A schematic picture is shown in Fig. 2.4. Contacts on

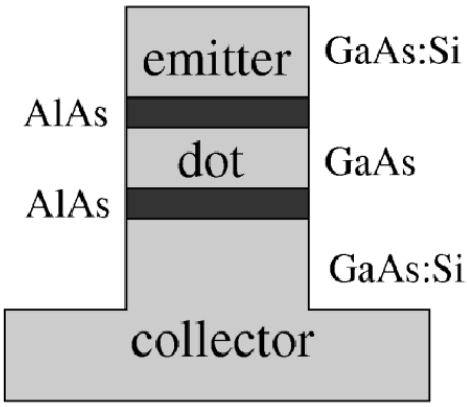

Figure 2.4: *Schematic picture of a vertical QD structure. The AlAs and GaAs layers are typically several nm thick.*

the upper and lower side of the dot structure allow for two terminal measurements of current and shot noise. The introduction of a gate as for the lateral QDs is technically more difficult. On the other hand controlled preparation of fixed tunnel barriers (typically of energy height ~ 100 meV) is possible. The electrons couple more or less uniformly to the entire area of the QD, whereas in lateral QDs the electrons tunnel into the edges.

The single particle energies of the electrons on the dot structure have a certain spacing $\Delta\varepsilon$. A continuous spectrum with $\Delta\varepsilon \to 0$ describes a metallic island, whereas a discrete spectrum with a large level spacing $\Delta\varepsilon \to \infty$ the extreme case of a single level quantum

dot. We are interested in a region in between, where one up to several levels contribute to the transport, which is the case in molecular transport as well.

Theoretically, transport through quantum dots in general is described very well in terms of the 'orthodox theory', where the barrier hight (connected to the lifetime of electrons on the structure or the total linewidth Γ as introduced in the last section) is small compared to other energies, such as the charging of the dot. There are however situations, when a weak coupling description is insufficient or wrong, such as in the Coulomb-blockade regime, where transport is strongly suppressed. Here the picture of single electrons hopping one after the other onto and off the dot structure (sequential tunneling) can not be applied. Now, processes allowing to tunnel through the whole structure via intermediate virtual states, so called 'co-tunneling' processes play an important role. Theoretically such processes are described by a perturbation expansion in the parameter Γ to higher (second) order, reflecting an intermediate (stronger) coupling region. For the non-interacting case, results for the current and shot noise in these regimes (Coulomb-blockade and transport) have been presented in the last section. A theoretical discussion will follow also in the next chapter.

Measurements of the current have been done for lateral [52] as well as vertical QDs [53] in the sequential tunneling regime. Co-tunneling effects have been observed also in lateral [54] and vertical [55] structures, where elastic and especially inelastic processes enhance the current at specific energies corresponding to the level structure of the dot. Typically, these additional processes, showing up in conductance peaks within the Coulomb-blockade region are illustrated in Coulomb-diamond plots, where the peaks are indicated as dark regions (the higher, the darker) in the source- drain voltage versus the gate voltage plane. The coupling strength for co-tunneling processes to be visible is typically of the order, (or larger) of the temperature. For a level width Γ being very large compared to the temperature, Kondo behavior can be observed [56, 57], which arises from the interplay of charging effects and quantum fluctuations.

Measurements of the shot noise in quantum dots are still rare. Up to date, it has been measured only in vertical structures [15, 58, 59, 60], whereas in lateral QDs $1/f$-noise [61] and generation-recombination or random telegraph noise (RTN) [62] have been discussed. However, the lateral structures would be the more interesting objects to study, since a closer relation to molecular systems is given, with tunable coupling parameters, more degrees of freedom, etc.

The frequency dependent $1/f$ or generation-recombination noise has been shown in [58, 59, 60] to be eliminated for frequencies larger than some kHz. In Ref. [59] current I and Fano factor F (here denoted by α) are measured in dependence of the source-drain voltage $V_{\rm sd}$ (results are shown in Fig. 2.5). For small temperatures of $1.5K$ and $3.7K$ (~ 130 μeV and 320 μeV) and weak coupling ('orthodox theory' is applicable), current and shot noise have been measured for an InAs QD. In contrast to the fabrication

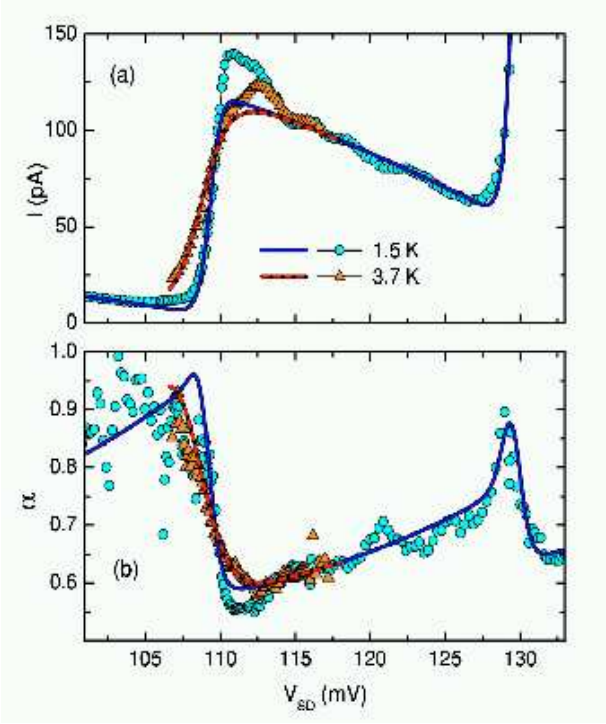

Figure 2.5: *Experimentally measured current (a) and Fano factor (b) vs. source-drain voltage for temperatures $T = 1.5K$ (circles) and $T = 3.7K$ (triangles). The experiment has been realized from A. Nauen in the group of R. J. Haug [59]. Sequential tunneling calculations are used to fit the results and extract the coupling parameters $\Gamma_{\mathrm{L}} \sim 0.4$ μeV and $\Gamma_{\mathrm{R}} \sim 1.6$ μeV.*

technique described above, these vertical QDs have been produced by a self-assembled growth of the layers. Experimental results for the two temperatures are indicated by symbols and theoretically calculated curves by solid lines. Since the current scales with the strength of the coupling, the experimental values (here hundreds of pA) can be taken, to estimate the absolute value of $\Gamma \sim 2$ μeV. The asymmetry $\Gamma_{\mathrm{R}}/\Gamma_{\mathrm{L}} = 4.4$ leading to values $\Gamma_{\mathrm{L}} \sim 0.4$ μeV and $\Gamma_{\mathrm{R}} \sim 1.6$ μeV is then extracted from the Fano factor. The underlying formulas, which allow for such a procedure are theoretical calculations in a lowest order perturbation expansion in Γ. It is shown in Ref. [59], that several QDs (in their case 3) with independent additive contributions can explain the experimental results, where each of them allows for tunneling through a spin degenerate ground state, where double occupancy is forbidden due to Coulomb interaction. The expressions, used to fit the experimental data, have been derived in [63, 64, 6], for example. They will be presented also in chapter 4. Peaks in the Fano factor in Fig. 2.5 can be explained by the sum of the contributions of several QDs.

The above example shows, that 'orthodox theory' can be applied very well in a finite transport regime for QD structures. This, however, will not be the case in the

Coulomb-blockade, where first order calculations turn out to be suppressed exponentially. Here, higher order calculations including co-tunneling processes will become relevant, although we are in a weak coupling situation in principle. Whereas vertical quantum dots may serve as a self-consistency test of a theory of shot noise, the same theory may be used for molecules the other way around, namely to determine the unknown system parameters.

2.2.2 Molecules

Transport through single molecules is a promising field of research [3, 4, 65, 66, 67, 68], since nanoscale electronic devices, due to many degrees of freedom, offer a potentially large number of possible device designs. What these degrees of freedom are, and how they may be handled, will be discussed in the next chapter, where theoretical descriptions of molecular transport are presented.

1) In experiment, two terminal transport through a single molecule has been achieved by deposition of the object between two fixed electrodes [69, 70, 71, 72, 73] by making use of a *mechanically controlled break-junction* technique (MCB). Transport is mea-

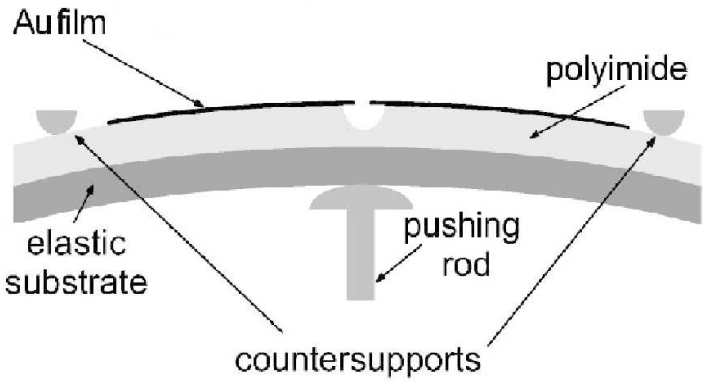

Figure 2.6: *Sketch of the mechanically controlled break-junction-technique to form a molecular device. Figure by courtesy of H. Weber.*

sured mostly in setups where organic molecules are attached via thiol (S) groups, providing a strong chemical bond, to gold (Au) electrodes. This is realized by a metallic wire substrate on a flexible substrate with a narrow bridge-like constriction. If the substrate is bent by a pushing rod, the bridge on top stretches, until it finally tears apart, resulting in a nanoscopic pair of electrodes facing each other. A sketch illustrating this procedure is shown in Fig. 2.6. A high precision (less than an Ångström) of distance control has been achieved within this technique, which reflects a high mechanical stability. Other advantages of this technique are clean contact surfaces (which

contain uncontaminated over several days), a wide range of operation (ultra high vacuum, low temperature). Not at least MCB can be employed to study various transport phenomena (shot noise, thermopower, Kondo effect, etc.).

In order to fabricate molecular devices, a solution of molecules is spilled over the junction (typically organic molecules e.g. benzene fabricated by chemists), and finally the distance of the gold electrodes is reduced, in the hope that at the end a single molecule is trapped in between. The direct observation of symmetric and asymmetric I-V-characteristics within measurements of symmetric and asymmetric molecules [71], has demonstrated uni-molecular transport. However, also experiments with molecular films have attracted much interest, since diode behavior [74, 75] and negative differential conductance (NDC) [76, 77] have been observed. Within a MCB-technique but also others, even the Coulomb-blockade effect and Kondo behavior, have been observed at low temperatures [78, 79, 80].

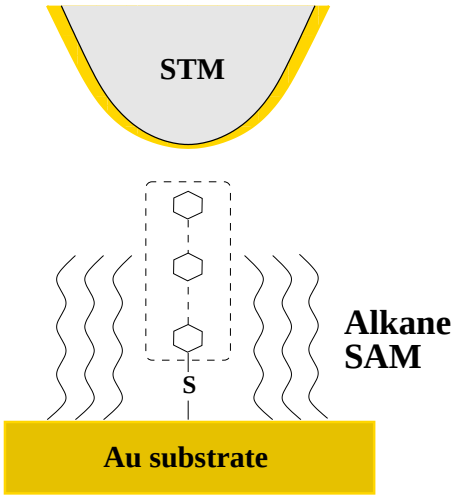

Figure 2.7: *Sketch of a conducting-tip STM above a molecule attached to a conducting gold (Au) substrate.*

One has to realize that the gold electrodes (good metal with well known electronic structure), having a cross section of about 20-50 nm, are relatively large compared to the molecules (electronic structure calculated from quantum chemistry) of nanometer scale. This qualitative difference in size and structure makes the contact or interface properties of the components to poorly understood parameters, especially in finite bias transport situations. With an adequate theoretical description of shot noise, many open questions could be answered by a comparison to experimental data.

2) Concerning the interface another possibility to measure transport through single molecules is provided by a scanning tunneling microscope (STM). The STM is widely used in both industrial and fundamental research to obtain atomic-scale images of

surfaces. It provides a three-dimensional profile of the surface which is very useful for characterizing surface roughness, observing surface defects, and determining the size and conformation of molecules and aggregates on the surface. Two terminal transport with a conducting-tip STM above a molecule attached to a conducting substrate has been achieved in experiment [81, 82, 83, 84]. An illustrative sketch is given in Fig. 2.7. The gap between the STM and the fixed electrode structure has to be adjusted such that only a single molecule has place to be trapped in between. The major problem of this technique is the fact that the STM is designed to operate in a feedback loop. I-V-curves can be obtained after switching off the feedback loop, which is usually done in a short time period, since the electrodes become sensitive to temperature drift and vibrations.

A shot noise measurement has been published in Ref. [34], where a small metal particle of 5 nm size has been deposited between the substrate and the STM. As discussed before, Fano factors between 1 and 1/2 have been observed, which is in agreement with theoretical predictions for the SET regime. Earlier measurements reported about $1/f$ and thermal noise [85]. However, shot noise in single molecules has not been measured so far. In comparison to the quantum dot structures as discussed before one needs to reach higher frequencies until a white noise behavior corresponding to shot noise is found. Noise measurements with single molecules using the MCB-technique have shown frequency dependent behavior due to $1/f$-noise, since only frequencies up to several kHz have been measured [86]. The expected shot noise is several orders of magnitude smaller compared to the measured noise, and will become visible therefore at much higher frequencies (above MHz). Technical problems will hopefully be solved soon so that experimental data become available in the near future.

Application of our theory to a specific experiment

In order to close the discussion on experiments on quantum dots and molecules we want to provide a short discussion about data, which are available at present. These are current measurements through single molecules. As an example we consider the current voltage characteristics of a terphenyl-type molecule. This molecule consists of three phenyl rings in series, which are directly coupled. A picture is given in Fig. 2.8. Thiol groups (S) on the left and right side of the molecule bind to the gold electrodes (Au) in experiment. Methyl groups make the phenyl rings about 60° rotated with respect to each other, leading to a suppressed π-conjugation between the rings. The coupling of the left and right phenyl ring to the central ring is therefore expected to be weak. Depending on the strength of the thiol bonds to the electrodes, the molecule might be described theoretically as a system of three coupled quantum dots or a single quantum dot, when these bonds are much larger compared to the coupling of the phenyl rings. The latter situation is expected to be present here. Quantum chemical calculations

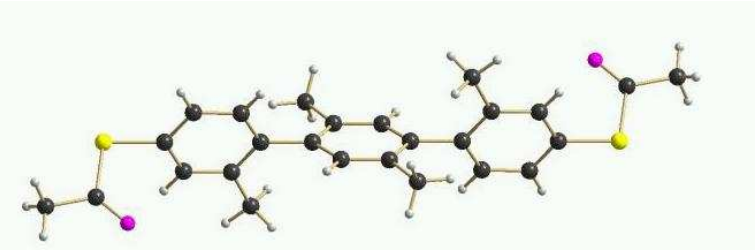

Figure 2.8: *Picture of the terphenyl molecule consisting of three phenyl rings. Methyl groups make the phenyl rings* 120° *rotated against each other, leading to a suppressed* π*-conjugation. Figure by courtesy of M. Elbing [87].*

could fix the electronic energy parameters and reduce the free model parameters to a minimum. We will show here, that even a simple single level model system can explain most of the features being observed in the current and the conductance.

In Fig. 2.9 we find a current measurement through terphenyl at a temperature of $T = 30K$ ($\sim$ 3 meV). The current I (thin solid line) and the differential conductance $G(V_b) = \partial I(V_b)/\partial V_b$ (thick solid line) vs. the bias as experimental results are compared to theoretical calculations of a single level system up to second order in Γ (dashed black lines) in Fig. 2.9. These calculations have been done within our diagrammatic theory we will discuss in the next chapter, and should serve here to illustrate the applicability of our theory even to complex systems like molecules. We depicted only a single measuring cycle from -0.8V_b to +0.8V_b and back, in order to permit an easier comparison of experiment to theory. In general of course many such cycles are performed and at the end the data is smoothed.

We are able to extract considerably much information from our single level model. The broadening of the conductance peaks is due to a combination of temperature and coupling, about $6(k_{\mathrm{B}}T + \Gamma)$. This allows us to determine the total linewidth, which we estimate to be about $\Gamma \sim 9$ meV. The comparison of Γ and T tells us that neither a weak $\Gamma << k_{\mathrm{B}}T$ nor a strong $\Gamma >> k_{\mathrm{B}}T$ coupling situation is present, but an intermediate one.

Transport sets in at a bias of $V_{seq} = 0.5V_b$, which we model with a corresponding excitation energy of the single level. We find an asymmetry in the conductance peaks, where the left peak in Fig. 2.9 is about twice as large as the one on the right side. This can be modeled only, when taking into account a finite Coulomb-interaction in our model and when choosing a very asymmetric coupling $\Gamma_{\mathrm{L}}/\Gamma_{\mathrm{R}} \sim 2000$. Less asymmetric couplings would be found, when modeling the data with several orbitals (levels). This can be explained, since at finite transport (above the sequential threshold V_{seq}) the current in first order (orthodox theory) is calculated to be

$$I^{(1)}(V_b > V_{\mathrm{seq}}) \sim \frac{2e}{\hbar}\frac{\Gamma_{\mathrm{L}}\Gamma_{\mathrm{R}}}{(\mathrm{N}\Gamma_{\mathrm{L}} + \Gamma_{\mathrm{R}})}, \tag{2.23}$$

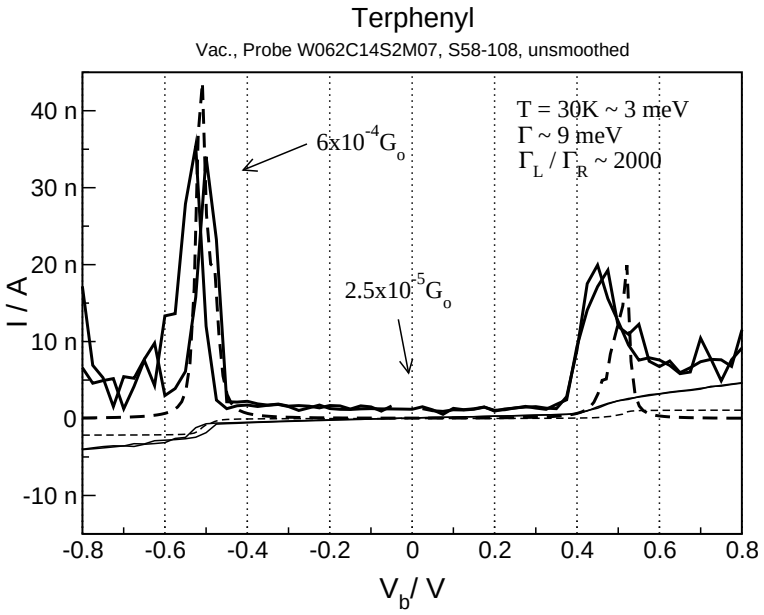

Figure 2.9: *Current (thin line) and conductance (thick line) vs. bias voltage for terphenyl measured by M. Di Leo in the group of H. Weber with a MCB-technique. The dashed lines are theoretical results of a single level model for an intermediate coupling regime, being relevant here.*

where N denotes the number of states available to enter the molecule (there is only one possibility to leave the molecule from each of the N states). For the present single level model N equals 2 because of the two spin states. Inserting the extracted parameters in Eq. 2.23, we find that the predicted current to be in agreement with the experimentally small measured current of some nA for larger bias. In our model a positive bias is due to a positive choice of the left chemical potential and a negative for the right one. Γ_L and Γ_R have to be exchanged, when reversing the bias. The need of additional levels to model the data becomes obvious also in the large bias regime, where the theoretical curve for the current lies below the experimental result. When additional channels are included, the theory will be able to better fit the experimental data.

The only feature which can not be qualitatively understood with our model is the conductance at small bias, which lies about a factor 20 below the experimental data of $2.5\text{x}10^{-5}G_0$ ($G_0 = 2e^2/h = 77\mu S$ is the quantum of conductance). We explain the experimental excess conductance by an ohmic offset due to additional transmission of electrons through the setup that does not include the molecule.

We find that information about absolute coupling, asymmetry, excitation energies, interaction effects and the number of conducting channels can be extracted from a relatively simple model. Much better statements could be given with the availability of shot noise data, as the current provides information only about a particular combination of the coupling constants (Eq. 2.23). One has to realize that asymmetric values

of Γ_L, Γ_R compensate for a stronger absolute value of Γ. A definitive answer on the real absolute and relative coupling strength can be given by the shot noise measurements. Since especially the low bias regime (Coulomb-blockade and above) permits a good comparison between experiment and theory, a theoretical description of molecules should include co-tunneling effects.

We are aware of the fact that a molecular device is a complicated system with a complex electronic structure, where vibrational, photon-relaxation effects, etc. may play a role. We also did not account for the spatially delocalized nature of the molecular orbitals of the molecule as shown in Fig. 2.8. In ***chapter 4.4*** the impact of such effects is studied in more detail. In addition the geometry of the environment and the orientation of the molecule will influence the transport properties. It has been shown in theoretical studies, for example, that the conductance can be different by orders of magnitude for different orientations of the molecule [88, 89]. On the other hand, transport measurements on molecules are still limited. The relevance of the above mentioned influences has not been studied extensively. Sometimes it is even unclear, if really a single molecule has been measured, or an ensemble of them. This is another reason, why *shot noise measurements in molecular devices* are important, since the behavior of the noise or the Fano factor may provide information about the presence of certain effects. Additionally, as we see from Fig. 2.9 an intermediate coupling situation is likely to be present in many experiments, which makes a theoretical inclusion of higher order *co-tunneling processes* necessary.

3 Theory

To date, many theories exist that attempt to describe transport through general nanoscale systems (quantum dots, atoms, molecules, nanotubes, DNA, etc.). In order to really describe such systems in a realistic manner, the electronic structure of both, the nanoscale system and the macroscopic electrodes would have to be characterized within a microscopic theory. Such a theory would have to account for all relevant many-body effects, and therefore go beyond a single-particle picture. Let us introduce a parameter $\mathbf{U}$ that shall represent all classes of many-body interaction effects (described by two-particle operators).
Now, one wishes to connect both components of transport (nanoscale island and reservoir electrodes) which introduces a further characteristic parameter, namely the coupling strength $\mathbf{\Gamma}$. The coupling to electrodes however affects the electronic structure of the nanoscale island and hence further complicates the whole problem of computing transport.
If now a bias is applied to the setup we obtain a complex system out of equilibrium. We disregard the geometry of the different components, the environment, mechanical, optical and other effects, which may additionally play a role in finite transport situations and even further complicate matters. A third parameter we want to introduce here, which determines physical effects one observes in transport measurements, is the temperature $\mathbf{T}$.
Therefore, we are interested therefore in a microscopic theory describing non-equilibrium transport phenomena, while allowing for a complete treatment of all these parameters $\mathbf{U}, \mathbf{\Gamma}$ and $\mathbf{T}$. This theory should be applicable to arbitrary complex systems.

Such a theory however does not exist. Several communities of researchers have formed specializing on electronic transport through the different systems and focusing on different regimes of the above discussed parameters. Current through quantum dots, molecular electronics, spintronics, etc. are some of the fields concerned with electronic transport. A recently formed field of research deals with shot noise as a non-equilibrium phenomenon, applied to study transport in variety of systems connected to superconducting, ferromagnetic, etc. leads.
But what are the theories currently used to study current as well as shot noise in such systems, and what are the regimes for which their approximations are valid? The main problem consists in the exact treatment of the two-particle operators, thus correctly accounting for interaction effects. There may be systems and transport situations in which those effects are of minor importance and can be neglected. This is the case for ballistic transport, which we discussed in the last chapter.

Electronic transport in mesoscopic structures in this picture can be studied by using the ***Landauer-Büttiker approach*** [90, 91, 92, 93, 5, 21] to conductance in nanometer-sized coherent systems. Here, *coherent* means, that the quantum mechanical coherence

length is longer then the sample size (no energy relaxation takes place in this region), and electrons originating from the reservoirs maintain their phase coherence. To view the electrons as non-interacting ($U = 0$) particles in phase coherent systems makes sense only, if the system couples via many channels (or at least a few almost open channels) to the reservoirs. This reflects a situation of ballistic transport. The number of channels is related to the conductance in the Landauer-Büttiker approach. The above requirement therefore implies a good conductance and hence a strong coupling between reservoirs and system, such that the mesoscopic system itself could be regarded as an impurity at which the electrons are scattered. This approach has been introduced in the last chapter and is the underlying theory for the physical situation as discussed in *chapter 3.1.1.* If the condition of large conductance is not given, interactions play a dominant role, since electrons will more likely be localized within the system compared to the reservoirs.
At this point we stress that exact formulas for current and shot noise have been derived within a scattering formalism in the non-interacting case [5, 21]. However, as discussed above the flow of electrons through a mesoscopic conductor may be correlated due to Coulomb interactions. The importance of these correlations is determined by the strength of Coulomb interactions for which the charging energy (energy cost for adding or removing electrons) is a qualitative measure in a mesoscopic system. The charging energy can be of the order of meV for quantum dots or even of order eV in the case of molecules.

One qualitative theory taking into account interaction effects is the so called ***mean field theory***. The basic idea is to include the electron correlations on the average, and hence account for the effects of other particles by introducing a mean density (mean field) of other electrons which a specific particle feels when moving around. The reduction to an effective single-particle picture makes the problem soluble again. Mean field theories are often used to study phase transitions as in superconductors (BCS-theory) or for Bose-Einstein condensates (BEC). In transport they have been used to describe current and shot noise addressing the Kondo problem (at small temperatures T_K) [94, 95, 96, 97, 98, 99]. So called slave-boson techniques as well as the description within a Hartree-Fock approximation are examples for mean field theories. Although the mean field approximation in many cases is sufficient to understand important physical features, it still fails, if explicitly the dynamic electron-electron correlations are needed to realistically describe transport and two-particle effects cannot be disregarded. This is certainly the case if the system is so small, that charging of the system costs more energy than can be provided by other energy scales like temperature T or the coupling Γ.
Another possibility to deal with the dynamical aspects of interacting many-body systems is the ***equation of motion technique***, where a series of coupled differential equations is generated, by differentiating the correlation function (Green functions)

a number of times. In general such a set of differential equations is not soluble and only a small set of Hamiltonians describing interacting systems can be solved exactly. Additional approximations like mean-field theories or random phase approximations (RPA) need to be applied, making this approach similar to the other mean field theories discussed before.

Many body systems out of equilibrium can be described by the ***Keldysh technique*** [100] which allows to deal with the real-time evolution of the system at finite temperature. Transport can be expressed in terms of non-equilibrium Green functions (NEGF) which may be derived within an equation of motion technique or a direct expansion of the S-matrix. Exact formulas have been derived for the current and shot noise also in this approach for the non-interacting case and for the current including interaction effects [22, 101]. For the shot noise however it turns out to be difficult to express two-particle Green functions (present here because of current-current correlations) in terms of one-particle Green functions. All formulas presented so far for the shot noise within a NEGF-formalism make use of Wick's theorem (which can be applied to non-interacting systems only) and therefore do not account properly for the interaction effects.
However, a Keldysh-formulation of the shot noise is able to handle all three above discussed parameters $\mathbf{U}, \mathbf{\Gamma}, \mathbf{T}$ in transport situations, in principle. It is our aim in this chapter to show this. We express current and noise in terms of irreducible self-energy diagrams (or transition rates) which are closely related to the Green functions. The general technical problem that always remains is the calculation of the objects containing the information about the systems transport properties, whether it is the S-matrix, Green function or, in our case the transition rates.
In order to do so, one usually expands in either the interaction U (**Hartree approximation**) [29, 30] or the coupling strength Γ (**orthodox theory**, golden rule) [26, 27] up to the lowest non-vanishing (first) order. [Only few works expand to higher orders in U [102, 103] and Γ [104, 105].] Especially for the latter approach which describes sequential (incoherent) transport by considering first order perturbation theory in Γ there exists a lot of work. This weak coupling limit will be discussed in more detail in *chapter 3.1.2*.
If we want to study transport for arbitrary choices of the above parameters we would either have to do a perturbation expansion up to infinite order or make use of a non-perturbative treatment (e.g by using renormalization group methods, resonant tunneling approximation, etc.) which however would restrict us to a very limited number of model systems. We are interested in describing an intermediate coupling regime by using the perturbative approach as we motivate in *chapter 3.1.3*. We find a ***diagrammatic technique*** to be able to deal with this problem.

We further show that our theory as presented in this chapter can be extended to describe ***coherent transport***, meaning the inclusion of non-diagonal elements in the

density matrix. This should allow for physical investigation of coherence effects in delocalized systems as was investigated by Gurvitz [106, 107, 108, 109]. The disadvantage of the latter approach is a restriction to zero temperatures and a large (infinite) bias voltage. Recently, two different groups, presented an 'extension' of the theory of Gurvitz, meant to valid for high temperature ($T \gg \Gamma$) and arbitrary bias voltage, within 'orthodox theory' [110, 111].

Approach	Γ	U	T	Ref.
Landauer-Büttiker	any	non-interacting	any	[91, 5]
Landauer-Büttiker with DFT	any	self-consistent	$T > T_K$	[112, 113]
slave boson mean field	any	infinite U	$T \ll T_K$	[94, 96]
Equation of motion	any	self-consistent	$T \gtrsim T_K$	[114, 115]
Hartree approximation in U and beyond	any	first or higher order	$T > T_\mathrm{K}$	[29, 30] [102, 103]
Orthodox theory	first order	any	$T \gg \Gamma$	[27, 26]
Our diagrammatic technique	higher order	any	$T \gtrsim \Gamma$	[9, 10]
'Gurvitz approach'	any	any	$T = 0$	[106, 107]

Table 3.1: *A simplified overview over the validity regime of different approaches describing mesoscopic transport (current and/or shot noise). Note that all theories can describe arbitrary finite bias situations except the 'coherent transport' approach of Gurvitz, which is strictly valid only at infinitely large bias.*

In Tab. 3.1 a somewhat simplified overview over the different theories (allowing to calculate current and shot noise) and validity of parameter regimes is given. An exact treatment of interaction, while considering an intermediate coupling regime and an arbitrary finite transport situation is provided by our diagrammatic technique, as introduced in the following.

In the following we present a theory for current and shot noise in mesoscopic systems (e.g. quantum dots or molecules), derived within a diagrammatic technique. We start with a short discussion of the extreme limits of the coupling parameter (strong and weak), which theories are applied in these cases and what they are able to describe. We hereby focus on the field of molecular electronics to learn about the difficulties one has to overcome in order to realistically describe transport through molecules. We will further motivate why it is interesting and necessary to push a theory towards an intermediate regime.
The class of Hamiltonians being able to describe the systems we are interested in is introduced and we discuss in detail the derivation of a current and noise formula within a diagrammatic technique, which can be interpreted on the Keldysh contour, and hence allows for a non-equilibrium treatment of the problem. We discuss the range

of validity of our theory, which we expand order by order in the coupling strength Γ. The equivalence and advantage of the zero frequency shot noise formula to the finite frequency noise is discussed and a way for a description of higher order correlators (as calculated within full counting statistics) will be shown. The inclusion of coherent processes allowing to describe delocalized general systems is discussed at the end.

3.1 Strong vs. weak coupling

Theoreticians working in the field of molecular electronics are interested in a theory describing electronic transport through single molecules or molecular layers adequately. However, there are two main difficulties making this problem particularly hard.

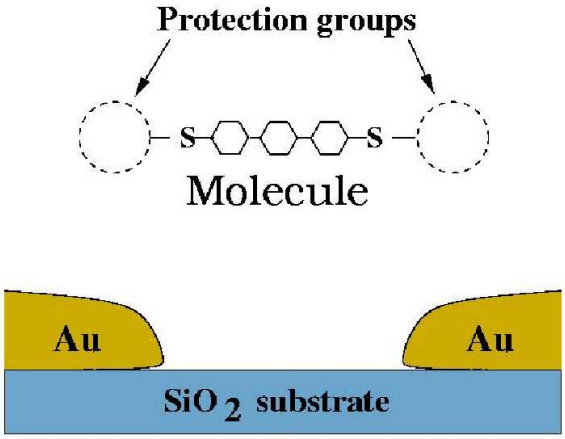

Figure 3.1: *Illustration of the independent parts of the metallic gold electrodes and the molecule, before building a molecular device. The isolated system parts are well understood.*

First, transport takes place through a hybrid system, consisting of mostly metallic electrodes and a semiconducting molecule (i.e. a system with a gapped excitation spectrum). Bringing these systems into contact, interface physics like charge transfer and the resulting barriers as well as the possibility of Coulomb blockade complicate matters, since transport is strongly influenced by these effects. Therefore, knowledge of the separated system parts (molecule and electrodes) in general is not by itself sufficient to describe transport through the combined system.
Second, one needs to know more of the molecular electronic structure than necessary for the description of thermodynamic or equilibrium properties. To describe transport, one needs to know the true single-particle excitation spectrum of the molecule in contact to the electron reservoirs of the electrodes. These are out of equilibrium, due to the applied bias V_b.

This is illustrated, when considering the situation as sketched in Fig. 3.1, where two gold (Au) electrodes on a SiO_2 substrate are shown, separated by a gap of size about 2 nanometers. Above the gap a molecule is approaching the electrodes. Protection groups prevent unwanted chemical reactions to take place. The choice of thiol (S) as connection groups is due to chemical feasibility and stability considerations, since Au-S is a strong chemical bond and hence allows reproducible measurements in experiment. The electronic structure of the three separated parts (left electrode, right electrode and the molecule) is indicated in Fig. 3.2. The electrodes can be considered as 'Fermi seas' of electrons with a continuous density of states filled to the corresponding chemical potential (Fermi energy).

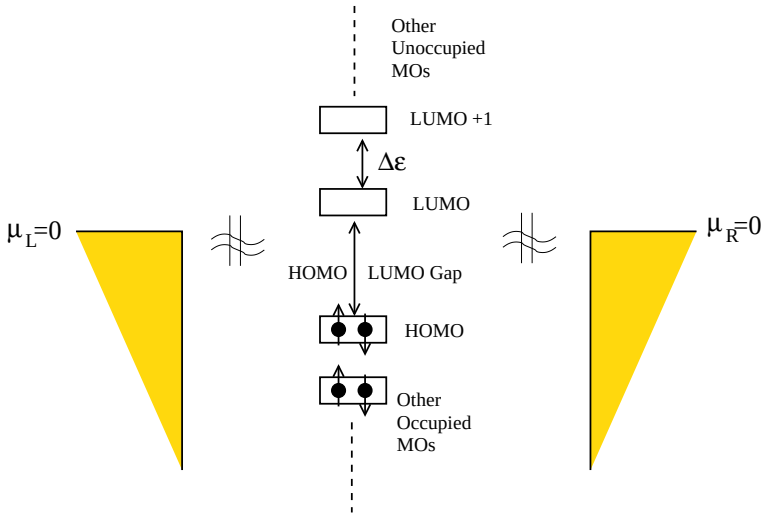

Figure 3.2: *Sketch of the isolated systems as illustrated in Fig. 3.1: metallic electrodes, with chemical potentials μ_L and μ_R (considered as non-interacting electrons) and the molecules, with molecular orbitals separated by an energy $\Delta\varepsilon$ (calculated from quantum chemical calculations).*

The molecule in isolation is a finite quantum system and has a spectrum of discrete quantum states (Molecular Orbitals, MOs) that are either occupied or unoccupied. For simple organic molecules, the MOs are occupied by two electrons (spin up and down) up to the Highest Occupied MO (HOMO). All MOs above the HOMO are unoccupied, starting with the Lowest Unoccupied MO (LUMO). Between the HOMO and the LUMO the electronic spectrum has a gap (HOMO-LUMO gap) that can be associated to the light absorption spectrum of the molecule in isolation, since the lowest energy process for absorption of a photon would be an excitation where one kicks an electron out of the HOMO and deposits it in the LUMO. The electronic structure of the nanosize organic molecule can be calculated by means of quantum chemistry.

If the molecule approaches the gap between the electrodes, the thiol groups (S) prefer a covalent bond to the gold atoms of the electrodes. The protection groups are removed

and will diffuse away. The new situation is depicted in Fig. 3.3. Now the molecule is bound covalently to both electrodes, meaning that the formerly separated electronic systems are coupled. The electrodes with a cross section of 20-50nm are huge compared to the molecule of nanometer size. The different components interact with each other in many complex ways. Field effects, screening, dielectric effects, vibrations, electro-mechanical effects and relaxation via electromagnetic radiation all can play a role.

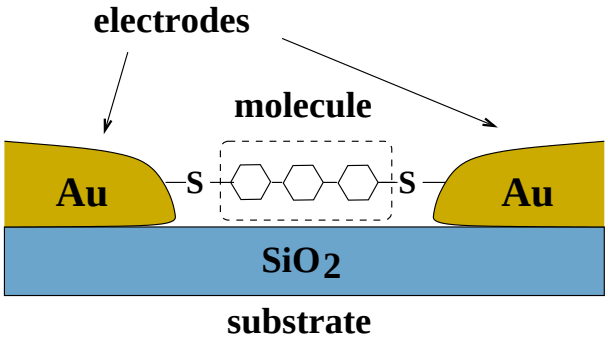

Figure 3.3: *The molecule approaching the gap between the electrodes (Au) is bound covalently to the electrodes via the thiol groups (S).*

Which of these effects takes the dominant role in an experiment is almost impossible to establish without making use of theoretical studies. The importance of different effects, however will be mainly determined by the way the different parts of the systems couple together. To understand this, we consider for simplicity three parameters: the coupling strength Γ, the level (molecular orbital) spacing $\Delta\varepsilon$ and the charging energy E_C. Depending on the strength of the coupling (compared to the other energy parameters) two extreme scenarios of transport can be considered: a *strong* or a *weak* coupling situation.

3.1.1 Strong coupling

If the molecule-electrode coupling is strong (i. e. $\Gamma >> \Delta\varepsilon, E_C$) the combined system of electrodes and molecule can lower its free energy by hybridizing states of the electrodes and the molecule. From the point of view of the molecular states, this means that the formerly sharp quantum states become broadened, i.e. they acquire a finite life time, as electrons in the new hybrid states will spend some time in the electrode and not on the molecule. A sketch of this situation is given in Fig. 3.4. In addition to the broadening, there will be a (differential) shift of the molecular orbitals due to the fact that in contact a spatially uniform electrochemical potential will be established. This results in charge transfer (typically from the electrode to the molecule) and a corresponding electrostatic potential at the interface region, similar to a Schottky barrier at semiconductor-metal

interfaces. The electronic transport in this situation can be understood by scattering theory, in the sense that the current is carried by scattering states that extend from the left electrode over the molecule into the right electrode. This is the Landauer approach we have discussed in the last chapter. Because of the coherent quantum states that span the entire system, we call this scenario the *coherent transport picture*.

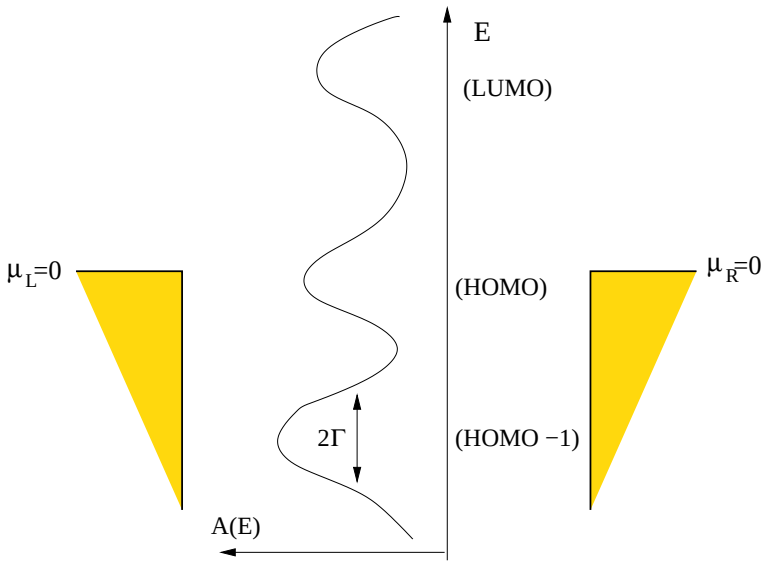

Figure 3.4: *Sketch of a strong coupling situation of the molecule to the electrodes. Formally sharp quantum states are smeared out to a continuous density of states* $A(E)$.

Simplistically, the current can be understood as a product of a transmission rate and an effective continuous density of states on the molecule as depicted in the figure above. As the electrochemical potential will often lie in the region of low density of states that was formerly the HOMO-LUMO gap, the conductance $G(V_b) = \partial I(V_b)/\partial V_b$ will be low at small bias. As the bias is increased, at some bias a resonance due to the broadened molecular orbital will be captured by the bias window. The current will increase rapidly and the conductance will show a peak. If one ignores the influence of the bias on the electronic states, the conductance peak will show at a bias approximately twice the energy difference of the electrochemical potential and the closest resonance (typically, but not always, the resonance related to the former HOMO). Naturally, the problem is how to compute the transmission function in a quantitative way. The transmission function can be expressed in terms of non-equilibrium Green functions. Nowadays still the best method to compute these Green functions is based on Density Functional Theory (DFT). However, DFT was never meant to be used for transport through nanoscopic systems. It is by now well known that its application to transport has intrinsic shortcomings, because the DFT Green functions are by no means assured to capture all the physics. In general, DFT calculations show a low bias conductance

that is orders of magnitude too high in comparison to experiment. At larger bias, the agreement with experiment is qualitatively better, but still insufficient for quantitative predictions [116, 117, 118, 119, 89].

3.1.2 Weak coupling

Weak molecule-electrode coupling (i. e. $\Gamma << \Delta\varepsilon, E_C$) effectively means high tunnel barriers between the electrode and (parts of) the molecule. In this case one can ignore to first approximation the broadening of the molecular states, so the orbitals remain well defined and discrete states [120]. This is illustrated in Fig. 3.5. Electrons spend

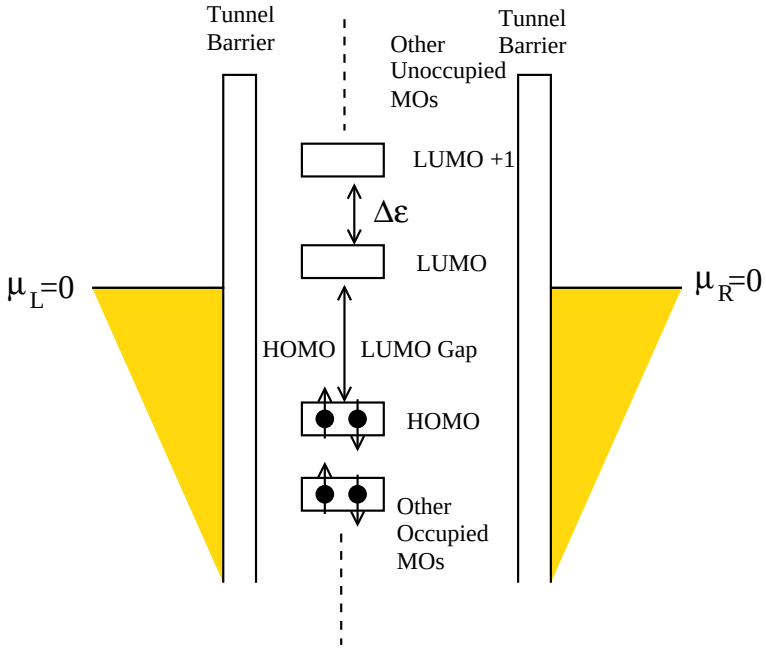

Figure 3.5: *Sketch of a weak coupling situation of the molecule to the electrodes. The molecular orbitals remain discrete quantum states.*

enough time on the molecule for charging effects to become important. The transport can be described as a sequence of incoherent hops of single electrons on and off the molecule. Due to the dominant interaction effects the Landauer approach breaks down here. We call this scenario the *(incoherent) tunneling transport picture*. The theory usually applied in this scenario has the name 'orthodox theory'. It computes transport in a perturbative expansion to first order in the coupling Γ, which is nothing but the golden rule approximation. Semiquantitative calculations of molecular transport with this theory have been performed for the current in Ref. [121].

At first glance, not much has changed from the physical picture of transport described above for strong coupling. One still would expect low (exponentially small) conductance at small bias and a rapid rise of the current and a peaked conductance as soon as

the first resonance (that is now very close to the molecular state of the separated components) is captured by the bias window. However, this picture almost certainly fails for the molecules of interest in the weakly coupled situation. The underlying reason for this failure is the phenomenon of 'Coulomb blockade', also known from transport through mesoscopic quantum dots [51, 122]. To understand this, consider an initially electrically neutral island, somehow isolated from its environment. Little work is required to bring an electron on the island. The occupied island, with charge e, however produces an electric field. Therefore, an additional electron has to overcome a force to occupy the island. The energy needed, to further charge the island is called charging energy

$$E_C = \frac{e^2}{2C}, \tag{3.1}$$

with C being the island capacitance. For an integer number N of excess charges ($Q = Ne$) and $Q_g = n_g e = CV_g$ (since a gate voltage allows to tune the charge number) we can write the total charging energy generally as

$$E_{ch}(N, n_g) = E_C(N - n_g)^2. \tag{3.2}$$

It is obvious, that n_g can be tuned continously, where the ground state energy will always take a minimal value. This leads to the fact, that for temperatures and bias voltages small compared to E_C, the number of island electrons N will be a fixed integer, as long as n_g is away from half-integer values. As an example take $n_g \sim 0$, than the energy difference for the charge states $N = 0$ and $N = 1$ is about E_C, whereas for $n_g \sim 1/2$ the difference is zero. In the first case neither energetically (bias) nor thermally the charge state can be changed, whereas in the second case it is possible.

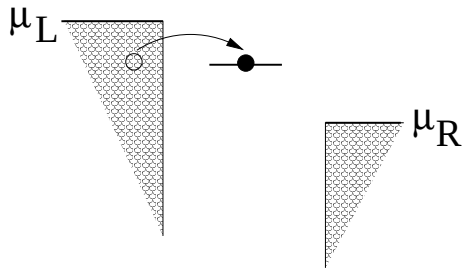

Figure 3.6: *An example for a sequential tunneling process. At finite bias a single electron hop leads to an occupied molecular orbital (level). Double occupancy would be possible only at much larger bias due to the Coulomb repulsion, although the level is already in the bias window defined by the chemical potentials.*

For a weak coupling situation considered here, the quantized charge e therefore leads to a gap due to the charging energy, blocking the transport through the island. Applying

methods that work well in a strong coupling picture (using e.g. mean field theories), an average number of charges is predicted to occupy the island that generally will be a fraction of e. A small but finite current would be the consequence, in contradiction to the blocking effect explained above. An intuitive picture of this blocking can be given when considering the kind of processes being dominant in the weak coupling regime. In Fig. 3.6 an example is given for such an incoherent single electron hop on a molecular orbital. Here, a finite bias situation is indicated, where a sequential tunneling process from the left reservoirs leads to an occupied orbital. Another hop into the right reservoir would be allowed next, but double occupancy is forbidden for sufficiently large Coulomb interaction.

Assuming the single level to lie below the equilibrium Fermi energy and considering an arbitrary small bias voltage, the ground state will be a singly occupied one. Transport will be suppressed exponentially unless the bias is sufficient to further charge (or uncharge) the system.

3.1.3 Why co-tunneling?

The theoretical approaches to the strong and weak coupling limits can be viewed as nearly orthogonal. Whereas transport in the coherent transport picture is dominated by the contact, it is dominated by the interactions on the molecule in the tunneling transport picture. As we have seen in the last chapter, the presence and relevance of interaction effects is quite probable in quantum dots as well as molecules. On the other hand, an extremely weak coupling situation (e.g. as often studied in experiments with quantum dots), can not be guaranteed to be present in experiments with molecules, but a strong coupling scenario is doubtful as well. A theory taking into account dynamic interaction effects, while describing an intermediate coupling regime might be the adequate candidate to describe transport through molecular devices.

An intermediate coupling regime can be described theoretically by considering higher order contributions (second order in Γ) in tunneling processes. An example of such co-tunneling processes is given in Fig. 3.7. An initially unoccupied orbital can be charged with an electron and uncharged again, thus allowing an electron to cross the molecule via a virtual intermediate state. The same can happen for a hole with an occupied state. Since for such processes no energy is needed, they take place even at arbitrarily small bias voltage. Processes that excite the molecule leading an electron effectively into an energetically higher lying orbital, are possible at larger bias, corresponding to energy difference. The first kind of processes are called elastic co-tunneling processes (left side of Fig. 3.7) and the others inelastic co-tunneling processes (right side of Fig. 3.7). The co-tunneling processes will dominate in the Coulomb blockade regime, where the first order, sequential tunneling processes are exponentially suppressed. Current in the

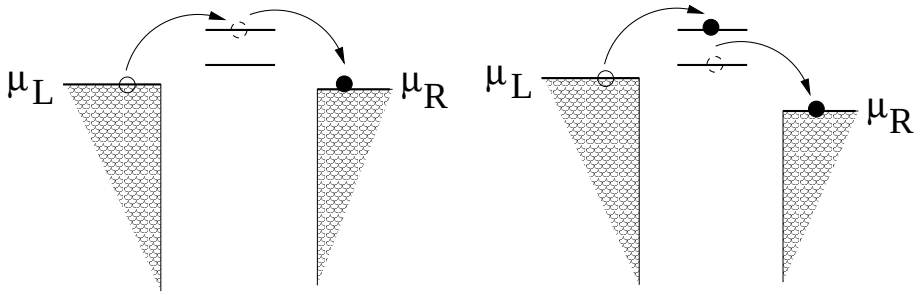

Figure 3.7: *An example for an elastic (left side) and an inelastic (right side) co-tunneling process. Even at arbitrary small bias, tunneling into the right reservoir is possible via a virtual intermediate state. Elastic processes can occur even at vanishing bias, since they do not require any energy. Inelastic processes require an energy, corresponding to the difference of the two energy levels and take place at the corresponding bias.*

co-tunneling regime has been calculated in Refs. [123, 124, 125, 126], for example. The reasons *why co-tunneling* is interesting or relevant to be studied in transport through molecules and quantum dots can be answered now.

First, in comparison to much better controlled quantum dot structures (which provide the possibility to test theoretical predictions with experimental results), co-tunneling current and shot noise may adequately describe realistic transport situations in molecular devices.

Second, co-tunneling effects dominate in the *Coulomb-blockade* regime, where 'orthodox theory' fails to describe the physics of transport. Since shot noise is more sensitive to various processes, we expect promising information can be extracted from the noise or Fano factor. But even in the regime of finite transport, under certain conditions, higher order tunneling effects may become important. This will be the case, e.g. when *asymmetric coupling* parameters suppresses sequential tunneling, whereas co-tunneling processes can still occur.

Third, even the behavior of transport at bias voltages around the excitation energies, might be altered, as the interplay of first and second order processes leads to *step structures* in the current and noise characteristics, which can provide further information on system parameters.

Last, the additional consideration of co-tunneling processes provides a complete picture of transport being applicable to the whole bias regime. While of no consequence in itself, it is one of the intellectually most satisfying points of this work to have achieved this.

3.2 Hamiltonian

For the description of the transport through a nanoscale island like a quantum dot or a molecule, we consider a generalized Anderson impurity model. In order to keep our discussion as clear as possible, we will limit ourselves to the language of quantum dots in the following. The standard Hamiltonian can be written as $H = H_0 + H_\mathrm{T}$, where H_0 describes the decoupled system and H_T the tunneling between the leads and the island. The decoupled system consists of noninteracting electrons in the left (L) and right (R) leads (in general $r = \mathrm{L}, \mathrm{R}$) and interacting electrons in the dot (D)

$$H_0 = H_\mathrm{L} + H_\mathrm{R} + H_\mathrm{D}, \tag{3.3}$$

with

$$H_r = \sum_{k\sigma} \varepsilon_{k\sigma r} a^\dagger_{k\sigma r} a_{k\sigma r} \tag{3.4}$$

and

$$H_\mathrm{D} = \left(\sum_{ij\sigma} \varepsilon_{ij\sigma} c^\dagger_{i\sigma} c_{j\sigma} + \sum_{ijkl\sigma\sigma'} V_{ijkl} c^\dagger_{i\sigma} c^\dagger_{j\sigma'} c_{k\sigma'} c_{l\sigma} \right). \tag{3.5}$$

The Fermi operators $a^\dagger_{k\sigma r}, (a_{k\sigma r})$ and $c^\dagger_{i\sigma}, (c_{i\sigma})$ create (annihilate) electrons in the electrodes and the dot. The energy of the electrons in the reservoirs and the dot are $\varepsilon_{k\sigma r}$ (with wave vector k) and $\varepsilon_{ij\sigma}$. The two-particle operator in H_D, allowing to consider interaction effects, has its most general form with elements V_{ijkl}. The indices $i, j, k, l = 1 \ldots N$ are due to N dot-levels and σ describes the spin state (spin $\downarrow$ or $\uparrow$). For appropriate choices of these elements capacitive effects with a charging energy as well as Coulomb interaction effects for double occupancy of electronic levels can be described. This allows for a study of models like the Anderson impurity model, the Hubbard model and others.

Tunneling between the leads and the quantum dot levels is modeled by

$$H_{\mathrm{T},r} = \sum_{ik\sigma} \left(t^{kr}_{i\sigma} a^\dagger_{k\sigma r} c_{i\sigma} + h.c. \right) \tag{3.6}$$

with $H_\mathrm{T} = \sum_r H_{\mathrm{T},r}$ and $t^{kr}_{i\sigma}$ being the tunneling matrix elements. These parameters describe the coupling of the dot system to the electronic environment and hence lead to a finite lifetime τ of the dot states, which in turn defines an intrinsic level broadening (line width) $\Gamma = \hbar/\tau$. The coupling strength to the reservoirs is related to these amplitudes via

$$\Gamma^{i\sigma}_r(\omega) = \frac{2\pi}{\hbar} \sum_k |t^{kr}_{i\sigma}|^2 \delta(\omega - \varepsilon_{kr}), \tag{3.7}$$

which is obtained from golden-rule arguments. Assuming a constant density of states in the two electrodes and tunneling elements independent of k, we obtain the energy independent coupling $\Gamma_r^{i\sigma} = 2\pi|t_{i\sigma}^r|^2\rho_e$.

So far, we have specified a model allowing for a transport description through a small island with an arbitrary complex electronic structure. If we want to include further effects like vibration, relaxation, etc. effects we may couple additionally to a bosonic bath (e.g. of photons or phonons).

We therefore add a Hamiltonian

$$H_{\mathrm{B}} = \sum_q \omega_q d_q^\dagger d_q \tag{3.8}$$

and

$$H_{\mathrm{B-D}} = \sum_{q\sigma ij} g_q^{ij}(d_q^\dagger + d_q)c_{i\sigma}^\dagger c_{j\sigma} \tag{3.9}$$

where $d_q^\dagger, d_q$ are the corresponding Bose operators. The term H_{B} describes the unperturbed boson bath (with wave vector q) and $H_{\mathrm{B-D}}$ the interaction with the dot structure, where a coupling is given by constants g_q^{ij}. Charge relaxation and excitation due to bosons is given for $i \neq j$, whereas "boson-assisted tunneling" is described when choosing $i = j$. [Such a diagonal term would lead to additional steps in the I-V when the boson bath has a discrete spectrum [127, 128, 129].] Analogously to the fermionic coupling strength we define a coupling

$$\alpha_{ij}(\omega) = \frac{2\pi}{\hbar}\sum_q |g_q^{i,j}|^2\delta(\omega - \omega_q), \tag{3.10}$$

where again we assume the amplitudes g^{ij} to be independent of q. This allows us to rewrite $\alpha_{ij}(\omega) = 2\pi|g^{ij}|^2\rho_{\mathrm{b}}(\omega)$, with $\rho_{\mathrm{b}}(\omega)$ being the density of states of the bosonic bath.

In chapter 4 we will discuss various models which are special choices of the general Hamiltonian presented here. A further specification of the various coupling constants will be made as well. However, our theory can deal with its general form. All transport properties of interest are expressed in terms of self-energy diagrams (transition rates) which are calculated via diagrammatic rules. These rules are discussed in Appendix A and account for all features described by the general Hamiltonian $H = H_0 + H_{\mathrm{T}}$. Note, that by inclusion of a bosonic bath we rewrite the Hamiltonian of the decoupled system as $H_0 = H_{\mathrm{L}} + H_{\mathrm{R}} + H_{\mathrm{D}} + H_{\mathrm{B}}$, and the one, containing the parts which are treated perturbatively as $H_{\mathrm{T}} = H_{\mathrm{T}} + H_{\mathrm{B-D}}$.

3.3 Diagrammatic technique

In the following we present a general transport theory which is based on a real-time diagrammatic approach Ref. [129, 130, 131, 132]. The basic idea of the diagrammatic technique is to integrate out all reservoir degrees of freedom and thus end up with a formally exact kinetic equation for the reduced density matrix of the dot states in the quantum dot. The reduced density matrix contains a series of irreducible blocks, which are identified as self-energies or transition rates, and can be calculated straightforward by applying diagrammatic rules (these will be presented in the appendices).

This theory allows to perform a systematic perturbation expansion of the current and shot noise (current noise) or even higher correlators. The great advantage compared to other theories (e.g. non-equilibrium Green functions techniques) is the description of all transport properties in terms of such self-energy diagrams (transition rates), which allow to study systems of higher complexity, such as described by the Hamiltonian introduced before, without additional extensions.

3.3.1 Keldysh contour and Diagrams

We want to calculate the quantum-statistical expectation value of an operator A at time t [133], which is given by

$$\langle A(t)\rangle = Tr(\rho_0 A(t)_H) = Tr(\rho(t)A), \tag{3.11}$$

with $A(t)_H = \exp[iH(t-t_0)]A\exp[-iH(t-t_0)]$ being the operator in the Heisenberg picture with respect to the initial time t_0 and $\rho_0 = \rho(t_0)$. Using permutation under the trace leading to A in the Schrödinger picture, we write the time evolution of the density matrix

$$\rho(t) = \exp[-iH(t-t_0)]\rho(t_0)\exp[iH(t-t_0)], \tag{3.12}$$

which governs all transport properties. If we assume, that the initial density matrix factorizes into parts of the dot D and leads electrons $r = \mathrm{L}, \mathrm{R}$ (fermionic bath), we may write

$$\rho_0 = \rho_0^{\mathrm{D}}\rho_0^{\mathrm{L}}\rho_0^{\mathrm{R}} \qquad \text{or} \qquad \rho_0 = \rho_0^{\mathrm{D}}\rho_0^{\mathrm{L}}\rho_0^{\mathrm{R}}\rho_0^{\mathrm{B}}, \tag{3.13}$$

when coupling additionally to a bosonic bath B. We consider the leads to be large reservoirs of thermally equilibrated noninteracting electrons with fixed chemical potentials μ_r and $\mu_D = 0$. The leads thus can be described by Fermi functions $f_r(\omega)$ and the density matrix reads

$$\rho_0^r = \frac{1}{Z_0^r} e^{-\beta(H_r - \mu_r N_r)}, \tag{3.14}$$

with the inverse temperature $\beta = 1/k_{\mathrm{B}}T$ and the number operator $N_r = \sum_{k\sigma} a^\dagger_{k\sigma r} a_{k\sigma r}$. The normalization factor Z_0^r is determined by $\mathrm{tr}\rho_0^r = 1$. Correspondingly the same can be written for ρ_0^B, with the bosonic free Hamiltonian, describing the bosons by Bose functions $n_b(\omega)$

$$\rho_0^B = \frac{1}{Z_0^B} e^{-\beta_{\mathrm{B}} H_B}. \tag{3.15}$$

The remaining part of the dot electrons is not described by equilibrium reservoirs. We assume, its initial distribution to be diagonal in some basis $|\chi\rangle$, which labels the many-body dot states, and includes all correlations within the island. We write

$$\rho_0^D = \sum_\chi p_\chi^{\mathrm{init}} |\chi\rangle\langle\chi|, \tag{3.16}$$

where probability conservation yields $\sum_\chi p_\chi^{\mathrm{init}} = 1$. In the stationary limit, when long enough time has passed by, such that the system has forgotten its initial distribution, it becomes obvious that physical quantities do not depend on the choice of p_χ^{init}. We denote the initial time t_0 (which later will be shifted to minus infinity), when we adiabatically switch on tunneling between the reservoirs and the dot.

We change to the interaction picture with respect to H_0 and find

$$A(t)_H = \tilde{T}\mathrm{exp}\left(-i\int_t^{t_0} dt' H_{\mathrm{T}}(t')_I\right) A(t)_I T\mathrm{exp}\left(-i\int_{t_0}^{t} dt' H_{\mathrm{T}}(t')_I\right), \tag{3.17}$$

where T and $\tilde{T}$ denote the time and anti-time ordering operators. We further write the integrals as one contour integral over the *Keldysh contour*, where the time t' runs forward from t_0 to t (where the operator A acts) and then backwards from t to t_0. This yields

$$\langle A(t)\rangle = \mathrm{tr}\left[\rho_0 T_K \mathrm{exp}\left(-i\int_K dt' H_{\mathrm{T}}(t')_I\right) A(t)_I\right], \tag{3.18}$$

where we introduced the Keldysh time-ordering operator T_K, which orders all following operators along the Keldysh contour, such that the one with the later time along the contour appears at a further right position. In a diagrammatic language, the Keldysh contour is represented by horizontal lines running from the left to the right (upper) and then back to the left (lower), as illustrated in Fig. 3.8 (details to be explained in the following). Since the time now labels the physical time and additionally the information, on which part of the contour the corresponding operator lies, we can understand such diagrams (as Fig. 3.8) as real-time expansions of the reduced dot system.

This becomes more transparent, when we further manipulate Eq. 3.18 to

$$\langle A(t)\rangle = \sum_{\chi} p_{\chi}^{\text{init}} \langle\chi|\Pi A(t)_I|\chi\rangle, \tag{3.19}$$

where we summarized

$$\Pi = \text{tr}_\text{L}\text{tr}_\text{R}\text{tr}_\text{B}\left[\rho_0^L\rho_0^R\rho_0^B T_K \text{exp}\left(-i\int\limits_K dt' H_\text{T}(t')_I\right)\right]. \tag{3.20}$$

and inserted the above defined initial density matrix. When expanding the exponential in Eq. 3.20, we get

$$T_K \text{exp}\left(-i\int\limits_K dt' H_\text{T}(t')_I\right) = \tag{3.21}$$
$$\sum_{m=0}^{\infty}(-i)^m \int\limits_K dt_1 \int\limits_K^{t_1>t_2>...>t_m} dt_2 ... \int\limits_K dt_m \; T_K[H_T(t_1)_I H_T(t_2)_I ... H_T(t_m)_I] \quad .$$

The following points need to be made:

1) The Keldysh time-ordering operator in Eqs. 3.19 with 3.20 acts on all operators on the right, including A, which puts this operator in infinite many possible configurations (between the tunneling Hamiltonians) on different positions in time, located on the Keldysh contour. Both types of operators H_T and A are diagrammatically represented by vertices (see Fig. 3.8), which are either *internal* (for H_T) or *external* (for A) ones.

2) Instead of only one external vertex, there may also be arbitrary many vertices A_i (with $i = 1..n$), describing the n-th correlator (here we describe the situation with $n = 1$). As an example, the second correlator with $n = 2$ is required to describe the shot noise, as discussed in the following. Again, each of these operators will have to be placed at all possible positions between the tunneling Hamiltonians.

3) All operators H_T and A (i.e. for A representing the current operator) contain combinations of dot and reservoir operators ($c_{i\sigma}, a_{k\sigma r}, d_q$ and the creation operators respectively). The only part of the system, which is not in equilibrium is the dot. The reservoir operators can be separated therefore from the dot operators (this will give a sign due to exchanging operators) and contracted into pairs by applying Wick's theorem. Wick's theorem in this case holds, since the Hamiltonian H_0 is bilinear in the operators of the reservoirs. Contractions between pairs of field operators are included from H_T as well as from A in general. This allows to integrate out the reservoirs degrees of freedom leading to Fermi and Bose functions. For the dot operators, the Schrödinger equation has to be solved exactly. These operators act on the many-body dot states.

4) Thus Eq. 3.20 (without external vertices) can be understood as the reduced propagator of the dot system, which describes time evolution of the system via coupling to the reservoirs.

Another way to write down the matrix elements, describing the non-equilibrium time evolution of the density matrix from dot state χ_1 at time t_0 forward to state χ_1' at time t and then backward from χ_2' to χ_2 is

$$\Pi^{\chi_1,\chi_1'}_{\chi_2,\chi_2'} = \langle\chi_2|\left[\Pi(|\chi_2'\rangle\langle\chi_1'|)(t)_I\right]|\chi_1\rangle = \tag{3.22}$$
$$\mathrm{tr_L tr_R tr_B}\left[\langle\chi_2|\tilde{T}\mathrm{exp}\left(-i\int_t^{t_0} dt' H_\mathrm{T}(t')_I\right)|\chi_2'\rangle\langle\chi_1'|T\mathrm{exp}\left(-i\int_{t_0}^{t} dt' H_\mathrm{T}(t')_I\right)|\chi_1\rangle\right]$$

This allows us to understand Fig. 3.8, which visualizes the propagation. The upper and lower lines describe the forward and backward time propagation along the contour, where tunneling vertices, H_T, change the many-body dot states χ, which are indicated in our example for a single level system with states empty (0), spin $\uparrow$, spin $\downarrow$ or doubly occupied. The vertices are connected in pairs (Wick's theorem) by tunneling lines, corresponding to reservoirs $r = \mathrm{L}, \mathrm{R}$. Since with each vertex a tunneling amplitude t can be associated, a tunneling line will provide a factor $\Gamma \propto |t|^2$.

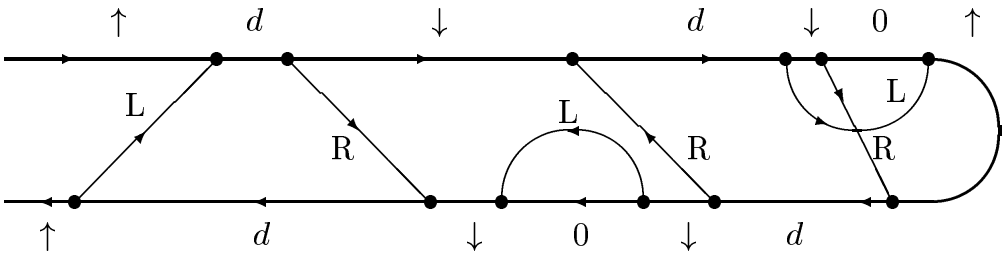

Figure 3.8: *An example for the time evolution of the reduced density matrix. The upper and lower line represent the forward and backward time propagation along the Keldysh contour, respectively. Tunneling lines correspond to the reservoirs* L, R *connecting pairs of vertices. The resulting changes between the dot states are indicated (here four different, as would be relevant for a single level model).*

For the following discussion, we assume the reduced density matrix to be diagonal ($\chi_1 = \chi_2 = \chi$ and $\chi_1' = \chi_2' = \chi'$). For the case of the Anderson model, e.g. conservation of spin and transverse channel number guarantee that the reduced density matrix stays diagonal for all time, although it is not necessarily the case in general. The general case of a non-diagonal density matrix will be discussed in chapter 3.8.

Considering the different kinds of tunneling lines in Fig. 3.8, we see, that doing a vertical cut at a certain time, we may either cut zero, one, two, ... up to infinitely

many tunneling lines. This allows us to rewrite the full propagation as a sequence of irreducible blocks (self-energy) $W_{\chi'\chi}(t',t)$ containing one or more tunneling lines. They are associated with transitions from state χ at time t to state χ' at time t'. Parts without tunneling lines describe a free propagation and are written as $\mathbf{\Pi^{(0)}} = \mathbf{1}$ for the diagonal density matrix. This leads to the Dyson equation for the propagator

$$\mathbf{\Pi}(t',t) = \mathbf{1} + \int_t^{t'} dt_2 \int_t^{t_2} dt_1 \, \mathbf{W}(t_2,t_1)\mathbf{\Pi}(t_1,t) \tag{3.23}$$

where the bold face indicates matrix notation related to the dot state labels (for N states $\chi = 1..N$ this defines a $N \otimes N$ matrix). To be more general we use a time t instead of t_0, which is associated with the initial time. Additionally, since in matrix notation we read from right to left, the order of times is the other way around, compared to the diagrammatical representation. Eq. 3.23 is illustrated in Fig. 3.9.

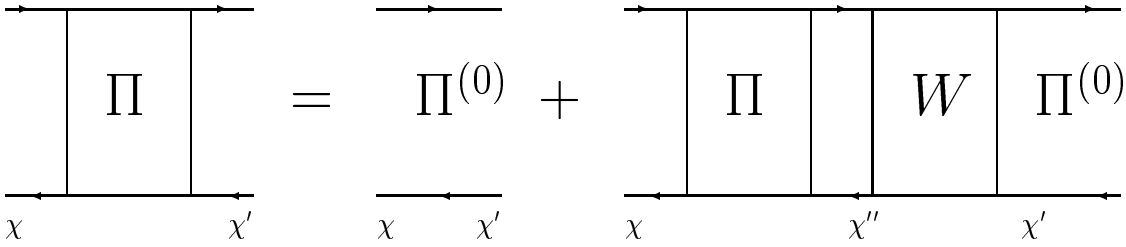

Figure 3.9: *Illustration of the Dyson equation, which describes an infinite series of irreducible self energy diagrams* $\mathbf{W}$ *interrupted by free propagators* $\mathbf{\Pi^{(0)}}$*. The full propagator* $\mathbf{\Pi}$ *thus describes a reducible diagram.*

For the irreducible blocks, containing one or more tunneling lines, an illustrative example is shown in Fig. 3.10. The simplest diagram containing one tunneling line describes the transition from a state with spin $\uparrow$ into a doubly occupied state, via an electron hopping onto the dot out of the left reservoir. Since the tunneling line provides a factor Γ, the process describes a first order, sequential tunneling process. A co-tunneling process described by two tunneling lines respectively, is shown as well. Higher order contributions ($k > 2$) in a perturbative expansion of the coupling strength are described diagrammatically by blocks containing more tunneling lines. In general we can write $\mathbf{W} = \sum_{k=1}^{\infty} \mathbf{W}^{(k)}$.

Note that diagrams with k lines may contain 0 to k tunneling lines and k to 0 boson lines. This is trivial in lowest order (since only diagrams with either one tunneling or one boson line appear) but for higher order contributions (e.g. second order) this means, that two tunneling lines, one tunneling and one boson line or two boson lines may be present. All kinds of diagrams have to be regarded.

As discussed above, k Fermi or Bose functions, together with k couplings $\Gamma_r^{i\sigma}$ and α_{ij} will appear, describing the structure of the tunneling and boson lines. The $2k$ integrals over times (associated with vertices) can be reduced to $(2k-1)$, when choosing the final time to be zero. Propagation between different times $t-t'$ is described by an exponential $\exp[-i\varepsilon_\chi(t-t')]$ with the dot state χ, being realized between two vertices. Changing from time space to energy space, via a Laplace transform, we obtain $(2k-1)$ resolvents of the kind $1/(-i\varepsilon_\chi+\eta)$, where $\eta \to 0^+$ is a convergence factor, and accounts for an adiabatic switching on of the perturbation H_T. At the end k integrations due to the number of lines remain to be carried out over the combined functions (see also the discussion of diagrammatic rules in time and energy space in appendix A).

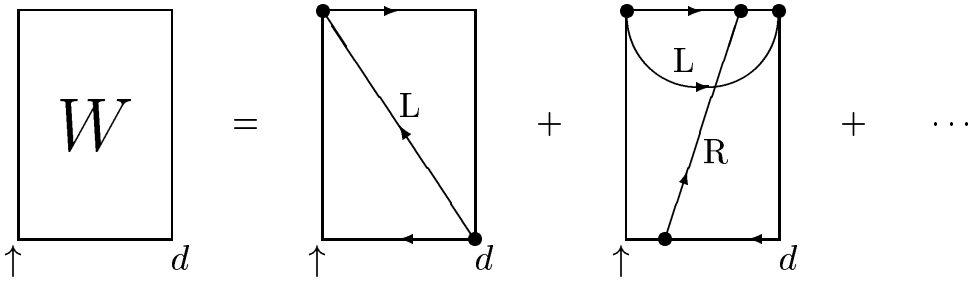

Figure 3.10: *An example of an irreducible self-energy diagram with one, two, etc. tunneling lines, connecting the dot with reservoirs* $r = \mathrm{L}, \mathrm{R}$. *The number of tunneling lines is directly related to the order of* Γ *in a perturbation expansion.*

A crucial point, which simplifies calculations, is the use of symmetries, allowing to reduce the number of diagrams tremendously until finally only really topologically different diagrams remain. One example is the fact, that when changing all directions of lines in a diagram and reflecting it horizontally, the complex conjugated is obtained. This is known as the *mirror rule*. Another example is, that when changing the position of the rightmost vertex H_T in a diagram from the upper to the lower branch of the contour (or vice versa), the sign of the diagram changes. This can be summarized in the *sum rule* $\sum_{\chi'} W_{\chi'\chi} = 0$.

Since this is not the place to go into further details, we refer to Refs. [129, 130, 131, 132], where the rates $\mathbf{W}$ are exactly related to self-energies $\mathbf{\Sigma}$ via $\Sigma_{\chi\chi'} = iW_{\chi'\chi}$. The reason for our new choice is the desire to use purely real objects (the rates Σ are mostly purely imaginary), making an interpretation as transition rates more transparent.

So far, we have developed an approach to determine the self-energies diagrammatically in a straightforward way. If all transport properties (e.g. current, shot noise, etc.) we are interested in can be expressed in terms of diagrams $\mathbf{W}$, it will be a question of book keeping only to calculate all contributions.

3.3.2 Master equation and stationary probabilities

When taking the long-time limit, i.e. time differences $t' - t$ larger than the relaxation time the system approaches the stationary state. It is obvious that the propagator Eq. 3.23 itself must become stationary, i.e. a constant in time. Thus we have

$$\lim_{t_0 \to -\infty} \mathbf{\Pi}(t' - t_0) = \mathbf{p}^{\mathrm{st}} \otimes \mathbf{e}^T, \tag{3.24}$$

where $\mathbf{e}^T = (1, .., 1)$, and $\mathbf{p}^{\mathrm{st}}$ is the vector of the stationary probabilities of the dot, independent of t' . $\mathbf{p}^{\mathrm{st}}$ describes the probabilities of the dot to occupy the possible quantum states χ. Eq. 3.24 can be obtained by taking the derivative of Eq. (3.23) with respect to t' and setting the derivative to zero, corresponding to the stationary state. An arbitrary initial state $\mathbf{p}^{\mathrm{init}} = \lim_{t_0 \to -\infty} \mathbf{p}(t_0)$ will develop always into the same stationary state $\lim_{t_0 \to -\infty} \mathbf{\Pi}(0, t_0)\mathbf{p}(t_0) = \mathbf{p}^{\mathrm{st}}$.

To obtain an equation to determine the stationary probabilities $\mathbf{p}^{\mathrm{st}}$ we first introduce the Laplace transform of the transition rates $\mathbf{W}(z) = \hbar \int_{-\infty}^{0} dt e^{zt} \mathbf{W}(0, t)$ with the definition $\mathbf{W} = \mathbf{W}(z)|_{z=0^+}$. From Eq. (3.23) we find

$$\mathbf{W}\mathbf{p}^{\mathrm{st}} = \mathbf{0}, \tag{3.25}$$

independent of the initial density matrix (since $\mathbf{e}^T \mathbf{p}^{\mathrm{init}} = \mathbf{1}$ because of the probability conservation). As $\mathbf{W}$ has a zero eigenvalue, it cannot be inverted (remember the sum rule $\mathbf{e}^T \mathbf{W} = \mathbf{0}$). With the normalization condition $\mathbf{e}^T \mathbf{p}^{\mathrm{st}} = 1$ we obtain the stationary probabilities $\mathbf{p}^{\mathrm{st}}$ by solving

$$\tilde{\mathbf{W}}\mathbf{p}^{\mathrm{st}} = \mathbf{v}, \tag{3.26}$$

where $\tilde{\mathbf{W}}$ is identical to $\mathbf{W}$ but with one (arbitrarily chosen) row χ_0 being replaced by $(\Gamma, .., \Gamma)$ and $\mathbf{v}$ defined by $v_\chi = \Gamma \delta_{\chi\chi_0}$.

For a well-defined perturbation expansion in powers k of the coupling strength Γ we write $\mathbf{W} = \sum_{k=1}^{\infty} \mathbf{W}^{(k)}$, $\tilde{\mathbf{W}} = \sum_{k=1}^{\infty} \tilde{\mathbf{W}}^{(k)}$, and $\mathbf{p}^{\mathrm{st}} = \sum_{k=0}^{\infty} \mathbf{p}^{\mathrm{st}(k)}$. Since the order in Γ corresponds to the number of tunneling lines contained in the irreducible blocks, $\mathbf{W}$ and $\tilde{\mathbf{W}}$ start with first order in Γ, whereas $\mathbf{p}^{\mathrm{st}}$ starts in zeroth order. The zeroth-order stationary probabilities are

$$\mathbf{p}^{\mathrm{st}(0)} = (\tilde{\mathbf{W}}^{(1)})^{-1} \mathbf{v}, \tag{3.27}$$

and higher-order corrections are obtained iteratively by

$$\mathbf{p}^{\mathrm{st}(k)} = -\left(\tilde{\mathbf{W}}^{(1)}\right)^{-1} \sum_{m=0}^{k-1} \tilde{\mathbf{W}}^{(k-m+1)} \mathbf{p}^{\mathrm{st}(m)}, \tag{3.28}$$

for $k = 1, 2, \ldots$. The stationary probabilities are thus expressed in terms of blocks $\mathbf{W}^{(k)}$, which are calculated diagrammatically.

3.4 Current

The current flowing through the barriers $r = \mathrm{L}, \mathrm{R}$ is defined by the current operator

$$\hat{I}_r(t) = -e\frac{d}{dt}N_r(t), \tag{3.29}$$

where the time dependence of dot number operator $N_r(t)$ in the Heisenberg picture is given by the equation of motion $\frac{d}{dt}N_r(t)_H = i[H, N_r](t)_H = i[H_T, N_r](t)_H$, which leads to

$$\hat{I}_r(t) = -i(e/\hbar)\sum_{ik\sigma}\left(t^{kr}_{i\sigma}(a^\dagger_{k\sigma r}c_{i\sigma})(t) - h.c.\right). \tag{3.30}$$

In order to describe transport, a finite bias voltage enters the difference of the electrochemical potentials μ_r for the left and right leads. For the current we use $\hat{I}$ in order to distinguish from the expectation value $I = \langle\hat{I}\rangle$. We furthermore define a symmetrized notation $\hat{I} = (\hat{I}_\mathrm{R} - \hat{I}_\mathrm{L})/2$, which will enable a compact description of the noise and facilitates an easier calculation when using the diagrammatic technique. Of course, we could write also $\hat{I} = \hat{I}_\mathrm{R} = -\hat{I}_\mathrm{L}$, which holds due to the continuity equation.

The current operator eq. 3.30 represents a possible choice of an operator A, as introduced in section 3.3.1. For a diagrammatic representation of the current, we introduce a block $\mathbf{W}^I$, in which one (internal) tunneling vertex due to $H_{\mathrm{T,r}}$ is replaced by an (external) one due to $\hat{I}_r$. This leads to additional diagrammatic rules, accounting for prefactors and signs, which are given in appendix A. The diagrammatic approach now allows for a visualization of the different expressions we will encounter (see Fig. 3.11). The objects are indicated here in the order as they appear in the formulas due to matrix notation.

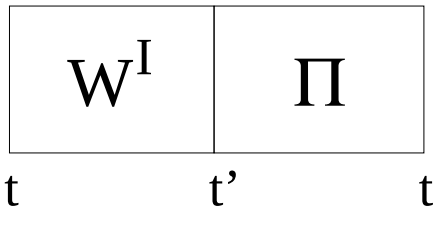

Figure 3.11: *Visualization of the blocks contributing to the current. For $t_0 \to -\infty$ and turning to the energy representation, the blocks take the form $\mathbf{W}^I\mathbf{p}^{\mathrm{st}} \otimes \mathbf{e}^T$.*

The current (expectation value) in time-representation is written as

$$I(t) = \lim_{t_0\to-\infty}\left[\frac{e}{2\hbar}\int_{t_0}^{t} dt'\mathbf{e}^T\hbar\mathbf{W}^I(t,t')\mathbf{\Pi}(t',t_0)\mathbf{p}(t_0)\right] \tag{3.31}$$

In the limit $t_0 \to -\infty$ we are free to chose $I(t) = I(0) = I$. However, in our discussion of the shot noise (next section), we will have to manipulate expressions while keeping t_0 at a finite value. If a sequence of transition rates $\mathbf{W}^I$ interrupted by propagators $\mathbf{\Pi}$ is considered, one has to take care of the exact time ordering of the objects. An exact treatment is possible only, if the time t_0 is taken to be finite until this has been achieved.

For the current this is uncritical, since as $t_0 \to -\infty$ the propagator in Eq. 3.31 leads to time-independent stationary states, such that the Laplace transform of the only remaining object $\mathbf{W}^I(t, t')$ can be performed, choosing $t = 0$ because of time-translational invariance. Hence, for the *current* we find

$$I = \frac{e}{2\hbar}\mathbf{e}^T\mathbf{W}^I\mathbf{p}^{\mathrm{st}} \tag{3.32}$$

where we used $\mathbf{e}^T\mathbf{p}^{\mathrm{init}} = 1$ again. Expanding this expression order by order in the coupling strength Γ, we obtain

$$I^{(k)} = \frac{e}{2\hbar}\mathbf{e}^T\sum_{m=0}^{k-1}\mathbf{W}^{I(k-m)}\mathbf{p}^{\mathrm{st}(m)} \tag{3.33}$$

for $k = 1, 2, \ldots$, and the total current is $I = \sum_{k=1}^{\infty} I^{(k)}$. The factor $1/2$ corrects for double counting of the current vertex being on the upper and lower branch of the Keldysh contour. Since the stationary probabilities are expressed in terms of irreducible blocks $\mathbf{W}^{(k)}$, the current is expressed by rates $\mathbf{W}^{(k)}$ and $\mathbf{W}^{I(k)}$ only.

In first order the current reads

$$I^{(1)} = \frac{e}{2\hbar}\mathbf{e}^T\mathbf{W}^{I(1)}\mathbf{p}^{\mathrm{st}(0)}, \tag{3.34}$$

and in the second order corrections

$$I^{(2)} = \frac{e}{2\hbar}\mathbf{e}^T(\mathbf{W}^{I(2)}\mathbf{p}^{\mathrm{st}(0)} + \mathbf{W}^{I(1)}\mathbf{p}^{\mathrm{st}(1)}). \tag{3.35}$$

We will present results in the next chapter, which have been derived by calculations up to second order, with a current $I = I^{(1)} + I^{(2)}$. The stationary probabilities needed to compute the current up to second order are determined from Eqs. 3.27 and 3.28. The only task remaining is the calculation of rates $\mathbf{W}^{(1)}, \mathbf{W}^{I(1)}$ in first and $\mathbf{W}^{(2)}, \mathbf{W}^{I(2)}$ in second order.

An equivalent expression to Eq. 3.32 in terms of self-energies $\mathbf{\Sigma}$ has been derived in Ref. [132]. It has been shown there that the current can be expressed in terms of greater and lesser single-particle Green functions $(C^{>}, C^{<})$ as well, which again is equivalent to the current formula derived in a non-equilibrium Green's function formalism in Ref. [22]. We will explain later, why there is no trivial extension of this to the shot noise, where two-particle Green functions appear.

3.5 Zero frequency shot noise

We want to expand the diagrammatic approach to describe the *shot noise*, which is related to the current-current correlations in time. When taking the zero frequency limit of the definition from chapter 2.1, we find

$$S = \int_{-\infty}^{\infty} dt \langle \delta\hat{I}(t)\delta\hat{I}(0) + \delta\hat{I}(0)\delta\hat{I}(t)\rangle, \tag{3.36}$$

with $\delta\hat{I}(t) = \hat{I}(t) - \langle\hat{I}\rangle$, which we expand to

$$S = 2\int_{-\infty}^{0} dt \left[\langle\hat{I}(t)\hat{I}(0) + \hat{I}(0)\hat{I}(t)\rangle - 2\langle\hat{I}\rangle^2\right]. \tag{3.37}$$

Due to our symmetrized definition of the current, a compact description of the noise is possible, which consists of the parts $S = (S_{\mathrm{LL}} + S_{\mathrm{RR}} - S_{\mathrm{LR}} - S_{\mathrm{RL}})/4$. This summation is hidden in the diagrammatic rules, which account for the different pre-factors.

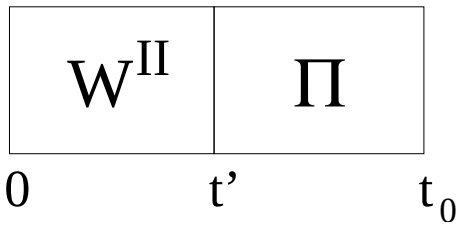

Figure 3.12: *Visualization of irreducible current-current contributing to the noise. For $t_0 \to -\infty$ and turning to the energy representation, the contribution takes the form $\mathbf{W}^{II}\mathbf{p}^{\mathrm{st}} \otimes \mathbf{e}^T$.*

The shot noise involves expectation values of two current operators which either appear both in a single irreducible block, which we denote by $\mathbf{W}^{II}$, or in two different blocks $\mathbf{W}^{I}$. In analogy to the current, the first part of the noise (with both current vertices in one irreducible block) is found to be

$$S_{II} = \lim_{t_0\to-\infty}\left[\frac{e^2}{\hbar}\int_{t_0}^{0} dt' \mathbf{e}^T\hbar\mathbf{W}^{II}(0,t')\mathbf{\Pi}(t',t_0)\mathbf{p}(t_0)\right] \tag{3.38}$$

where the factor 2 in the above definition has canceled against the correction factor 1/2 for double counting. This expression is visualized in Fig. 3.12 containing a block $\mathbf{W}^{II}$. The external integration from Eq. (3.37) is taken over the time t at which the second current operator acts. As the time t is earlier than the time 0 this leads to the

possibility of arbitrary positions of one current vertex within the block $\mathbf{W}^{II}$. In energy representation (Laplace transform) we find

$$S_{II} = \frac{e^2}{\hbar}\mathbf{e}^T\mathbf{W}^{II}\mathbf{p}^{\rm st} \tag{3.39}$$

The other part of the noise contains current vertices in two different blocks $\mathbf{W}^I$ as visualized in Fig. 3.13. [We note here that the factor 2 from the noise definition

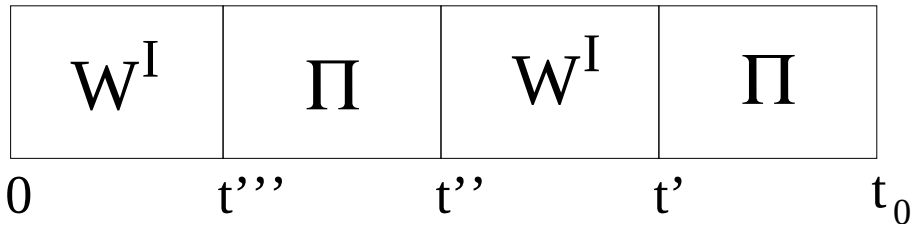

Figure 3.13: *Visualization of the blocks contributing to the noise part $S_{I\Pi I}$. The propagator between times t''' and t'' takes the stationary form $\mathbf{p}^{\rm st}\otimes\mathbf{e}^T$ in the long time limit. Thus the integration over t'' leads to a divergence.*

cancels only once, since for the second object $\mathbf{W}^I$ acting on the propagator in Eq. 3.40 all positions of the current vertex have to be considered (no double counting).] The propagator $\mathbf{\Pi}(t''',t'')$ in Eq. 3.40 will approach $\mathbf{p}^{\rm st}\otimes\mathbf{e}^T$ in the long-time limit. As we have to integrate over the time t'', we find this expression to be divergent. We write the term corresponding to Fig. 3.13 as

$$S_{I\Pi I} = \tag{3.40}$$
$$\lim_{t_0\to-\infty}\left[\frac{e^2}{\hbar}\int_{t_0}^{0}dt'''\mathbf{e}^T\hbar\mathbf{W}^I(0,t''')\int_{t_0}^{t'''}dt''\frac{1}{\hbar}\mathbf{\Pi}(t''',t'')\int_{t_0}^{t''}dt'\hbar\mathbf{W}^I(t'',t')\mathbf{\Pi}(t',t_0)\mathbf{p}(t_0)\right].$$

On the other hand, we find from Eq. 3.37 that we still have to subtract the part $S_{I^2} = -4\int_{-\infty}^{0}dt\langle\hat{I}(0)\rangle\langle\hat{I}(t)\rangle$ which also diverges (being an infinite integral over a constant). The two divergencies must cancel in the final expression for the shot noise. Our following manipulations will show that they indeed do cancel. Inserting Eq. 3.31 at the different times we may rewrite this part as

$$S_{I^2} = \tag{3.41}$$
$$-4\lim_{t_0\to-\infty}\int_{t_0}^{0}dt\left[\frac{e^2}{4\hbar^2}\mathbf{e}^T\int_{t_0}^{0}dt'''\hbar\mathbf{W}^I(0,t''')\mathbf{\Pi}(t''',t_0)\mathbf{p}(t_0)\mathbf{e}^T\int_{t_0}^{t}dt'\hbar\mathbf{W}^I(t,t')\mathbf{\Pi}(t',t_0)\mathbf{p}(t_0)\right]$$

Now Eq. 3.41 is manipulated as follows: we rename $t\to t''$ and split the domain of the integral, $\int_{t_0}^{0}dt''\to\int_{t_0}^{t'''}dt''+\int_{t'''}^{0}dt''$. As we will later let $t_0\to-\infty$ we can also use

$\mathbf{\Pi}(t''', t_0)\mathbf{p}(t_0)\mathbf{e}^T \to \mathbf{\Pi}(t''', t_0)$ in the middle of Eq. 3.41. Forming the sum of Eq. 3.40 and the first part of the t'' integral $\int_{t_0}^{t'''} dt''$ of Eq. 3.41, we encounter an object

$$\mathbf{P}(t''', t_0) = \int_{t_0}^{t'''} dt'' \, \frac{1}{\hbar} \left[\mathbf{\Pi}(t''', t'') - \mathbf{\Pi}(t''', t_0) \right] \tag{3.42}$$

that in the limit $t_0 \to -\infty$ (and by setting $t''' = 0$) is recognized as another Laplace transform, which we denote by $\mathbf{P}$. $\mathbf{P}$ might be called a "decaying" propagator, as it has the stationary part of the propagator, i.e. the part that does not decay as $t_0 \to -\infty$, subtracted. Due to time-translational invariance the times t'' and t''' in the objects $\mathbf{W}^I(t'', t')$ and $\mathbf{P}(t''', -\infty)$ can be set to zero allowing for the Laplace transformation. The idea is to start taking the limit $t_0 \to -\infty$ at the right side of the expressions leading to time independent stationary probabilities. The whole sequence of objects can be shifted in time, since the internal time ordering of the objects is maintained. Therefore, the Laplace transformation can be taken for one object after the other until we obtain a term in the form

$$\sim \mathbf{e}^T \mathbf{W}^I \mathbf{P} \mathbf{W}^I \mathbf{p}^{\mathrm{st}}.$$

The second part of the time integral $\int_{t'''}^{0} dt''$ of Eq. 3.41 simply evaluates to $-t'''$. The t''' integral also contains $\mathbf{W}^I(0, t''')\mathbf{\Pi}(t''', t_0)$. In the limit $t_0 \to -\infty$ the propagator $\mathbf{\Pi}(t''', t_0)$ approaches the stationary probabilities $\mathbf{p}^{\mathrm{st}}$, and therefore can be considered independent of t'''. The remaining integral over t''' reads $\hbar \int_{t_0}^{0} dt''' t''' \mathbf{W}^I(0, t''')$ (a minus sign canceled with the minus sign in front of Eq. 3.41). In the limit $t_0 \to -\infty$ this expression is written as the derivative of the Laplace transform $\mathbf{W}^I(z) = \hbar \int_{-\infty}^{0} dt e^{zt} \mathbf{W}^I(0, t)$ as $\partial \mathbf{W}^I = \left(\partial \mathbf{W}^I(z)/\partial z \right) |_{z=0^+}$. The t' integral of Eq. 3.41 has been untouched and evaluates to $\mathbf{e}^T \mathbf{W}^I \mathbf{p}^{\mathrm{st}} = \langle I \rangle$. Collecting factors, we obtain another noise term of the form

$$\sim \left(\mathbf{e}^T \partial \mathbf{W}^I \mathbf{p}^{\mathrm{st}} \right) \left(\mathbf{e}^T \mathbf{W}^I \mathbf{p}^{\mathrm{st}} \right)$$

that is a product of two scalars (it is derived from $\langle I \rangle^2$). We can reorganize the terms to obtain a rather short expressions of the form

$$S_{I\Pi I} + S_{I^2} = \frac{e^2}{\hbar} \mathbf{e}^T \mathbf{W}^I \left[\mathbf{P} \mathbf{W}^I + \mathbf{p}^{\mathrm{st}} \otimes \mathbf{e}^T \partial \mathbf{W}^I \right] \mathbf{p}^{\mathrm{st}}. \tag{3.43}$$

A central assumption we have to make here, is that the kernels $\mathbf{W}^I$ (and $\mathbf{W}$ since the same expression will appear again below) decay faster than $1/t^2$, $\lim_{t \to -\infty} t^2 \mathbf{W}^I(0, t) = \mathbf{0}$ so that the object $\partial \mathbf{W}^I$ exists. This is the case for the situations we will consider later, where $\mathbf{W}^I(0, t)$ decays exponentially with t. The appearance of the object $\partial \mathbf{W}^I$ is related to non-Markovian processes and will be discussed below.

The total shot noise Eq. 3.37 can finally be expressed as ($S = S_{II} + S_{I\Pi I} + S_{I^2}$)

$$S = \frac{e^2}{\hbar} \mathbf{e}^T \left[\mathbf{W}^{II} + \mathbf{W}^I (\mathbf{P} \mathbf{W}^I + \mathbf{p}^{\mathrm{st}} \otimes \mathbf{e}^T \partial \mathbf{W}^I) \right] \mathbf{p}^{\mathrm{st}} \tag{3.44}$$

Before expanding the expressions order by order in Γ, we still have to find an equation which determines the object

$$\mathbf{P} = \lim_{t_0 \to -\infty} \int_{t_0}^{0} dt_1 \, \frac{1}{\hbar} \left[\mathbf{\Pi}(0, t_1) - \mathbf{\Pi}(0, t_0) \right] \tag{3.45}$$

from transition rates $\mathbf{W}$. (The introduction of time t_1, as opposed to t', t'', t''' allows an easier identification of the parts of the Dyson equation we derive the object $\mathbf{P}$ from). We consider again the Dyson-equation Eq. 3.23 for the propagator $\mathbf{\Pi}(0, t_0)$. By changing the integration times and making use of time-translational invariance, we can write the equation as

$$\mathbf{\Pi}(0, t_0) = \mathbf{1} + \int_{t_0}^{0} dt_1 \int_{t_1}^{0} dt_2 \, \mathbf{W}(0, t_2) \mathbf{\Pi}(t_1, t_0). \tag{3.46}$$

We split the domain of the integral $\int_{t_1}^{0} dt_2 \to \int_{t_1}^{t_0} dt_2 + \int_{t_0}^{0} dt_2$ and add and subtract once the expression $\int_{t_0}^{0} dt_2 \mathbf{W}(0, t_2) \int_{t_0}^{0} dt_1 \mathbf{\Pi}(0, t_0)$. In the limit $t_0 \to -\infty$ we can use again the Laplace transformation and find

$$\mathbf{W}\mathbf{P} = (\mathbf{p}^{\mathrm{st}} \otimes \mathbf{e}^T - \mathbf{1}) - \partial \mathbf{W} \mathbf{p}^{\mathrm{st}} \otimes \mathbf{e}^T. \tag{3.47}$$

Again we assumed the transition rates to decay fast enough such that $\lim_{t \to -\infty}(t^2 \mathbf{W}(0, t)) = \mathbf{0}$. Since $\mathbf{W}$ cannot be inverted we need an extra condition to determine $\mathbf{P}$. The necessary condition is $\mathbf{e}^T \mathbf{P} = \mathbf{0}$, which follows from the definition of $\mathbf{P}$, the Dyson equation, and $\mathbf{e}^T \mathbf{W} = \mathbf{0}$. We rewrite Eq. 3.47 as

$$\tilde{\mathbf{W}}\mathbf{P} = \tilde{\mathbf{1}}(\mathbf{Q} + \mathbf{R}) \tag{3.48}$$

with the objects $\mathbf{Q} = \mathbf{p}^{\mathrm{st}} \otimes \mathbf{e}^T - \mathbf{1}$, $\mathbf{R} = -\partial \mathbf{W} \mathbf{p}^{\mathrm{st}} \otimes \mathbf{e}^T$ and $\tilde{\mathbf{1}}$ being the unit matrix, where one (arbitrary) row χ_0 has been set to zero. We now have all parts in place to expand $\mathbf{P}$ and the shot noise in powers of Γ. For $\mathbf{P}$, we observe that $\mathbf{P}$ starts in order $\Gamma^{(-1)}$ as

$$\mathbf{P}^{(-1)} = \left(\tilde{\mathbf{W}}^{(1)} \right)^{-1} \mathbf{Q}^{(0)} \tag{3.49}$$

($\mathbf{Q}^{(0)} = \mathbf{p}^{\mathrm{st}(0)} \otimes \mathbf{e}^T - \mathbf{1}$). Higher orders $k = 0, 1, ...$, can be computed from

$$\mathbf{P}^{(k)} = \left(\tilde{\mathbf{W}}^{(1)} \right)^{-1} \left[\tilde{\mathbf{1}} \left(\mathbf{Q}^{(k+1)} + \mathbf{R}^{(\mathrm{k}+1)} \right) - \mathbf{S}^{(k+1)} \right] \tag{3.50}$$

where

$$\mathbf{Q}^{(k+1)} = (\mathbf{p}^{st(k+1)} \otimes \mathbf{e}^T), \tag{3.51}$$

$$\mathbf{R}^{(k+1)} = -\sum_{m=0}^{k} (\partial \mathbf{W}^{(k-m+1)} \mathbf{p}^{\mathrm{st}(m)} \otimes \mathbf{e}^T) \tag{3.52}$$

and

$$\mathbf{S}^{(k+1)} = \sum_{m=-1}^{k-1} (\tilde{\mathbf{W}}^{(k-m+1)} \mathbf{P}^{(m)}). \tag{3.53}$$

Finally, we expand the noise Eq. 3.44 to

$$S^{(k)} = \frac{e^2}{\hbar} \mathbf{e}^T \sum_{m=0}^{k-1} \left[\mathbf{W}^{II(k-m)} + \mathbf{X}^{(k-m)} \right] \mathbf{p}^{\mathrm{st}(m)} \tag{3.54}$$

with

$$\begin{aligned} \mathbf{X}^{(k-m)} = &\sum_{m'=1}^{k-m} \left(\sum_{m''=-1}^{k-m-m'-1} \mathbf{W}^{I(k-m-m'-m'')} \mathbf{P}^{(m'')} \mathbf{W}^{I(m')} \right) \\ &+ \sum_{m'=1}^{k-m} \left(\sum_{m''=0}^{k-m-m'-1} \mathbf{W}^{I(k-m-m'-m'')} \mathbf{p}^{\mathrm{st}(m'')} \otimes \mathbf{e}^T \partial \mathbf{W}^{I(m')} \right) \end{aligned} \tag{3.55}$$

for $k = 1, 2, \ldots$. Again, the full shot noise is given by $S = \sum_{k=1}^{\infty} S^{(k)}$. The set of matrix equations Eqs. (3.27, 3.28, 3.33, 3.49, 3.50, 3.54 and 3.55) constitute the starting point for calculations which are done in a perturbative expansion. Since in the next chapter we will discuss results, based on calculations of the current and shot noise up to second order, we write down the first and second order contributions to the noise explicitely. In first order in Γ (sequential tunneling) this noise simplifies to

$$S^{(1)} = (e^2/\hbar)\, \mathbf{e}^T \left(\mathbf{W}^{II(1)} + \mathbf{W}^{I(1)} \mathbf{P}^{(-1)} \mathbf{W}^{I(1)} \right) \mathbf{p}^{\mathrm{st}(0)}, \tag{3.56}$$

and all contributions involving the derivatives $\partial \mathbf{W}$ and $\partial \mathbf{W}^I$ disappear as a consequence of the fact that $\mathbf{W}$ starts at order Γ, $\mathbf{p}^{\mathrm{st}}$ at Γ^0, and $\mathbf{P}$ at Γ^{-1}. For the second order corrections we find

$$S^{(2)} = \frac{e^2}{\hbar}\, \mathbf{e}^T \left[(\mathbf{W}^{II(2)} + \mathbf{X}^{(2)}) \mathbf{p}^{\mathrm{st}(0)} + (\mathbf{W}^{II(1)} + \mathbf{X}^{(1)}) \mathbf{p}^{\mathrm{st}(1)} \right] \tag{3.57}$$

with

$$\mathbf{X}^{(1)} = \mathbf{W}^{I(1)} \mathbf{P}^{(-1)} \mathbf{W}^{I(1)} \mathbf{p}^{\mathrm{st}(1)}, \tag{3.58}$$

$$\begin{aligned} \mathbf{X}^{(2)} = &\mathbf{W}^{I(2)} \mathbf{P}^{(-1)} \mathbf{W}^{I(1)} + \mathbf{W}^{I(1)} \mathbf{P}^{(-1)} \mathbf{W}^{I(2)} \\ &+ \mathbf{W}^{I(1)} \mathbf{P}^{(0)} \mathbf{W}^{I(1)} + \mathbf{W}^{I(1)} (\mathbf{p}^{\mathrm{st}(0)} \otimes \mathbf{e}^T) \partial \mathbf{W}^{I(1)}, \end{aligned} \tag{3.59}$$

and objects $\mathbf{P}^{(-1)}$ and $\mathbf{P}^{(0)}$ being determined by Eqs. 3.49 and 3.50. Again, it remains to calculate the rates $\mathbf{W}^{(1)}, \partial\mathbf{W}^{(1)}, \mathbf{W}^{I(1)}, \partial\mathbf{W}^{I(1)}, \mathbf{W}^{II(1)}$ in first and $\mathbf{W}^{(2)}, \mathbf{W}^{I(2)}, \mathbf{W}^{II(2)}$ in second order.

All difficulties are reduced to book-keeping of diagrams, which could be handled by a numerical program code. This allows for a microscopic description of more complex mesoscopic systems with many internal degrees of freedom (electronic structure, coupling to fermionic or bosonic degrees of freedom, etc.).

First order calculations, using the theory presented above, have been performed for a single level system [6] but also more complex systems [7, 8] up to structures approaching a description of molecules [12, 13]. The inclusion of bosonic degrees of freedom has been considered in [7, 8]. In second order we have studied the Coulomb-blockade regime and spin-dependent transport for arbitrary bias [9, 10, 11].

We close this section with some comments on the theory we developed here:

1) The derivatives $\partial\mathbf{W}$ and $\partial\mathbf{W}^I$ are associated with *non-Markovian* behavior of the system, and are not present in Refs. [26, 27] and [6] which describe "orthodox theory" (first order perturbation theory). However they become important for second- and higher-order corrections. (For a discussion of non-Markovian effects see also Ref. [134].) In Ref. [105, 104] co-tunneling shot noise was discussed in the Coulomb-blockade regime by making use of a S-matrix expansion. In these works terms related to the non-Markovian corrections have been neglected. This can be done only if first order contributions are suppressed sufficiently strong compared to second order terms. This becomes transparent in our expression for the noise, where the corresponding term can be written as $2eI(\mathbf{e}^T\partial\mathbf{W}^I\mathbf{p}^{\rm st})$. Counting the powers in Γ we see that the second order contributions to the noise contains the current I to first order. The first order current, however, is exponentially small in the Coulomb blockade region. We may understand the situation as follows: sequential tunneling events are rare since thermal excitations of the excited states are exponentially suppressed. A long time will pass between two such events and the system thus is most likely to recover the ground state in between (by co-tunneling processes). Therefore, the system loses its memory between sequential tunneling events deep in the Coulomb blockade region. This will not be the case anymore, if we are closer to the onset of sequential tunneling. Therefore, neglecting the memory effects is a reasonable approximation only deep in the Coulomb blockade regime, far away from the sequential tunneling threshold.

2) Higher derivatives than the first derivative will not appear for the shot noise even for higher-order corrections ($k > 2$). We will discuss this in more detail in section 3.7, where further extensions of our theory to describe *higher correlators*, as is the objective of full counting statistics (FCS), are discussed.

3) Since Eqs. 3.26, 3.32, 3.44 and 3.48 are valid for arbitrary order perturbation theory

in Γ, we have derived a theory here, which could in principle describe *Kondo physics* as well, when considering a corresponding choice of diagrams (as was done in [132], within a resonant tunneling approximation). The main problem to be solved, is the appropriate calculation of diagrams containing two current vertices $\mathbf{W}^{II}$, which are the most difficult to relate to the 'pure' transition rates $\mathbf{W}$. However, we have to realize that our main assumption was the factorization of the density matrix into parts of the reservoirs and the island. This, in principle, restricts us to a perturbative approach, which can be expanded to infinite order. The description of the Kondo problem may be possible due to an approximative mapping to capture the relevant physics.

4) Another assumption is the restriction to consider the diagonal elements of the density matrix only. *Coherence effects* therefore are not taken fully into account. However, we show in chapter 3.8 that the structure of the noise formulas we derived here will remain unchanged, and only the objects $\mathbf{p}^{\mathrm{st}}$ and $\mathbf{P}$ have to be calculated differently.

5) The description of *finite frequency* shot noise poses no problem within our theory as well. In chapter 3.6 we show the relation of our zero frequency theory we developed here to a theory accounting for finite frequencies.

6) An alternative description of the shot noise in terms of *non-equilibrium Green functions*, as has been developed for the current, poses a stronger problem, since two-particle Green functions are encountered now. When an exact treatment of interaction effects is desired, as we did in our approach, a reduction to a single particle picture or application of Wick's theorem is not allowed. This is reflected in the objects, we encounter within our theory of shot noise. The rates $\mathbf{W}^{I}$ in the current are easily related to the rates $\mathbf{W}$, since due to the sum rule the only truly relevant position of the current vertex is the rightmost in the diagrammatic representation. A relation between the Green functions and irreducible blocks $\mathbf{W}$ is found almost trivially [132]. In contrast, the rates $\mathbf{W}^{II}$ or $\partial\mathbf{W}, \partial\mathbf{W}^{I}$ are not linked in an obvious way to the blocks $\mathbf{W}$, and hence the Green functions. This is a problem especially for $\mathbf{W}^{II}$.

3.6 Finite frequency shot noise

In this section we show that a description of finite frequency noise is straightforward in our diagrammatic approach. We begin again with its definition

$$S = \int_{-\infty}^{\infty} dt \, \left[\langle \hat{I}(t)\hat{I}(0) + \hat{I}(0)\hat{I}(t) \rangle - 2\langle \hat{I} \rangle^2 \right] e^{i\omega t}. \tag{3.60}$$

The last term can be expressed in terms of the Dirac-Delta-function, since $\delta(\omega) = \int_{-\infty}^{\infty} dt e^{i\omega t}$ vanishes for finite frequencies. Therefore, at finite frequencies we do not have to subtract the $\langle \hat{I} \rangle^2$ part, which in the zero frequency limit led to a divergence. Also the noise part with the propagator between two irreducible blocks does not diverge, as we will see next. In analogy to all other calculations in the last section we can write down the symmetrized noise as

$$S(\omega) = \frac{e^2}{2\hbar} \mathbf{e}^T \left[\mathbf{W}^{II}(\omega) + \mathbf{W}^I_<(\omega) \mathbf{\Pi}(\omega) \mathbf{W}^I_>(\omega) \right] \mathbf{p}^{\mathrm{st}} + (\omega \to -\omega). \tag{3.61}$$

The frequency dependent propagator takes finite values as long as $\omega \neq 0$ and reads

$$\mathbf{\Pi}(\omega) = \left[i\omega \mathbf{1} - \mathbf{W}(\omega) \right]^{-1}. \tag{3.62}$$

In the zero frequency limit the divergence was due to the zero eigenvalue of the matrix $\mathbf{W}(\omega = 0)$. We find that again all quantities are expressed in terms of irreducible blocks $\mathbf{W}, \mathbf{W}^I$ and $\mathbf{W}^{II}$. Although Eqs. 3.61 and 3.62 are more compact in appearance we want to explain why this does not mean that the noise is easier to calculate at finite frequencies. In contrary, we encounter more complicated objects here, since in addition to the blocks as introduced in the last section we now have to account for an external frequency line running through the diagrams. This is illustrated for the

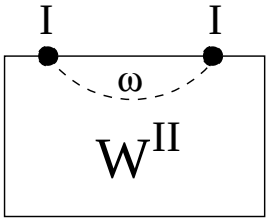

Figure 3.14: *An example for the frequency dependent diagrams $\mathbf{W}^{II}(\omega)$, where an external line, connecting the two current vertices runs through the whole, or parts of the diagram.*

diagrams including two current vertices in Fig. 3.14 and 3.15. Since the external vertices may sit on arbitrary positions between the internal vertices, the frequency line connecting the current vertices can cover the whole, or only parts of a diagram. In

section 3.3 we discussed a special symmetry of diagrams, when changing the direction of all lines and reflecting them on a horizontal cut. This mirror rule allowed for a compactification of diagrams, which led to $\mathbf{W} + \mathbf{W}^* = 2\mathrm{Re}\mathbf{W}$ (in Ref. [132] this was $\mathbf{\Sigma} + (-\mathbf{\Sigma}^*) = 2\mathrm{Im}\mathbf{\Sigma}$). This rule cannot be applied anymore, since the external frequency line is fixed in direction. The blocks $\mathbf{W}$ cannot be written as real objects anymore, which makes their evaluation considerably harder, and additionally enhances the number of diagrams drastically. Diagrammatically, the frequency line with index ω is accounted for by adding its energy $\hbar\omega$ appropriately to the energies of internal lines, which keeps the rules from appendix A unchanged. We only have to sum over a larger number of diagrams later on. For the second contribution of Eq. 3.61 we find

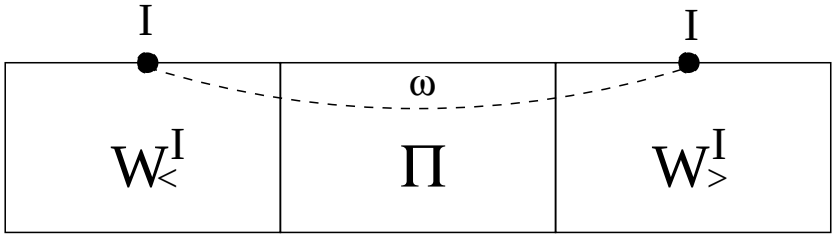

Figure 3.15: *An example for the second frequency dependent term in Eq. 3.61. The current vertex in a block* $\mathbf{W}^I_<(\omega)$ *is connected to another in block* $\mathbf{W}^I_>(\omega)$.

diagrams $\mathbf{W}^I_<(\omega), \mathbf{W}^I_>(\omega)$, which have open frequency lines to the right or left side, with a propagator, expressible in terms of diagrams $\mathbf{W}(\omega)$, with a line crossing the whole block. This visualizes that for lines covering parts of $\mathbf{W}^I_<(\omega), \mathbf{W}^I_>(\omega)$ on both sides current events at different times are connected, making Fig. 3.15 'irreducible' in a sense. [Note that there are also combinations where a current vertex sits on the edge, where the propagator begins]. Diagrams of the kind as shown above will provide contributions which we attributed to memory effects in the last section. Indeed, when calculating the first order contribution to the noise we find that contributions resulting from structures like Fig. 3.15 also provide a second order contribution. A well defined perturbation expansion in the coupling strength to the reservoirs only (in principle one could think to consider a combination of Γ and ω) is therefore not possible, and one has to select different order terms 'by hand'.

In the following, we want to show, that our zero frequency noise formula is exactly recovered, when taking the limit $\omega \to 0$ of Eq. 3.61. This will show that the frequency dependent noise, as applied to lowest order calculations for example in Refs. [135, 136], can describe higher order contributions correctly as well and thus accounts for the non-Markovian memory effects. We could take this limit in the present energy representation, by performing a spectral eigenvalue decomposition of the propagator. In analogy to our zero frequency calculations in the last section however, we formally rewrite Eq. 3.61 in time space in terms of frequency dependent objects and include

the contribution again, which we neglected due to the Delta function. We recover an object

$$\mathbf{P}(\omega, t''') = \lim_{t_0 \to -\infty} \int_{t_0}^{t'''} dt'' \, \frac{1}{\hbar} e^{-i\omega(t'''-t'')} \left[\mathbf{\Pi}(t''', t'') - \mathbf{\Pi}(t''', t_0)\right] \tag{3.63}$$

which gives $\mathbf{P}(\omega, 0) = \mathbf{P}(\omega)$ when shifting the time t''' to zero. Doing an analoguous calculations to before, we find that by splitting the exponential in the definition Eq. 3.60 as $e^{i\omega t} = e^{-i\omega(0-t''')} e^{-i\omega(t'''-t'')} e^{-i\omega(t''-t)}$ allows us to attach the frequency ω directly to the objects appearing in the noise expression. We end up with a corresponding noise formula to Eq. 3.61

$$S^+(\omega) = \frac{e^2}{2\hbar} \mathbf{e}^T \left[\mathbf{W}^{II}(\omega) + \mathbf{W}^I_<(\omega)\mathbf{P}(\omega)\mathbf{W}^I_>(\omega) + \left(\mathbf{W}^I_<(\omega) - \mathbf{W}^I\right) \frac{\mathbf{p}^{\mathrm{st}} \otimes \mathbf{e}^T}{i\omega\hbar} \mathbf{W}^I_>(\omega)\right] \mathbf{p}^{\mathrm{st}}, \tag{3.64}$$

with one block being independent of frequency. Note that a difference of two irreducible blocks appears which is due to integrations over two different times, connected with a frequency. The full noise reads

$$S(\omega) = S^+(\omega) + S^-(\omega), \tag{3.65}$$

where $S^-(\omega) = S^+(-\omega)$. The equation which determines the object $\mathbf{P}(\omega)$ is found as usual from the Dyson equation. Together with $\mathbf{P}(\omega) = \mathbf{\Pi}(\omega) + \frac{i}{\omega}\mathbf{p}^{\mathrm{st}} \otimes \mathbf{e}^T$ this leads to

$$\left[\mathbf{W}(\omega) - i\omega\mathbf{1}\right] \mathbf{P}(\omega) = \left[\mathbf{p}^{\mathrm{st}} \otimes \mathbf{e}^T - \mathbf{1}\right] - \frac{1}{i\omega} \mathbf{W}(\omega) \mathbf{p}^{\mathrm{st}} \otimes \mathbf{e}^T. \tag{3.66}$$

The Eqs. 3.64, 3.65 and 3.66 are equivalent to Eqs. 3.61 and 3.62. If one wants to expand these equations in perturbation theory, it is significant that a fixed order of the right hand side of Eq. 3.66 requires terms of different orders for $\mathbf{P}(\omega)$ on the left side, since $\mathbf{W}(\omega)$ starts with first order in Γ and $i\omega\mathbf{1}$ is independent of Γ (zeroth order).

When taking the limit $\omega \to 0$ we have to make use of l'Hospitals rule and find derivatives with respect to the frequency, which is equivalent to our former definition of $\partial\mathbf{W}$ as $\left(\partial\mathbf{W}(\omega)/\partial\omega\right)|_{\omega=0^+} = i\left(\partial\mathbf{W}(z)/\partial z\right)|_{z=0^+} = \partial\mathbf{W}$. The rates as defined above reduce to $\mathbf{W}, \mathbf{W}^I, \mathbf{W}^{II}$ in the zero frequency limit. In this limit we recover our zero frequency noise formula Eq. 3.44 and the determination equation (Eq. 3.47).

The equivalence of the zero and finite frequency noise formulas in the limit $\omega \to 0$ shows that both account for non-Markovian memory effects relevant for higher order contributions in the coupling strength. It is straightforward to perform calculations of finite frequency shot noise within our diagrammatic technique, however the zero frequency formula (although more lengthy in appearance) allows a much easier calculation of the irreducible self energy diagrams, since symmetries reduce the number of needed diagrams. In chapter 4 we only consider the zero frequency noise, as motivated in chapter 2.2 (white noise behavior up to high frequencies).

3.7 Higher correlators

In the last years the idea of *Full Counting Statistics* (FCS) for electron transport has attracted much interest. This theory counts the probability of N electrons having passed a mesoscopic system during a time t and was introduced from [137, 138, 139] and further extended and studied from [140, 141, 142, 143, 144, 145, 146, 134]. The full information about all transport properties of a given system is contained in the probability distribution $P(N,t)$, which is related to the cumulant generating function (CGF)

$$S(\lambda) = -\ln\left[\sum_{N=-\infty}^{\infty} e^{iN\lambda} P(N,t)\right] \tag{3.67}$$

depending on a so called counting field λ. The quantum mechanical form of this function is found to be

$$e^{-S(\lambda)} = \left\langle T e^{-i\frac{\lambda}{2e}\int_0^{t_0} dt\hat{I}(t)} \tilde{T} e^{-i\frac{\lambda}{2e}\int_0^{t_0} dt\hat{I}(t)} \right\rangle. \tag{3.68}$$

with T and $\tilde{T}$ being the time and anti-time ordering operators. When expanding Eq. 3.68 it becomes clear, that higher order current correlators ($\hat{I}(t)$ being the current operator) are encountered. Therefore another quantity has been defined, which is the n-th cumulant, related to the n-th derivative of the CGF

$$C_n = -(-i)^n \frac{\partial^n}{\partial\lambda^n} S(\lambda)|_{\lambda=0}. \tag{3.69}$$

The charm of FCS lies in the fact that higher correlator can be determined immediately after the calculation of only one functional. It is then straightforward to relate the first cumulant to the current expectation value $C_1 = -\frac{t_0}{e} I$ and the second one to the shot noise $C_2 = \frac{t_0}{2e^2} S$, where t_0 denotes the initial time (which we shift to minus infinity). [I and S are are the expectation values as defined in chapters 3.4 and 3.5. Note that n integrals are present in the n-th cumulant, which can always be reduced to $n-1$ integrals, since only the relative times between current measures are physically relevant.]

The limited literature on FCS deals mostly with a description of the weak coupling regime (first order in Γ). Very recently, a theory taking into account higher order contributions while describing two-particle interaction effects exactly has been derived [134] within FCS. In Ref. [134] it is shown that non-Markovian memory effects appear in the shot noise beginning at second order perturbation theory in Γ. This is in agreement with our theory of shot noise, as discussed in chapter 3.5. All results derived in Ref. [134] are reproduced within our theory. The memory effects show up in terms containing a derivative of irreducible self energy blocks with respect to a convergence factor. Ref. [134] shows that the highest derivative in the n-th cumulant is given by

$[min(k,n)-1]$ where k is the order of the perturbation expansion. Since $n=1$ for the current and $n=2$ for the shot noise, we find that only a single derivative beginning in second order contributions to the noise will appear, whereas in the current non-Markovian effects do not play a role at all.

All this can be understood from the perspective of our diagrammatic technique as well. Since for higher correlators $(n-1)$ external integrals have to be done they will produce terms of the kind $t^{(n-1)}\mathbf{W}(0,t)$ by rearranging objects in terms of $\mathbf{P}$. The maximal derivative we have to expect will therefore be of the order $(n-1)$, present in objects $\partial^{n-1}\mathbf{W}$. We find that the n-th current correlator is composed of products of up to the n-th correlator with up to the $(n-1)$-th derivative. Since each correlator starts with first order in Γ, we find that for a given order in perturbation theory k at most the $(k-1)$-th derivative will appear. The prediction from Ref. [134] is therefore in agreement with our expectations for arbitrary current-correlators. As an example consider the third correlator, described by objects of the kind $\mathbf{W}^{III}$, $\mathbf{W}^{II}\mathbf{\Pi}\mathbf{W}^{I}$, $\mathbf{W}^{I}\mathbf{\Pi}\mathbf{W}^{II}$ and $\mathbf{W}^{I}\mathbf{\Pi}\mathbf{W}^{I}\mathbf{\Pi}\mathbf{W}^{I}$. Together with contributions of the current I and the shot noise S the propagators $\mathbf{\Pi}$ can be expressed in terms of objects $\mathbf{P}$ again. The object $\mathbf{W}^{I}\mathbf{\Pi}\mathbf{W}^{I}\mathbf{\Pi}\mathbf{W}^{I}$ has to be combined with current terms of the form I^3. This is the place where second derivatives will appear, since the two external integrals are taken over constant objects in time, leading to expressions of the kind $\hbar\int_{-\infty}^{0} t^2 e^{zt}\mathbf{W}(0,t)$.

Our theory can thus be generalized to describe higher current correlators as well. The tedious work of calculating a general expression needs to be done first. After this is done, arbitrary correlators could be computed immediately, since the rules of how to expand diagrams containing an arbitrary number of current vertices remain unchanged.

On the other hand we should ask, why higher cumulants or correlators are interesting to study, besides the technical achievement of providing a 'compact' theory. Low frequency current fluctuations give rise to a large number of irreducible correlation functions. The current-current correlation function (shot noise) still provides only partial information about the current fluctuations. For a complete picture additionally higher correlators should have to be considered. The current tells about the mean electronic transport, the shot noise tells about its fluctuations. The third correlator (skewness) tells us about asymmetry in the distribution function. It can be shown that odd correlators (current, skewness, etc.) vanish at equilibrium and are not masked by thermal fluctuations. Therefore, they can be used for probing non-equilibrium properties at relatively high temperatures. Furthermore, they depend on the direction the current is flowing (not only its absolute value), in contrast to even correlators, which in turn also capture the physics of thermal fluctuations and random transmissions of particles.

Up to date only a single measurement of a higher moment than the shot noise has been published, namely an experiment on the *skewness*, in Ref. [147]. However it still

is not clear, what quantity is measured indeed in experiment, the third cumulant (as derived from Eq. 3.68), the third correlator (as we would describe within our theory) or a combination of first, second and third cumulants or correlators. A discussion of different regimes (if the decay time t_0 is large or small compared to the electrons flight time between detector and scatterer) using different generating functions CGF (one is Eq. 3.68, another related to our approach) has been published in Ref. [148]. The problem may become more transparent by explicitly writing down the third cumulant as defined above. We find $i\frac{\partial^3 Z(\lambda)}{\partial\lambda^3}|_{\lambda=0} = C_1+3C_1C_2+C_3$ with the definition $Z(\lambda) = e^{-S(\lambda)}$. The problem we are confronted with is the fact, that there is no trivial relation to the third correlator,

$$\sim \int_0^{t_0} dt_3 \int_0^{t_0} dt_2 \int_0^{t_0} dt_1 \left\langle \sum_{Perm.} [\hat{I}(t_3)\hat{I}(t_2)\hat{I}(t_1)] \right\rangle, \tag{3.70}$$

including all permutations of times. Our diagrammatic approach would straight forwardly provide expressions related to this correlator. However, from Eq. 3.68 we find

$$\begin{aligned} \frac{\partial^3 Z(\lambda)}{\partial\lambda^3}|_{\lambda=0} = \frac{i}{8e^3} \int_0^{t_0} dt_3 \int_0^{t_0} dt_2 \int_0^{t_0} dt_1 \\ \Big\langle T[\hat{I}(t_3)\hat{I}(t_2)\hat{I}(t_1)] + \tilde{T}[\hat{I}(t_3)\hat{I}(t_2)\hat{I}(t_1)] \\ +T[\hat{I}(t_3)\hat{I}(t_2)]\hat{I}(t_1) + \hat{I}(t_1)\tilde{T}[\hat{I}(t_2)\hat{I}(t_3)] \\ +T[\hat{I}(t_2)\hat{I}(t_1)]\hat{I}(t_3) + \hat{I}(t_3)\tilde{T}[\hat{I}(t_1)\hat{I}(t_2)] \\ +T[\hat{I}(t_1)\hat{I}(t_3)]\hat{I}(t_2) + \hat{I}(t_2)\tilde{T}[\hat{I}(t_1)\hat{I}(t_3)]\Big\rangle \end{aligned} \tag{3.71}$$

which is different to the third correlator. The third cumulant C_3 is therefore non-trivially related to the third correlator. Technically, it could be interesting to relate the two approaches to each other. However, for the experimental comparison it is more relevant to clarify first what quantity is measured in reality and what would be a natural definition for this quantity.

3.8 Off-diagonal elements and coherent processes

For the derivation of the current and shot noise we assumed the density matrix to be diagonal, which, strictly speaking, restricts us to consider localized level structures. This assumption was made only for the objects $\mathbf{p}^{\mathrm{st}}$ and $\mathbf{P}$ where the Dyson equation enters. If we want to include the off-diagonal elements also, we have to derive new equations to determine these (off-diagonal) objects. However, the general form of the current and noise formula remain unchanged. The only difference is that transition rates may also begin and end in mixed states, leading to rates depending on all four (instead of two) state labels on the Keldysh contour. This increases the complexity of calculations significantly, but it is not a fundamental technical problem. In order to account for off-diagonal elements of the density matrix as well, we rewrite the Dyson equation in its most general form

$$\begin{aligned}\Pi^{\chi_1'\chi_1}_{\chi_2'\chi_2}(t,t_0) &= \Pi^{(0)\,\chi_1'}_{\quad\chi_2'}(t,t_0)\delta_{\chi_1,\chi_1'}\delta_{\chi_2,\chi_2'} \\ &\quad + \sum_{\chi_1'',\chi_2''}\int_t^{t'} dt_2 \int_t^{t_2} dt_1\, \Pi^{(0)\,\chi_1'}_{\quad\chi_2'}(t,t_2) W^{\chi_1'\chi_1''}_{\chi_2'\chi_2''}(t_2,t_1)\Pi^{\chi_1''\chi_1}_{\chi_2''\chi_2}(t_1,t_0),\end{aligned} \tag{3.72}$$

where $\Pi^{(0)\,\chi_1'}_{\quad\chi_2'}(t,t_0) = \exp[-i(\varepsilon_{\chi_1'} - \varepsilon_{\chi_2'})(t-t_0)]$ is the propagator of the isolated dot. Furthermore the density matrix of the dot at time t' reads

$$p^{\chi_1'}_{\chi_2'}(t) = \langle|\chi_2'\rangle\langle\chi_1'|(t)\rangle \tag{3.73}$$

which is related to the Dyson equation by

$$p^{\chi_1'}_{\chi_2'}(t) = \sum_{\chi_1,\chi_2}\Pi^{\chi_1'\chi_1}_{\chi_2'\chi_2}(t,t_0)p^{\chi_1}_{\chi_2}(t_0). \tag{3.74}$$

Now we insert Eq. 3.73 into Eq. 3.74, sum over χ_1, χ_2 and differentiate with respect to t. This yields

$$\frac{d}{dt'}p^{\chi_1'}_{\chi_2'}(t) + i(\varepsilon_{\chi_1'-\chi_2'})p^{\chi_1'}_{\chi_2'}(t) = \sum_{\chi_1'',\chi_2''}\int_{t_0}^{t} dt_1\, W^{\chi_1'\chi_1''}_{\chi_2'\chi_2''}(t,t_1)p^{\chi_1''}_{\chi_2''}(t_1), \tag{3.75}$$

This is the most general kinetic equation for the reduced density matrix. We want to consider the stationary limit again and choose $t = 0$ and the limit $t_0 \to -\infty$, where we can take out the Laplace transformation of the irreducible blocks.

$$\sum_{\chi_1'',\chi_2''}[W^{\chi_1'\chi_1''}_{\chi_2'\chi_2''} - i(\varepsilon_{\chi_1'-\chi_2'})\delta_{\chi_1',\chi_1''}\delta_{\chi_2',\chi_2''}]p^{\mathrm{st}\,\chi_1''}_{\quad\chi_2''} = 0 \tag{3.76}$$

Eq. 3.76 reflects a quantum rate equation, since an interpretation of the off-diagonal elements as classical probabilities is not possible. The sum over the diagonal elements

of $p^{\mathrm{st}}{}^{\chi_1''}_{\chi_2''}$ has to be conserved and equals unity. Note that Eq. 3.76 simplifies to the master equation for diagonal matrix elements if $\chi_1' = \chi_2' = \chi'$ and $\chi_1'' = \chi_2'' = \chi''$. The off-diagonal elements can be understood as possible realizations of linear combinations of quantum states. This is typical for delocalized systems (e.g. a number of coupled quantum dots), where electrons entering the system from a reservoir can not remain localized on a certain dot if participating in transport. Quantum rate equations describing *coherence effects* in mesoscopic systems have been derived by Gurvitz [106, 107]. Restrictions to a fixed bias regime (far away from resonances) and vanishing temperatures however limit this approach. Theories attempting to extend the Gurvitz approach to finite temperatures and bias voltages have been proposed in [110, 111] in a lowest order perturbation approach in the coupling Γ.

After solving Eq. 3.76 the current as introduced in chapter 3.4 can be computed, with objects $\mathbf{W}^I$ depending now on four dot states labels. However, it is clear that at a fixed time only mixed states within the same charge sector can be realized, which will limit the additional number of diagrams.

Transmission amplitudes connecting different times may have different quantum numbers (since the electrons can not be located in certain dot levels). The operator algebra generalizes from expressions like $|t_q\langle\chi'|c_p|\chi\rangle|^2$ to $t_q t_{q'}\langle\chi_2|c_{p'}|\chi_2'\rangle\langle\chi_1'|c_p|\chi_1\rangle$ (q, q', p, p' define quantum numbers again). A diagrammatic description of non-diagonal rates is therefore not a technical problem, but simply a book keeping one.

However we want to emphasize here, that one has to be careful with use of the terms like *coherence* and *delocalization*. It is clear that our description based on a diagonal density matrix cannot describe coherence effects in the sense as discussed in this section. However co-tunneling processes in situations of intermediate coupling approach a limit, where the quantum mechanical coherence time is longer than the time in which energy relaxation can take place in the scattering region or the dot system. This also implies coherence in a quantum sense. Thus, the word 'coherence' is connected with two different quantum effects. On the other hand, it is possible to describe delocalized systems (e.g. as relevant to describe coupled quantum dots or molecules) even while neglecting the off-diagonal elements. When diagonalizing the system Hamiltonian, we can change to a new basis, allowing to account for inter-dot couplings via the exact many body wavefunctions, whereas the coupling between electrodes and the dot system is still treated perturbatively. Transport through delocalized system is described correctly in that way, as long as the reservoir-dot coupling is small compared to the 'internal' coupling energies (coupled quantum dots are treated in this way in chapter 4.4). This restriction is lifted, if 'coherence' effects via off-diagonal elements of the density matrix are taken into account.

4 Results

In the following we want to review the main physical insights we can get about transport through systems like molecules or quantum dots in the sequential and co-tunneling regime. In chapters 3.4 and 3.5 we presented the first and second order formulas for current and shot noise ($I^{(1)}, I^{(2)}, S^{(1)}, S^{(2)}$). All quantities have been expressed in terms of transition rates, which are explained in more detail in the appendices B and C. In case of first order rates, we can write down explicitly analytical expressions, allowing therefore to compute straightforwardly systems of arbitrary complexity, including many electronic levels, interaction effects and even a coupling to bosonic degrees of freedom. For the second order rates we give the ingredients for a calculation and discuss the mathematical structure of the contributions. The diagrammatic rules can be formulated such that a straightforward numerical computation involving an operator-algebra becomes possible as well.

We will first specify three different model Hamiltonians which present special cases of the general Hamiltonian as introduced in chapter 3.2. After that, we discuss results for the current and shot noise for these models. In the present chapter we will thus study sequential and co-tunneling current and shot noise in systems like molecules or quantum dots in the Coulomb blockade, the finite transport regime and the crossover regime. We consider single and multi-level structures as well as photon relaxation effects. For spin-dependent coupling we can study the physics of spintronic devices. A brief outlook to more complex systems like several coupled quantum dots ('artificial molecules') will be given at the end. Most of the results presented in this chapter are taken from our former publications [6, 7, 8, 9, 10, 11, 12, 13]. We want to introduce the following conventions, to keep our language as clear as possible:

1) For the discussion of first order quantities we use $p_\chi^{(0)}$ if discussing probabilities, $I^{(1)}, S^{(1)}$ for current and noise and $F^{(1)} = S^{(1)}/2eI^{(1)}$ for the Fano factor.

2) For the discussion of second order quantities we use $p_\chi = p_\chi^{(0)} + p_\chi^{(1)}$ for the probabilities, $I = I^{(1)} + I^{(2)}$ and $S = S^{(1)} + S^{(2)}$ for current and noise and $F = S/2eI$ for the Fano factor (all objects including the second order corrections).

3) All energy parameters (e.g. level energies, interactions, temperature, etc.) are expressed in terms of the total linewidth Γ. The bias voltage V_b we give in terms of $2\Gamma/e$. Since a finite bias situation is described by different chemical potentials which we choose symmetrically $\mu_{\rm L} = eV_b/2$ and $\mu_{\rm R} = -eV_b/2$, resonance energies, leading to step structures in the transport curves, can be compared directly to the bias voltage.

4) In order to apply the results to quantum dots or molecules, the coupling strength should be chosen to $\Gamma \sim 10$ μeV in the first case and $\Gamma \sim 10$ meV in the latter case.

4.1 Model Systems

In chapter 3.2 we introduced a general Hamiltonian ($H = H_{\mathrm{L}} + H_{\mathrm{R}} + H_{\mathrm{D}} + H_{\mathrm{B}} + H_{\mathrm{T,L}} + H_{\mathrm{T,R}} + H_{\mathrm{B-D}}$) we can account for within our theory. Here we consider three specifications of this Hamiltonian, to model electron transport through a system with N levels. In this chapter we present results, based on calculations for these models. It is therefore possible to skip this section at the moment and come back to consider the corresponding models, when discussed in the text.

The electronic reservoirs with $r = \mathrm{L}, \mathrm{R}$ are described by

$$H_r = \sum_{k\sigma} \varepsilon_{k\sigma r} a^\dagger_{k\sigma r} a_{k\sigma r}, \tag{4.1}$$

and tunneling to the $i = 1, .., N$ levels is given by

$$H_{\mathrm{T},r} = \sum_{ik\sigma} \left(t^r_{i\sigma} a^\dagger_{k\sigma r} c_{i\sigma} + h.c. \right). \tag{4.2}$$

These parts of the general Hamiltonian will be the same for all our models. The main difference of our following models will therefore consist in the electronic structure of the island and a possible inclusion of bosonic degrees of freedom.

A) Our ***first model*** to be considered is a single-level Anderson impurity model (with $N = 1, c_{1\sigma} = c_\sigma, t^r_{1\sigma} = t^r_\sigma$) with the Hamiltonian

$$H_{\mathrm{D}} = \sum_{\sigma} \varepsilon_\sigma c^\dagger_\sigma c_\sigma + U n_\uparrow n_\downarrow \tag{4.3}$$

describing a single spin-dependent energy level including the Zeeman energy Δ due to an external magnetic field, when using the definition $\varepsilon_\downarrow = \varepsilon - \frac{\Delta}{2}$ and $\varepsilon_\uparrow = \varepsilon + \frac{\Delta}{2}$. Additionally we account for interaction effects via the Coulomb interaction U on the island ($n_\uparrow, n_\downarrow$ being the number operator for electrons with corresponding spin). We neglect bosonic degrees of freedom and set $H_B = H_{B-D} = 0$. Model A therefore describes the simplest model including interaction effects or a magnetic spin splitting and can be used in particular to study quantum dot structures or, as often denoted, 'artificial atoms'. This simple model-system was sufficient to describe the experimental features as discussed in chapter 2.

For the coupling parameters $\Gamma^{1\sigma}_r = \Gamma^\sigma_r$ we define $\Gamma_r = (\Gamma^\downarrow_r + \Gamma^\uparrow_r)/2$, $\Gamma^\sigma = \Gamma^\sigma_{\mathrm{L}} + \Gamma^\sigma_{\mathrm{R}}$, and $\Gamma = \Gamma_{\mathrm{L}} + \Gamma_{\mathrm{R}}$. A possible choice of spin-dependent couplings thus allows for a study of spin-dependent transport which is the subject of the field of spintronics. We may characterize a spin polarization of the magnetically polarized leads via a factor

$$p_{\mathrm{r}} = (\Gamma^\uparrow_{\mathrm{r}} - \Gamma^\downarrow_{\mathrm{r}})/(\Gamma^\uparrow_{\mathrm{r}} + \Gamma^\downarrow_{\mathrm{r}}). \tag{4.4}$$

This makes a further specification possible:

A1) By choosing $p = \pm p_{\mathrm{L}} = \pm p_{\mathrm{R}}$ the parallel $P^{\pm}$ configurations are realized (which lead due to their special left-right-symmetry to symmetric curves with respect to a finite bias voltage) and with $p = p_{\mathrm{L}} = -p_{\mathrm{R}}$ the antiparallel AP configuration is realized (a choice $p = -p_{\mathrm{L}} = p_{\mathrm{R}}$ is equivalent to considering the reversed bias region $V_b \to -V_b$). We furthermore assume $\Gamma_{\mathrm{L}} = \Gamma_{\mathrm{R}} = \Gamma/2$ here. This describes a ferromagnet-dot-ferromagnet (F-D-F) system.

A2) When choosing $p = \pm p_{\mathrm{L}}$ and $p_{\mathrm{R}} = 0$ or $p = \pm p_{\mathrm{R}}$ and $p_{\mathrm{L}} = 0$ (and $\Gamma_{\mathrm{L}} = \Gamma_{\mathrm{R}} = \Gamma/2$), a ferromagnet-dot-normal leads (F-D-N) and a normal-dot-ferromagnet (N-D-F) system are described.

A3) In the absence of spin-polarization, when $p = p_{\mathrm{L}} = p_{\mathrm{R}} = 0$ we can study a quantum dot coupled to normal leads (N-D-N), where an asymmetric situation with $\Gamma_{\mathrm{L}} \neq \Gamma_{\mathrm{R}}$ may be realized (for example we can choose $\Gamma_{\mathrm{L}} = a\Gamma$ and $\Gamma_{\mathrm{R}} = (1-a)\Gamma$).

Depending on the choice of configuration, two parameters remain to be fixed in model A: the total coupling Γ and an asymmetry factor a or polarization factor p with values between 0 and 1.

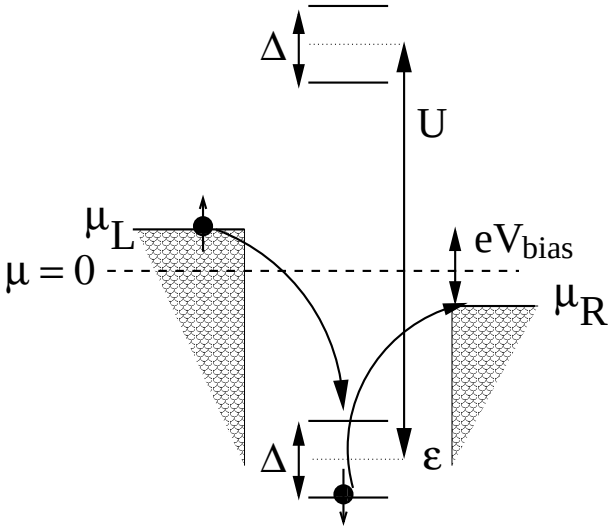

Figure 4.1: *Sketch of the excitation energies of the single level model (e.g. a single quantum dot), defined by an energy ε, a spin splitting Δ and the Coulomb interaction U. Here, a small bias situation is shown as an example, where co-tunneling processes (an inelastic one is indicated) provide the main contribution to transport.*

The model contains the following energy parameters: temperature $k_{\mathrm{B}}T$, level energy ε, spin-splitting Δ and Coulomb-interaction U, which are expressed in terms of Γ. Without loss of generality we can restrict ourselves to $U \geq 0$ and $\Delta \geq 0$. The energy ε can be chosen to be negative or positive. In Fig. 4.1 we sketch the excitation spectrum

of the single level model consisting of four excitation energies (not to be confused with a four level model), which is helpful to understand the relevant physical processes in different orders (of the coupling strength) for different choices of energy parameters.

The single-level Anderson impurity model contains four (4^N with ($N = 1$)) many-body dot states. Either an empty $|0\rangle$ state, an occupied state $|\downarrow\rangle$, $|\uparrow\rangle$ due to the spins or a doubly occupied state $|d\rangle$ can be realized on the dot.

B) A more generalized Anderson impurity model coupled to a bosonic bath is described by our ***second model*** with the Hamiltonian

$$H_{\rm D} = \sum_{i\sigma} \varepsilon_{i\sigma} c^\dagger_{i\sigma} c_{i\sigma} + U \sum_i n_{i\uparrow} n_{i\downarrow} + E_C \left(\sum_{i\sigma} n_{i\sigma} \right)^2 \tag{4.5}$$

where we consider $N = 2$ levels ($i = 1, 2$). We include a charging energy E_C which accounts for the classical energy cost to add a charge on a confined system with many electrons. We study photon relaxation effects by allowing processes where electrons on the dot can change the level by emitting or absorbing a photon by $i \neq j$ with the Hamiltonian

$$H_{\rm ph} = H_B + H_{B-D} = \sum_q \omega_q d^\dagger_q d_q + \sum_{q\sigma ij} g_{ph} (d^\dagger_q + d_q) c^\dagger_{i\sigma} c_{j\sigma}, \tag{4.6}$$

where we consider the constants $g^{ij}_q = (1 - \delta_{ij}) g_{ph}$ to be independent of i, j and q. This leads to a bosonic coupling constant $\alpha_{\rm ph}(\omega) = 2\pi g^2_{\rm ph} \rho_{\rm b}(\omega)$. For the relaxation

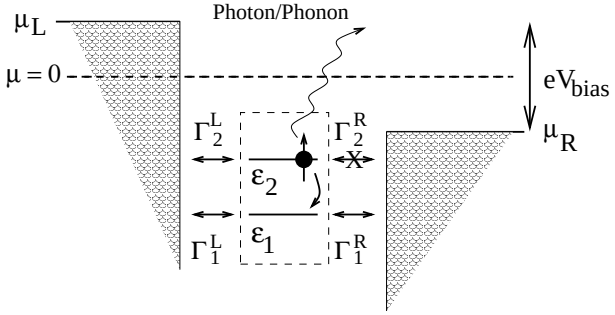

Figure 4.2: *Sketch of the two energy levels for model B. [Here no excitation spectrum is depicted, since there would be 16 excitation energies. The relevant excitation energies considered for this model are explained in the text.] The coupling parameters and an example for a relaxation process are indicated for a finite bias situation.*

due to photons we choose a power law behavior $\rho_{\rm b}(\omega) \propto \omega^3$, corresponding to photons with 3 spatial degrees of freedom. [Note that a diagonal coupling, $i = j$, would not be associated with relaxation but would give rise to 'boson-assisted tunneling', leading to additional steps in the I-V when the boson bath has a discrete spectrum [127, 128, 129].]

We take the coupling strength $\Gamma_r^{i\sigma}$ to be independent of the spin and write Γ_i^r (in order to distinguish from quadratic terms, which could appear for $i = 2$). Furthermore for equal tunneling couplings we choose $\Gamma_1^{\mathrm{L}} = \Gamma_1^{\mathrm{R}} = \Gamma_2^{\mathrm{L}} = \Gamma_2^{\mathrm{R}} = \Gamma$.

Model B therefore contains five different coupling parameters (Γ_i^r and α_{ph}). This is illustrated in Fig. 4.2, where the couplings to the two levels with energies $\varepsilon_1, \varepsilon_2$ and an example for a relaxation process with strength α_{ph} are indicated for a finite bias situation.

Concerning the energy parameters we limit ourselves to a vanishing Zeeman splitting ($\Delta = 0$) and therefore we find $k_{\mathrm{B}}T, \varepsilon_1, \varepsilon_2, U$ and E_C as parameters which we express in terms of Γ. We also choose the temperature of the photonic bath to be the same as the one of the electronic reservoirs ($T_b = T$).

In the case of the two level model we find 16 (4^N with ($N = 2$)) different many-body dot states. Model B is discussed in chapter 4.2.2.

C) The ***third model*** we want to consider describes a series of coupled quantum dots ('artificial molecule') and can be understood as a more realistic approximation to a molecular system with delocalized orbitals (levels). Results for this model are presented in chapter 4.4. In order to focus on the nature of the delocalized system we neglect again a coupling to a bosonic bath and choose $H_B = H_{B-D} = 0$. The dot Hamiltonian reads

$$H_{\mathrm{D}} = \varepsilon \sum_{i\sigma} c_{i\sigma}^\dagger c_{i\sigma} - t \sum_{(i\neq j)\sigma} c_{i\sigma}^\dagger c_{j\sigma} + U \sum_i n_{i\uparrow} n_{i\downarrow} + U_{nn} \sum_{(i\neq j)\sigma\sigma'} n_{i\sigma} n_{j\sigma'}, \tag{4.7}$$

with $i, j = 1...N$. We take $N = 3$, leading to 64 many-body states of the dot system.

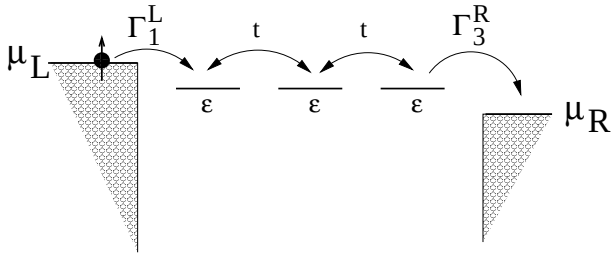

Figure 4.3: *Sketch of model C describing three coupled quantum dots (delocalized levels) with energy ε. Nearest neighbor hopping t and the two coupling parameters are indicated as well.*

We define the following energy parameters besides a temperature $k_{\mathrm{B}}T$: an on-site energy ε of the three dots, a nearest neighbor hopping t, an intra-dot U and a nearest neighbor inter-dot Coulomb repulsion U_{nn}. As the only non-vanishing dot-electrode coupling constants we choose $\Gamma_1^{\mathrm{L}} = \Gamma_3^{\mathrm{R}} = \Gamma/2$, meaning that the electrodes only couple to the adjacent dots.

4.2 Sequential tunneling

Current and shot noise within the sequential tunneling picture have been studied in a variety of systems (for example in Refs. [6, 7, 63, 64, 149, 150, 151]). Here we want to provide an overview over the main features to be expected when a weak coupling situation (first order Γ) determines the transport in mesoscopic systems. Possible candidates have been discussed in chapter 2 with the semiconductor quantum dots and the theoretical approach has been introduced in chapter 3 together with a discussion of the range of validity of this theory. However, we remind once again of the applicability of the following results to molecules as well, although we mostly use the technical language for descriptions of quantum dot structures. The expression of all parameters in terms of Γ allows for an appropriate choice of scales for quantum dots or molecules. Since the coupling parameter Γ in 'orthodox theory' has to be small compared to all energy parameters including the temperature, we choose $k_{\mathrm{B}}T = 10\Gamma$ in this section. We begin with the discussion of the Anderson impurity model (A) as introduced before and consider an extension to a multi-level system (B) after that.

4.2.1 Single-level systems

Normal leads

We choose a set of energy parameters: $\varepsilon = 150\Gamma$, $\Delta = 100\Gamma$ (or equivalently $\varepsilon_\downarrow = 100\Gamma, \varepsilon_\uparrow = 200\Gamma$) and $U = 400\Gamma$ for a single level quantum dot coupled to normal leads (model A3). Current $I^{(1)}$ and shot noise $S^{(1)}$ are plotted vs. the bias voltage V_b in Fig. 4.4. Electron transport becomes possible when charge excitations on the dot become energetically allowed. Generally, at low bias, transport is exponentially suppressed, unless a degeneracy of states with different net charge is present (this could be tailored by the application of a gate voltage, which we do not consider here). Each time when one of the four excitation energies $\varepsilon_\downarrow = (\varepsilon - \Delta/2)$, $\varepsilon_\uparrow = (\varepsilon + \Delta/2)$, $\varepsilon_\downarrow + U = (\varepsilon - \Delta/2 + U)$, or $\varepsilon_\uparrow + U = (\varepsilon + \Delta/2 + U)$ enters the energy window defined by the electrochemical potentials of the electrodes, a transport channel opens. This gives rise to plateaus, separated by thermally broadened steps. Due to the symmetric application of the bias, and the special scaling of the bias voltage as $eV_b/2\Gamma$, the steps occur at voltages of the corresponding excitation energy. The plateau heights depend on the coupling parameters Γ_{L} and Γ_{R} only, i.e. they are independent of U and T. This is the case since the excitation energies are large compared to the temperature and thus the region of broadening. This allows to extract analytic expressions for current, noise, and Fano factor (given in Tab. 4.1) of the different plateaus (labeled by $i = 0, ..., 4$).

The curves in Fig. 4.4 are normalized to $I_{\mathrm{norm}} = (e/\hbar)\Gamma/2$ and $S_{\mathrm{norm}} = (e^2/\hbar)\Gamma/2$, respectively. These values are reached in the large bias regime for symmetric couplings

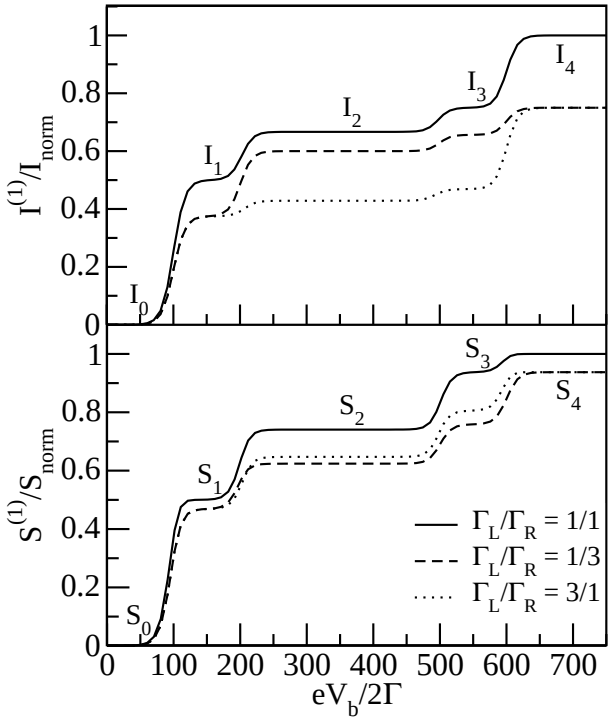

Figure 4.4: *Current $I^{(1)}$ and shot noise $S^{(1)}$ vs. bias voltage for energy parameters $\varepsilon_\downarrow = 100\Gamma, \varepsilon_\uparrow = 200\Gamma$ and $U = 400\Gamma$. The temperature is chosen to be $k_B T = 10\Gamma$ here and for the whole section 4.2. We find current and shot noise to be suppressed for asymmetric coupling compared to the symmetric one: $\Gamma_\mathrm{L}/\Gamma_\mathrm{R} = 1/1$ (solid line), 1/3 (dashed line) and 3/1 (dotted line). The height of the plateaus labeled by $i = 0, .., 4$ are given in Tab. 4.1. The curves are normalized to $I_\mathrm{norm} = (e/\hbar)\Gamma/2$ and $S_\mathrm{norm} = (e^2/\hbar)\Gamma/2$, respectively.*

$\Gamma_\mathrm{L} = \Gamma_\mathrm{R}$. For asymmetric coupling, the plateaus are reduced in height. In Fig. 4.4, we show the results for $3\Gamma_\mathrm{L} = \Gamma_\mathrm{R}$ (dashed lines) and $\Gamma_\mathrm{L} = 3\Gamma_\mathrm{R}$ (dotted lines) together with the case of symmetric coupling (equivalent to choices $a = 0.25$ and $a = 0.75$ in model A3). The symmetry of our setup implies that all plateau heights are invariant under simultaneous exchange of Γ_L with Γ_R and μ_L with μ_R. However, the plateau height can change if only Γ_L and Γ_R are exchanged, or if only the bias voltage is reversed, as shown in our example for the two plateaus labeled by 2 and 3. This opens the possibility to access the asymmetry $\Gamma_\mathrm{L}/\Gamma_\mathrm{R}$ experimentally by reversing the bias voltage and comparing the plateau heights. The fact that the plateau heights are not symmetric under exchange of $\Gamma_\mathrm{L} \leftrightarrow \Gamma_\mathrm{R}$ is an immediate consequence of the interaction U. For non-interacting systems, the plateau values would be symmetric.

Fig. 4.4 shows the result for one special choice of energy parameters and corresponding excitation energies. Nevertheless, Tab. 4.1 is complete in the sense that it contains all possible plateau values for any configuration of the excitation energies relative to the

i	0	1	2	3	4
I_i $[e/\hbar]$	0	$\frac{\Gamma_L\Gamma_R}{\Gamma_L+\Gamma_R}$	$\frac{2\Gamma_L\Gamma_R}{2\Gamma_L+\Gamma_R}$	$\frac{\Gamma_L\Gamma_R(\Gamma_L+2\Gamma_R)}{(\Gamma_L+\Gamma_R)^2}$	$\frac{2\Gamma_L\Gamma_R}{\Gamma_L+\Gamma_R}$
S_i $[e^2/\hbar]$	0	$\frac{2\Gamma_L\Gamma_R(\Gamma_L^2+\Gamma_R^2)}{(\Gamma_L+\Gamma_R)^3}$	$\frac{4\Gamma_L\Gamma_R(4\Gamma_L^2+\Gamma_R^2)}{(2\Gamma_L+\Gamma_R)^3}$	$\frac{2\Gamma_L\Gamma_R(2\Gamma_R+\Gamma_L)(\Gamma_L^3+\Gamma_R^3+3\Gamma_L^2\Gamma_R)}{(\Gamma_L+\Gamma_R)^5}$	$\frac{4\Gamma_L\Gamma_R(\Gamma_L^2+\Gamma_R^2)}{(\Gamma_L+\Gamma_R)^3}$
F_i	–	$\frac{\Gamma_L^2+\Gamma_R^2}{(\Gamma_L+\Gamma_R)^2}$	$\frac{4\Gamma_L^2+\Gamma_R^2}{(2\Gamma_L+\Gamma_R)^2}$	$\frac{\Gamma_L^3+\Gamma_R^3+3\Gamma_L^2\Gamma_R}{(\Gamma_L+\Gamma_R)^3}$	$\frac{\Gamma_L^2+\Gamma_R^2}{(\Gamma_L+\Gamma_R)^2}$

Table 4.1: *Current, shot noise and Fano factor for the different plateaus in the current-voltage characteristic shown in Fig. 4.4. The plateau values depend only on the coupling parameters* $\Gamma_{L,R}$.

electrochemical potentials of the electrodes. The classification of the configurations and the algorithm to find the corresponding analytic expressions in Tab. 4.1 is given in Tab. 4.2. Without loss of generality we restrict ourselves to $U \geq 0$ and $\varepsilon_\uparrow \geq \varepsilon_\downarrow$ (which is equivalent to $\Delta \geq 0$). The different configurations are classified by specifying which excitation energies lie within the energy window defined by the chemical potentials μ_L, μ_R. We find 13 different possibilities, as listed in Tab. 4.2. For each case, the index i indicates the column where the corresponding analytic expressions for current, noise and Fano factor can be found in Tab. 4.1. The indices 2^* and 3^* refer to columns 2 and 3 but with Γ_L and Γ_R being exchanged.

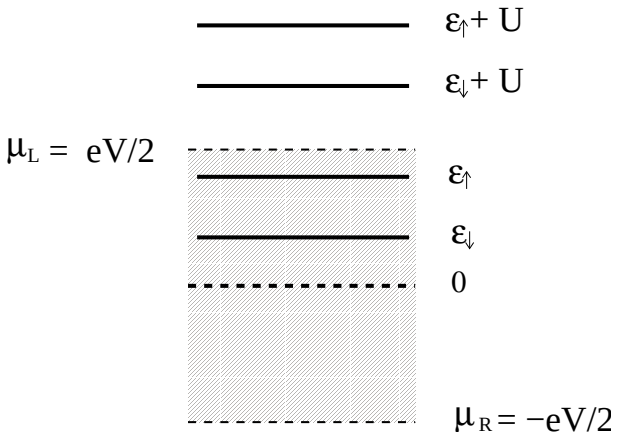

Figure 4.5: *A sketch of the configuration 2a listed in Tab. 4.2. The excitation energies* $\varepsilon_\downarrow$ *and* $\varepsilon_\uparrow$ *lie in the energy window defined by the electrochemical potentials* μ_L *and* μ_R*, and the energies* $\varepsilon_\downarrow + U$ *and* $\varepsilon_\uparrow + U$ *lie outside.*

In order to illustrate the use of the table we sketch the situation 2*a* in Fig. 4.5, realized

Case	$\epsilon_\downarrow$	$\epsilon_\uparrow$	$\epsilon_\downarrow + U$	$\epsilon_\uparrow + U$	i
0	-	-	-	-	0
$1a$	x	-	-	-	1
$1b$	-	x	-	-	0
$1c$	-	-	x	-	0
$1d$	-	-	-	x	1
$2a$	x	x	-	-	2
$2b$	x	-	x	-	1
$2c$	-	x	x	-	0
$2d$	-	x	-	x	1
$2e$	-	-	x	x	2^*
$3a$	x	x	x	-	3
$3b$	-	x	x	x	3^*
4	x	x	x	x	4

Table 4.2: *Classification of all possible configurations that are possible for $U \geq 0$ and $\varepsilon_\uparrow \geq \varepsilon_\downarrow$ ($\Delta \geq 0$). A cross (x) or minus (−) indicates that the corresponding excitation energy lies within or outside the energy window defined by the electrochemical potentials μ_L and μ_R, respectively. For each configuration, the analytic expression for current, noise and Fano factor can be found in Tab. 4.1 in column i. The indices 2^* and 3^* refer to column 2 and 3 with Γ_L and Γ_R being exchanged.*

in Fig. 4.4 in the region between $eV_b/2\Gamma = 200$ and 500. In this situation transport through both spin states is present as the single level gets charged/uncharged in the sequential tunneling events. Double occupancy is still out of reach, as the excitation energies $\varepsilon_\downarrow + U$ and $\varepsilon_\uparrow + U$ are outside the energy window opened by the applied voltage. [We use the notation of energies for the different spin states instead of the splitting Δ, in order to easier identify the position of excitation energies. The notation in terms of a spin-splitting Δ will be more convenient for the discussion of second order transport.]

For an arbitrary choice of energy parameters and bias voltage we can therefore identify one of the 13 cases as indicated in Tab. 4.2. The table then tells us, in which column of Tab. 4.1 the expressions of current, noise and Fano factor can be found. We will show in the following, that the same parameter extraction can be done in the case of

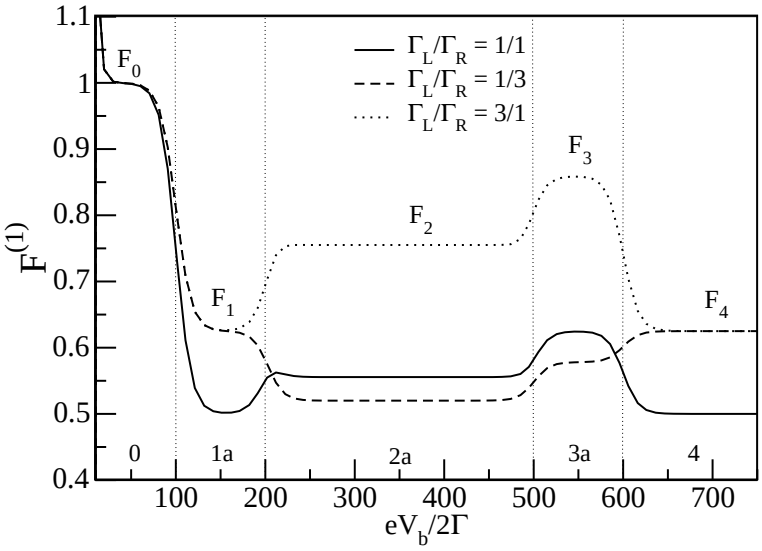

Figure 4.6: *Fano factor vs. bias voltage for for the same parameters as in Fig. 4.4 and* $\Gamma_{\rm L}/\Gamma_{\rm R}$ *= 1/1 (solid line), 1/3 (dashed line) and 3/1 (dotted line). The labels* $0, 1a, 2a, 3a, 4$ *refer to the cases listed in Tab. 4.2*

spin-dependent transport for the different configurations as introduced with the models A1 and A2.

We now turn to the discussion of the Fano factor $F^{(1)} = S^{(1)}/2eI^{(1)}$. In Fig. 4.6 we show the Fano factor as a function of bias voltage for the same parameters as in Fig. 4.4. Again we show three curves with $\Gamma_{\rm L}/\Gamma_{\rm R} = 1/1$ (solid line), 1/3 (dashed line) and 3/1 (dotted line). At small bias, $eV_b \ll k_{\rm B}T$, the noise is dominated by thermal noise, described by the well-known hyperbolic cotangent behavior which leads to a divergence of the Fano factor [5, 104], as we discussed in chapter 2 as well. The plateau for bias voltages below $eV_b/2\Gamma = 100$ corresponds to the Coulomb-blockade regime, where transport is exponentially suppressed (case 0 in Tab. 4.2). In the region between $eV_b/2\Gamma = 100$ and 200 (case $1a$) transport through only one spin state ($\downarrow$) is possible. The Fano factor F_1 for this case has been derived earlier in Ref. [28]. For very large bias (region F_4), all states of the single level are involved in transport, and the Fano factor F_4 is again identical to the well-known [5] formula for transport through a resonant level in the absence of Coulomb charging energy.

For the regions in between, corresponding to the cases $2a$ and $3a$, the Fano factor is different. The expression for F_2 has been derived in Ref. [146], while F_3, corresponding to region $3a$, has been presented in one of our former publications [6]. On similar grounds than for the current and the noise, we find that the expressions for the Fano factors F_2 and F_3 are not invariant under exchange of $\Gamma_{\rm L}$ and $\Gamma_{\rm R}$ alone, and also not invariant under reverse of the bias voltage alone. This is clearly seen in Fig. 4.6 in the very different plateau heights of the dotted and dashed curves, corresponding to

exchange of Γ_L and Γ_R. Furthermore, we see that all plateau heights lie between 1/2 and 1, and that the Fano factor, in general, is a non-monotonic function of the bias voltage. We find that $F_1 = F_4$ and $F_3 \geq F_2$ always holds, whereas $F_1 \geq F_2$ for $\Gamma_L/\Gamma_R \leq 1/\sqrt{2}$, and $F_1 \geq F_3$ for $\Gamma_L/\Gamma_R \leq 1/2$ only.

As a consequence, the pattern of the plateau sequence, in particular the relative height of the plateaus F_2 and F_3 compared to $F_1 = F_4$ indicate not only the presence of an interaction or charging energy, but also give *over-complete* information on the ratio Γ_L/Γ_R of the coupling strengths. This could be used in experiments to determine these parameters in a consistent way. In an experiment observing more than one plateau, the over-completeness would give narrow constraints (due to experimental uncertainty) on whether a single interacting level can explain the measured values. Of course, it is always possible to fit n plateaus with n non-interacting levels and different couplings per level, so an absolute decision on the presence of interactions is not possible without the additional application of a gate voltage. However, if a fit with an interacting level is feasible, the principle of parsimony should favor the model with fewer parameters.

In addition, we observe that sometimes a peak in the Fano factor shows up. This happens, for example, at the step between F_1 and F_2 for $\Gamma_L = \Gamma_R$, as seen in Fig. 4.6. The peak height 0.5625 exceeds that of the adjacent plateaus, 1/2 and 5/9. These features can even appear in the regime of negligible Coulomb charging energy, as previously shown in Ref. [63]. However, we point out that the behavior at the steps is going to be strongly affected by second-order tunneling events, as will be discussed in section 4.3. For example, the current steps will show additional broadening due to the intrinsic line width Γ. The plateau values, on the other hand, will mostly not be affected by second order effects. However, we will show that this is not the case in the Coulomb-blockade regime, since here second order effects will dominate the first order processes. This is, why we did not give values for the Fano factor in Tab. 4.1 for the plateau number 0. But also in the regime of finite bias voltage, deviations to the first order predictions may appear, when higher order processes gain importance over the first order ones (for example due to suppression of sequential tunneling because of asymmetric couplings).

We therefore may summerize the ***main features of first order transport*** as follows:

I) The electronic structure of the system, defined by ***energy parameters*** will always determine the ***step positions*** of the transport curves, connecting two regions with different number of 'transport channels'. The number of such steps is therefore directly linked to the number of transport channels or excitation energies.

II) The steps are broadened only by the ***temperature***. This ***broadening*** has been found in literature to be around 5.44 $k_B T$. The relatively large broadening with a factor of 5.44 is due to the fact that the Fermi functions do not determine directly the current and shot noise. The transport curves are composed of transition rates and probabilities in a non-linear way, where a temperature broadening enters as well. The

temperature is controlled reasonably well in experiment and therefore reflects another fixed parameter.

III) The ***coupling parameters***, being the last free parameters in our model, determine the ***plateau heights*** of the transport curves and can be determined, when all of the other parameters have been fixed. As discussed in chapter 2 and as we confirmed here, for the Fano factor values between 1/2 and 1 are typical ('sub-Poissonian noise'). In general however more than only two coupling parameters can determine the transport through the mesoscopic region. Even for the single level Anderson model, there may be four parameters, when considering the couplings to be spin dependent. But also for this spin-dependent model analytical expressions of the plateaus can be derived (see Tabs. 4.3, 4.4, 4.5, 4.6). In the low bias regime the first plateaus contributing to transport can be determined from the expressions we discuss in our tables. This is valid also for a system with more than one level and thus helpful to study even multi-level systems containing a large number of free coupling parameters. An iterative determination of additional parameters, when considering additional plateaus at larger bias can be imagined. A comparison of plateaus at positive and negative bias for the current, shot noise and the Fano factor helps to definitely fix these parameters.

IV) The only regime, where ***'orthodox theory' fails*** in a sense, is the ***Coulomb-blockade regime***. Aside of the qualitative prediction of a transport blockade only for sufficiently large temperatures we can trust the predictions. Here, second order calculations are unavoidable if a quantitative description of transport is asked for. We will continue the discussion of this point therefore in section 4.3, where second order results are presented.

The features I-III can be studied on the basis of a first order theory, and IV needs the application of second order calculations. There are two further features of particular interest, which have to be discussed within a complete picture considering sequential as well as co-tunneling processes, since an interplay of both kinds of effects will become important.

V) As we have seen, there may appear peaks in the Fano factor in the regions of the broadened steps. A peak and even a ***peak-dip structure*** can be observed under certain conditions even in the shot noise. Here we are in a region, which will be affected by stronger coupling to the electrodes. It therefore depends on the absolute height (depth) of such a structure as well as the stability of this effect, whether first or second order (or both) will give rise to such a behavior. Such an interplay of first and second order processes will be relevant especially in the crossover from the Coulomb-blockade to the finite bias regime. We will therefore discuss this point in more detail in section 4.3.

VI) Finally the presence of a finite ***Coulomb interaction*** accompanied by ***asymmetric coupling*** parameters can lead to the most striking effects in transport. In the

current a negative differential conductance (NDC) and in the noise a strong suppression or a large enhancement may be observed. Besides the typical values between 1/2 and 1, the Fano factor may show super-Poissonian ($F > 1$) or sub-Poissonian behavior with values even below 1/2. The identification of physical mechanisms leading to such a behavior will be our concern for the rest of this chapter. We will discuss several systems, where such 'anormalous' transport behavior arises.

Magnetic leads

In section 4.1, we introduced the models A1 and A2, allowing for a description of a single level system coupled to magnetically polarized leads. In Fig. 4.7 the effect of finite polarization on the coupling to the leads is illustrated for the anti-parallel (AP) and the two parallel ($P^{\pm}$) configurations. For sake of simplicity we indicate only

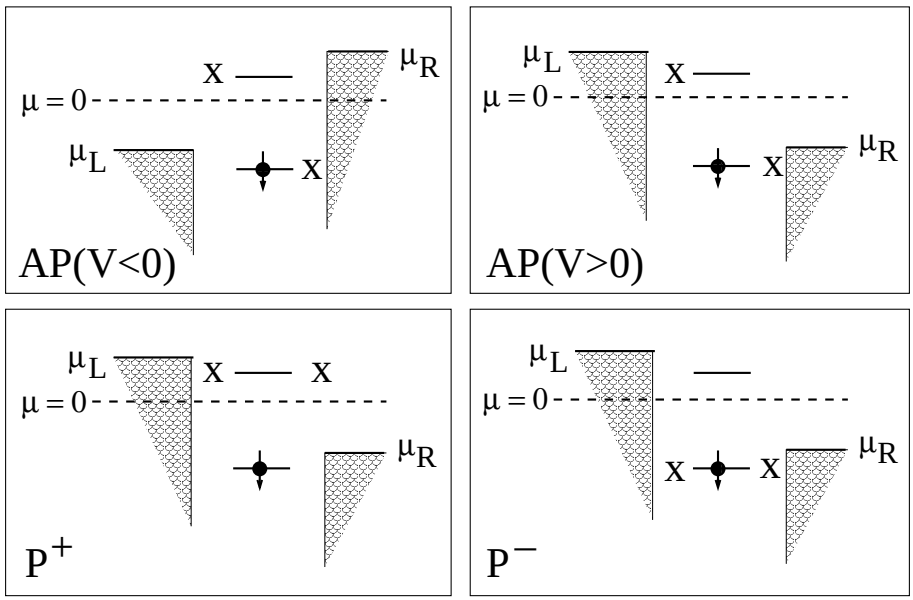

Figure 4.7: *Sketch of the different spin-polarization configurations as introduced in model A1. Crosses indicate which coupling parameters are suppressed with respect to the others for a finite polarization. The anti-parallel configuration AP is illustrated in the upper panel for a negative (left side) and a positive (right side) bias situation. The two parallel configurations $P^{\pm}$ (lower panel) have symmetric behavior if the bias is reversed.*

the two lowest excitation energies of this model ($\varepsilon_{\downarrow}$ and $\varepsilon_{\uparrow}$). The sketches have to be understood in such way that the lower line defines the energy, where transitions between states $\downarrow \leftrightarrow 0$ are allowed and the upper one, where transitions between states $\uparrow \leftrightarrow 0$ are allowed. The crosses in Fig. 4.7 indicate which coupling parameters are suppressed with respect to the others for a finite polarization. It thus becomes immediately clear

i	0	1	2	3	4
I_i $[e/\hbar]$	0	$\frac{(1-p^2)}{2}$	$\frac{2(1-p^2)}{(3+p^2)}$	$\frac{(3\mp p-3p^2\pm p^3)}{4}$	$(1-p^2)$
S_i $[e^2/\hbar]$	0	$\frac{(1-p^4)}{2}$	$\frac{4(1\pm p)(5\mp 5p+14p^2\mp 14p^3-3p^4\pm 3p^5)}{(3+p^2)^3}$	$\frac{(15\pm 4p-9p^2\mp 16p^3-3p^4\pm 12p^5-3p^6)}{16}$	$(1-p^4)$
F_i	–	$\frac{(1+p^2)}{2}$	$\frac{(5+14p^2-3p^4)}{(3+p^2)^2}$	$\frac{(5\pm 3p+3p^2\mp 3p^3)}{8}$	$\frac{(1+p^2)}{2}$

Table 4.3: *Current, shot noise and Fano factor for the different plateaus as discussed in Tab. 4.1 for the anti-parallel configuration (AP). Current and shot noise are normalized to I_{norm} and S_{norm}, such that the plateau values depend only on the polarization. The upper (lower) sign is due to a positive (negative) bias.*

that the two parallel configurations will show a symmetric behavior upon reversing of the bias voltage (exchange of μ_{L} and μ_{R}), whereas the anti-parallel configuration does not. Equivalently we can understand the configurations as introduced with the model A2 (F-D-N, N-D-F) to have fixed couplings on either the left or the right side, whereas the opposite side may be polarized, by reducing the coupling to the spin $\uparrow$ or $\downarrow$.

Analytic expressions for the possible plateaus of the magnetic systems are found in the same way as for the single level system with normal leads. They are given in Tabs. 4.3, 4.4, 4.5, 4.6. The plateau heights are determined now by the strength of the polarization p, which may have values between 0 and 1. The values for the anti-parallel configuration are given in Tab. 4.3, where current and shot noise have been normalized to the values they would reach in the large bias regime in the unpolarized case (I_{norm}, S_{norm}). These are the same values we introduced at the beginning of this section. It can be seen immediately, that for $p = 0$ the plateaus with number 4 lead to $I_4 = 1, S_4 = 1$ and $F_4 = 1/2$ as expected. The upper sign in Tab. 4.3 is due to a positive bias voltage and the lower sign due to a negative one. The opposite choice of the anti-parallel configuration in A1 would hence be modeled by exchanging the upper and lower signs and therefore does not yield additional information. Tab. 4.3 can be used the same way as Tab. 4.1 and thus allows for a consideration of arbitrary transport situations, when using Tab. 4.2.

The results for the two parallel configurations are given in Tab. 4.4 correspondingly, where the upper sign is due to the configuration P^+, and the lower due to P^-. The expression are the same for negative and positive bias.

For the F-D-N and N-D-F configurations the plateau values are shown in Tabs. 4.5

i	0	1	2	3	4
I_i $[e/\hbar]$	0	$\frac{(1\pm p)}{2}$	$\frac{2}{3}$	$\frac{(3\pm p)}{4}$	1
S_i $[e^2/\hbar]$	0	$\frac{(1\pm p)}{2}$	$\frac{4}{27}\frac{(5+3p^2)}{(1-p^2)}$	$\frac{(15\pm 13p+5p^2\mp p^3)}{16(1\pm p)}$	1
F_i	–	$\frac{1}{2}$	$\frac{1}{9}\frac{(5+3p^2)}{(1-p^2)}$	$\frac{(15\pm 13p+5p^2\mp p^3)}{8(1\pm p)(3\pm p)}$	$\frac{1}{2}$

Table 4.4: *Current, shot noise and Fano factor for the different plateaus as discussed in Tab. 4.1 for the parallel configuration. The plateau values depend only on the polarization. The upper (lower) sign is due to the configuration P^+ (P^-).*

and 4.6. Here, the upper signs reflect situations of suppressed couplings to the spin $\uparrow$ and the lower signs reflect situations of suppressed couplings to the spin $\downarrow$. The tables describe the transport at positive finite bias. It can be verified again because of symmetry reasons, that the plateaus for the negative bias region can be extracted, by exchanging the two tables.

As a consistency check for a vanishing polarization and symmetric choice of the left and right coupling to the reservoirs, all expressions presented in the five tables Tabs. 4.1, 4.3, 4.4, 4.5, 4.6 give the same values.

It is clear that the different tables presented above provide a lot of information, which could be visualized in a large number of plots. However our main interest consists in a discussion of physical mechanisms leading to a behavior of the current, shot noise and the Fano factor different to what has been found so far. An example of such 'anormalous' behavior would be, if the normalized current and shot noise show a non-monotonic behavior for a sequence of plateaus (NDC or negative differential noise), have values larger than unity (enhancement) or if the Fano factor has values others than between 1/2 and 1.

Let us use the same energy parameters as used for the discussion of Fig. 4.4. In this case the sequence of plateau values is given in the same order as presented in the tables. For the two parallel configurations in Tab. 4.4 we find a non-monotonic behavior in the current for larger polarization of the leads. A NDC behavior is found for the configuration P^+ between the first and second plateau, where in an extreme case ($p \to 1$) the current drops down from a value 1 to 2/3. For the negative configuration P^- this behavior can be seen between the plateaus two and three, where the current drops down from 2/3 to 1/2 for strong polarization. For the shot noise we find a strong

i	0	1	2	3	4
I_i $[e/\hbar]$	0	$\frac{(1\pm p)}{(2\pm p)}$	$\frac{2}{3}$	$\frac{(3-p^2)}{(4-p^2)}$	$\frac{2(2-p^2)}{(4-p^2)}$
S_i $[e^2/\hbar]$	0	$\frac{2(1\pm p)(2\pm 2p+p^2)}{(2\pm p)^3}$	$\frac{20}{27}$	$\frac{(60\pm 4p-55p^2\mp 5p^3+17p^4\pm p^5-2p^6)}{(4-p^2)^3}$	$\frac{4(16-12p^2+2p^4-p^6)}{(4-p^2)^3}$
F_i	–	$\frac{(2\pm 2p+p^2)}{(2\pm p)^2}$	$\frac{5}{9}$	$\frac{60\pm 4p-55p^2\mp 5p^3+17p^4\pm p^5-2p^6}{2(4-p^2)^2(3-p^2)}$	$\frac{(16-12p^2+2p^4-p^6)}{(4-p^2)^2(2-p^2)}$

Table 4.5: *Current, shot noise and Fano factor for the different plateaus as discussed in Tab. 4.1 for a ferromagnet-dot-normal leads system (F-D-N). The upper (lower) sign is due to suppression of the coupling to spin ↑ (↓).*

enhancement (theoretically $S \to \infty$) for one or two plateaus. Due to the finite values of the current this implies a super-Poissonian Fano factor. Such a strong enhancement of the shot noise has been discussed in spin-dependent transport [152, 153, 154] and is due to a ***dynamical bunching*** of electrons. Consider the second plateau (for configuration P^+), where the super-Poissonian behavior shows up for the first time. On this plateau, the state with spin ↑ lies in the window for sequential transport (additionally to the other spin state) and contributes to the transport with about the same probability as the state with spin ↓. However, due to the blocking of the tunneling through the state with spin ↑ (compare with Fig. 4.7), many electrons with spin ↓ will tunnel through the system until once the spin ↑ state is realized. Due to suppressed coupling the dot stays in the spin ↑ state for a long time. Both spins contribute to transport but have a very different role. Note that this effect would not show up for a vanishing Coulomb-interaction (the plateau would not exist). The mechanism of bunching is therefore due to a finite interaction together with a finite polarization (asymmetry of coupling parameters).

Another mechanism leading to super-Poissonian behavior of the Fano factor can be found for the system coupled to a normal metal on the left, but to ferromagnetic leads on the right side (N-D-F as discussed in Tab. 4.6). NDC is found when the spin state with the larger energy (spin ↑) is suppressed, as can be seen from the sequence of plateaus one and two. Here, the current and shot noise 'collapses' (for $p \to 1$), although transport through the lower spin state ↓ is possible in principle (transport through state ↑ would be possible in the absence of polarization). However, due to the suppressed coupling of the state with spin ↑ to the right reservoir, the probability to be in this state is practically unity and since double occupancy is still energetically forbidden,

i	0	1	2	3	4
I_i $[e/\hbar]$	0	$\frac{(1\pm p)}{(2\pm p)}$	$\frac{2(1-p^2)}{(3-p^2)}$	$\frac{(3\pm p-2p^2)}{(4-p^2)}$	$\frac{2(2-p^2)}{(4-p^2)}$
S_i $[e^2/\hbar]$	0	$\frac{2(1\pm p)(2\pm 2p+p^2)}{(2\pm p)^3}$	$\frac{4(1-p^2)(5+6p^2+p^4)}{(3-p^2)^3}$	$\frac{(60\mp 72p+33p^2\mp 18p^3+11p^4\mp 4p^5)(1\pm p)}{(4-p^2)^3}$	$\frac{4(16-12p^2+2p^4-p^6)}{(4-p^2)^3}$
F_i	–	$\frac{(2\pm 2p+p^2)}{(2\pm p)^2}$	$\frac{(5+6p^2+p^4)}{(3-p^2)^2}$	$\frac{(60\mp 72p+33p^2\mp 18p^3+11p^4\mp 4p^5)}{2(4-p^2)^2(3\mp 2p)}$	$\frac{(16-12p^2+2p^4-p^6)}{(4-p^2)^2(2-p^2)}$

Table 4.6: *Current, shot noise and Fano factor for the different plateaus as discussed in Tab. 4.1 for a normal-dot-ferromagnet system (N-D-F).The upper (lower) sign is due to suppression of the coupling to spin ↑ (↓).*

the other spin state is blocked. The origin of this ***blocking effect*** is due to a finite Coulomb interaction and asymmetric coupling to the reservoirs again, although the shot noise behaves the opposite way as before. The finite super-Poissonian value of the Fano factor ($F_2 = 3$ for $p = 1$ in Tab. 4.6) can be explained by the second term of the shot noise formula in first order (see chapter 3), which describes a propagation between two current events. This propagator involves processes leading into an empty state, which allows to tunnel onto the dot system again. However the dot will immediately be occupied by the spin ↑ state again. This is why the shot noise is a factor larger compared to the current, but vanishes as well (as $p \to 1$). The effect is destroyed again at a bias voltage, where the Coulomb interaction can be overcome energetically and transport via the doubly occupied state sets in.

This blocking effect is, in principle, very similar to the processes that lead to a super-Poissonian noise in the Coulomb-blockade regime. Here, the propagator can lead the system into an empty state, however the ground state will be occupied immediately again. In our example above we are in a finite bias situation, such that the current and shot noise are not suppressed exponentially as in the Coulomb-blockade. However, strong polarization may suppress processes in first order algebraically, where second order processes are still unaffected. Hence, a complete picture of sequential and co-tunneling processes may be important as $p \to 1$.

To ***summarize*** our findings, we characterized the current, shot noise and Fano factor for a single level system for arbitrary transport situations in lowest order. In the case of spin-dependent transport we identified two mechanisms leading to a super-Poissonian noise. The current in this case can show a NDC behavior, which however is not necessary for a super-Poissonian Fano factor. The noise may be strongly suppressed or enhanced. These mechanisms require a finite Coulomb interaction and an asymmetric

coupling situation giving rise to a dynamical bunching of electrons or the blocking of transport.

Current and shot noise in nanoscopic systems coupled to ferromagnetic leads have been studied theoretically in first order of the coupling to the leads in [152, 153, 154, 155, 156, 157, 158], for coherent transport in [159, 160] or diffusive wires with diffusion equations in [161]. Experimental work is mainly concerned with spectroscopy [162, 163]. Studies going beyond a first order approach are rare or still missing, especially for the shot noise.

In section 4.3.2 we will therefore discuss second order (co-tunneling) results for the current, shot noise and Fano factor, completing the limited sequential tunneling picture of first order. The tables presented in this section may serve as additional background to our discussion there. The model Hamiltonian A we considered here, is the simplest one that exhibits mechanisms leading to super-Poissonian noise. However, more than two coupling parameters are necessary to describe such a behavior. As we will see in the next section, a mapping onto a two-level system is relatively simple, in lowest order, leading to similar effects as we identified above.

4.2.2 Multi-level systems

We want to study a multi-level system as introduced with model B. The difference to a single level system is obviously a larger number of available states (transition channels), but also the possibility to include other kinds of interactions. The consideration of a charging energy E_C (energy cost to add an electron to the system) in addition to the 'Hubbard' interaction U (energy cost to doubly occupy a certain level) allows for a separation of different charge sectors (for the single level model the energies ε, U can account for the effect of E_C). This is also the simplest model allowing to describe relaxation effects, due to emission or absorption of bosons. This allows to study another kind of effects in quantum dots or molecules, and to identify the physics, which is typical for these kinds of effects.

We consider a system which is uncharged at zero bias, with energy parameters $\varepsilon_1 = -100\Gamma$, $\varepsilon_2 = 100\Gamma$, $U = 300\Gamma$ and $E_C = 200\Gamma$. The temperature is chosen to be $k_{\mathrm{B}}T = 10\Gamma$ again. An illustrative sketch of the system under study has been given in Fig. 4.2. The energy to occupy the first single particle level is $\varepsilon_1 + E_c = 100\Gamma$ (state D_1). Without coupling to the boson bath we find a negative differential conductance (NDC) regime, see Fig. 4.8 in dependence on the different coupling strength of the two levels and the reservoirs, as was previously discussed in Refs. [120, 164, 151, 150] and as we found also in the last section. The shot noise behaves qualitatively similar. If we chose equal tunnel coupling, $\Gamma_i^r = \Gamma$ (solid line), we find that current and shot noise $S^{(1)}$ increase, each time as a new transport "channel" (controlled by the excitation

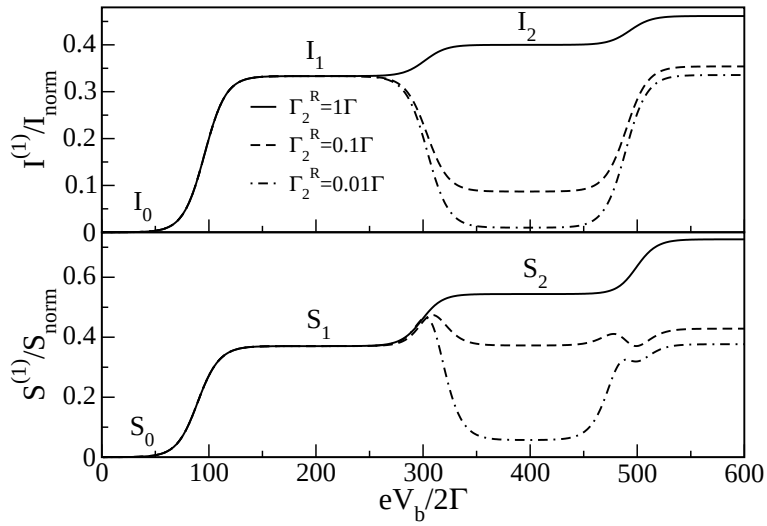

Figure 4.8: *Current $I^{(1)}$ and shot noise $S^{(1)}$ vs. voltage for the energy parameters as discussed in the text, symmetric bias and $\Gamma_1^{\rm L} = \Gamma_2^{\rm L} = \Gamma_1^{\rm R} = \Gamma$. The height of the plateaus labeled by $i = 0, 1, 2$ are discussed in the text and depend on the choice of the coupling parameters. For suppressed coupling $\Gamma_2^{\rm R}$ current and shot noise break down leading to negative differential conductance (NDC) at a threshold energy. The curves are normalized to $I_{\rm norm} = (e/\hbar)2\Gamma$ and $S_{\rm norm} = (e^2/\hbar)2\Gamma$, respectively.*

energies) opens. This leads to plateaus, separated by thermally broadened steps. The first four plateaus are shown and discussed in the following. At a bias voltage of $eV_b/2\Gamma = 100$, sequential transport through the state D_1 with one electron on the lower lying level becomes possible. At $eV_b/2\Gamma = 300$, additionally transport through the D_2 state opens up, with the upper level being occupied with one electron. The different regions of interest are labeled by I_i, S_i with $i = 0, 1, 2$. For a bias voltage above $eV_b/2\Gamma = 500$, transport channels with two or more electrons on the system open up. In the large-bias regime (not indicated in the plots) and for symmetric coupling, the values $I_{\rm norm} = (e/\hbar)2\Gamma$ and $S_{\rm norm} = (e^2/\hbar)2\Gamma$ are reached (note that due to the choice of the couplings, the sum of all electrode couplings is 4Γ and not Γ, which leads to other normalization factors as before).

If now the coupling parameter $\Gamma_2^{\rm R}$ is suppressed with respect to the other couplings, this leads to suppressed curves for the current and shot noise in region 2, resulting in NDC at the threshold of $eV_b/2\Gamma = 300$, when the state D_2 becomes relevant, see in Fig. 4.8 for $\Gamma_2^{\rm R} = 0.1\Gamma$ and 0.01Γ. The reason for the NDC is a combination of the Pauli principle, Coulomb blockade and suppressed coupling, as discussed in Ref. [120, 121]. It is, in principle, the same mechanism which led to the *blocking effect*, we discussed in the last section. In the present case, an electron, entering the upper level from the left electrode, cannot leave the system, if the coupling of this level to the right electrode is entirely suppressed. Transport through the lower level is also not possible, since

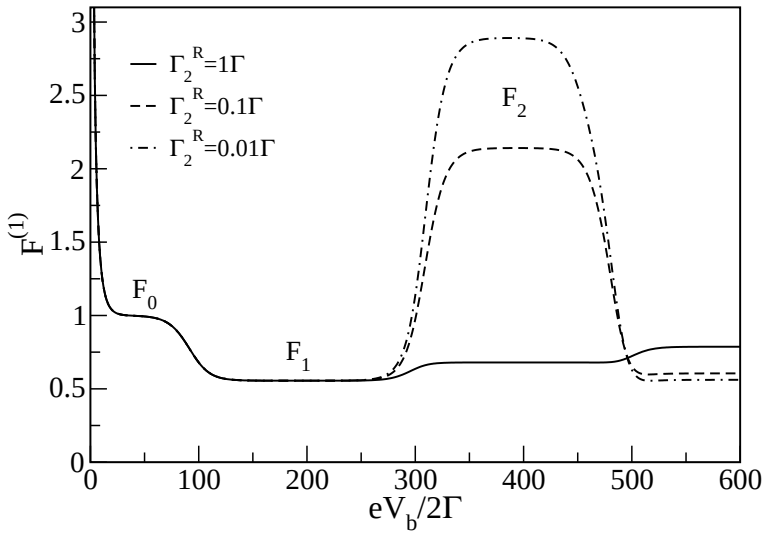

Figure 4.9: *Fano factor $F^{(1)}$ vs. bias voltage for the same parameters as in Fig. 4.8 and various coupling parameters Γ_2^{R}. The NDC effect results in a super-Poissonian value for the Fano factor.*

the simultaneous occupation of both levels is energetically forbidden in the considered bias regime. The electron gets stuck in the upper level blocking other electrons from tunneling through the system. Consequently, the current collapses. Since in lowest-order perturbation theory in Γ the plateau *heights* are given by the coupling parameters only, we find, that for $\Gamma_2^{\mathrm{R}} < 2/3\Gamma$ NDC can be observed, whereas the shot noise is suppressed below its lower bias plateau only, if $\Gamma_2^{\mathrm{R}} < 0.1\Gamma$.

If the shot noise is sufficiently suppressed in the NDC region, a peak in the shot noise appears around the resonance energy of the second level. This peak is due to temperature induced fluctuations that in certain situations enhance the shot noise over the surrounding plateau values (where charge fluctuations due to temperature are exponentially suppressed). As the resonance is approached from lower bias, within the range of temperature broadening the noise "detects" the opening of the second transport channel and increases. If the bias is beyond the resonance, the redistribution of occupation has taken place and the noise is algebraically suppressed. The result is the observed peak in the noise with width of the temperature. However, the peak height is only determined by the coupling parameters and is independent of the temperature. The current never shows such a peak, as it decreases proportional to the loss of occupation of the first level, the transport channel with "good" coupling.

The effect of NDC on the Fano factor is shown in Fig. 4.9. The plateau for bias voltages below $eV_b/2\Gamma = 100$ (region 0) corresponds to the Coulomb blockade regime, where transport is exponentially suppressed. In the regions 1 (2) transport through the state D_1 (D_2) is possible. The suppressed coupling strength Γ_2^{R} does not affect the plateau height F_1, whereas F_2 reaches values larger then 1, and up to 3 [151].

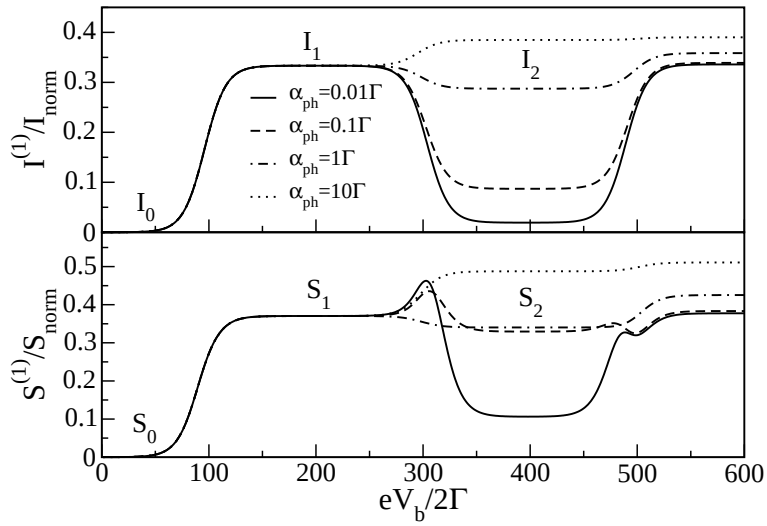

Figure 4.10: *Current I^1 and shot noise S^1 vs. voltage for the same parameters as in Fig. 4.8 but fixed coupling $\Gamma_2^{\rm R} = 0.01\Gamma$. Coupling to a bosonic bath allows for relaxation processes. The coupling parameter $\alpha_{\rm ph}$ which is varied relative to Γ. The NDC effect is destroyed by strong relaxation.*

This "super-Poissonian" noise ($F > 1$) is predicted for $\Gamma_2^{\rm R} < 0.44\Gamma$. If the bias is larger then $eV_b/2\Gamma = 500$ tunneling through states is allowed where both levels are occupied simultaneously, i.e. the system can be doubly occupied. The Fano factor is sub-Poissonian again ($F < 1$) in this regime. Comparing the Figs. 4.8 and 4.9 graphically allows one to determine roughly the strength of the suppression of $\Gamma_2^{\rm R}$.

Let us consider next the effect of relaxation processes on the current and shot noise curves. In Fig. 4.10 we keep the same set of energy parameters as in Fig. 4.8 and fix the coupling strength $\Gamma_2^{\rm R}$ at 0.01Γ suppressed relatively to the other dot-electrode couplings. Now a parameter $\alpha_{\rm ph}$ describes the coupling of the system with a boson bath. [A value of $\alpha_{\rm ph} = 0.01\Gamma$ is below even the relatively weak dipole coupling of photons to molecule states of small aromatic molecules such as benzene [121].] For this small photon coupling (solid line) current and shot noise are still reduced in region 2 relative to the plateau heights $I_1 = 1/3$ and $S_1 = 10/27$ in region 1. If now $\alpha_{\rm ph}$ increases, we find that both $I^{(1)}$ and $S^{(1)}$ also increase in the NDC region, at least initially. If the value $\alpha_{\rm ph} = 2\Gamma$ is exceeded, the NDC is gone.

The behavior of the shot noise peak at the resonance energy is now further complicated by the effect of relaxation. The noise value at the resonance energy is non-monotonic, i.e. it first decreases and then increases again with increasing relaxation. This is due to redistribution of occupation by the relaxation processes in favor of the first level.

For our chosen parameters, the value $\alpha_{\rm ph} = 2\Gamma$ is larger than a reasonable molecule-photon coupling. However, phonon (vibrational) couplings could easily be strong

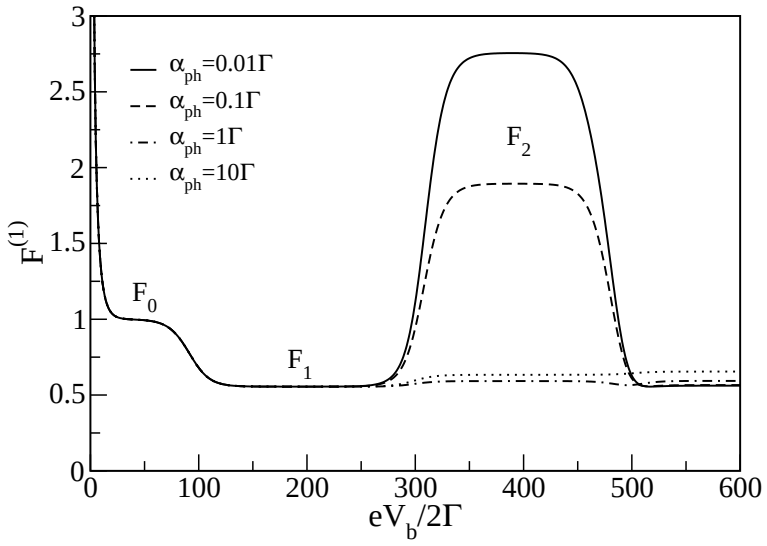

Figure 4.11: *Fano factor vs. bias voltage for for the same parameters as in Fig. 4.10 and various couplings to a bosonic bath* $\alpha_{\rm ph}$*. The super-Poissonian value of the Fano factor vanishes due to strong relaxation processes.*

enough to achieve such fast relaxation. On the other hand, molecule vibrations have a discrete spectrum, much different to the power law assumed in our calculations (see definition of model B). Relaxation due to phonons can be only effective, if the energies of a phonon and the electronic excitation match within the smearing provided by temperature. This obviously depends on the details of the molecule and can not be discussed within the model considered here.

The destruction of NDC by bosonic transition rates is easily explained. An electron which formerly was stuck on the upper level can now relax onto the lower one, from which tunneling to the right electrode is possible via the coupling $\Gamma_1^{\rm R}$.

For the Fano factor in Fig. 4.11 an increase of $\alpha_{\rm ph}$ leads to a decreasing value for the plateau F_2, which passes the Poissonian value $F = 1$ at $\alpha_{\rm ph} \sim 0.34\Gamma$. Different to the current, however, the Fano factor does not show monotonic behavior with increasing $\alpha_{\rm ph}$. The dashed-dotted line corresponding to $\alpha_{\rm ph} = 1\Gamma$ lies below the dotted one with $\alpha_{\rm ph} = 10\Gamma$. The non-monotonic behavior is even more pronounced for the shot noise. It has a maximum and a minimum for $0.2 \sim \alpha_{\rm ph}/\Gamma \sim 1$ before increasing again at $\alpha_{\rm ph} > \Gamma$. This has been discussed in further detail in [7]. The richness of the noise behavior in the NDC regime might allow a detailed determination of coupling-parameter values.

Since in lowest-order perturbation theory temperature only leads to a thermal broadening of the steps, the plateau heights in the different transport regimes are given by the coupling parameters, both the tunnel coupling as well as the relaxation strength. However, note that the actual relaxation *rate* depends also on the position of the energy levels via the boson density of states. This will complicate matters in the general

case with many levels, which are not equidistant from each other. In our case with two levels, we can extract analytical expressions for the plateau values of current, noise and Fano factor within the low bias transport regimes as indicated in the Figs. 4.8 to 4.11. We find for the plateau of the NDC-region 2 ($S_2 = 2I_2F_2$)

$$I_2 = \frac{\Gamma_1^{\mathrm{R}}(\alpha_{\mathrm{ph}} + \Gamma_2^{\mathrm{R}})(\Gamma_1^{\mathrm{L}} + \Gamma_2^{\mathrm{L}})/\Gamma}{2\Gamma_2^{\mathrm{L}}(\alpha_{\mathrm{ph}} + \Gamma_1^{\mathrm{R}}) + (2\Gamma_1^{\mathrm{L}} + \Gamma_1^{\mathrm{R}})(\alpha_{\mathrm{ph}} + \Gamma_2^{\mathrm{R}})} \tag{4.8}$$

for the current and

$$F_2 = \frac{\alpha_{\mathrm{ph}}(\alpha_{\mathrm{ph}}+2\Gamma_2^{\mathrm{R}})[(\Gamma_1^{\mathrm{R}})^2+4(\Gamma_1^{\mathrm{L}}+\Gamma_2^{\mathrm{L}})^2]+[8\Gamma_1^{\mathrm{L}}\Gamma_2^{\mathrm{L}}(\Gamma_1^{\mathrm{R}}-\Gamma_2^{\mathrm{R}})^2+4(\Gamma_1^{\mathrm{L}}\Gamma_2^{\mathrm{R}}+\Gamma_2^{\mathrm{L}}\Gamma_1^{\mathrm{R}})^2+(\Gamma_1^{\mathrm{R}}\Gamma_2^{\mathrm{R}})^2]}{[2\Gamma_2^{\mathrm{L}}(\alpha_{\mathrm{ph}}+\Gamma_1^{\mathrm{R}})+(2\Gamma_1^{\mathrm{L}}+\Gamma_1^{\mathrm{R}})(\alpha_{\mathrm{ph}}+\Gamma_2^{\mathrm{R}})]^2} \tag{4.9}$$

for the Fano factor.

Since only bosonic transition between singly occupied levels 1 and 2 are possible in this bias region, the above expressions include only one bosonic rate $\alpha_{\mathrm{ph}}(\Delta E = \varepsilon_2 - \varepsilon_1)$. Since the temperature is much smaller than ΔE, only relaxation processes matter for the plateau values.

In the absence of the photonic coupling and for electronic coupling parameters chosen such as in Fig. 4.9, where Γ_2^{R} is extremely suppressed, we find the Fano factor to take a value $F_2 = 3$. Comparison with plateau number 2 in Tab. 4.6 from the last section shows the same result for strong polarization $p \to 1$. This is no coincidence, but shows that a mapping from the single, spin-dependent model onto a two level model is indeed possible. The couplings Γ_r^σ in the first model are related to the couplings Γ_i^r of the other (two spin states $\leftrightarrow$ two levels). In order to account for the spin in the two level system again, one has to realize, that there are two possibilities to enter the system from the left electrode (positive bias choice) but only one to tunnel out into the right electrode. When choosing $2\Gamma_{\mathrm{L}}^\sigma = \Gamma_i^{\mathrm{L}}$ and $\Gamma_{\mathrm{R}}^\sigma = \Gamma_i^{\mathrm{R}}$, both models describe the same physics in the low bias regime, as discussed here. When comparing the parameter settings of the models A3 and B, it can be easily seen that this was exactly our choice. The underlying physical mechanisms are (as has been discussed in detail) in the first case due to a 'spin blockade' and in the latter due to a blocked transport level.

For completeness, we also give the expressions for the transport regime 1 (transport through the lower level only). They can be found from the above by setting the couplings Γ_2^{L} and α_{ph} equal to 0. Then electrons can never enter the upper level at positive bias, leading to an effective one level system with the result (compare to Tab. 4.1 second plateau)

$$I_1 = \frac{2\Gamma_1^{\mathrm{R}}\Gamma_1^{\mathrm{L}}}{(2\Gamma_1^{\mathrm{L}} + \Gamma_1^{\mathrm{R}})}\frac{1}{2\Gamma}\ ; \quad F_1 = \frac{4(\Gamma_1^{\mathrm{L}})^2 + (\Gamma_1^{\mathrm{R}})^2}{(2\Gamma_1^{\mathrm{L}} + \Gamma_1^{\mathrm{R}})^2}. \tag{4.10}$$

The derivation of analytical expressions in the low bias regime allows us a quick study of current, noise and Fano factor for arbitrary coupling situations. For the special

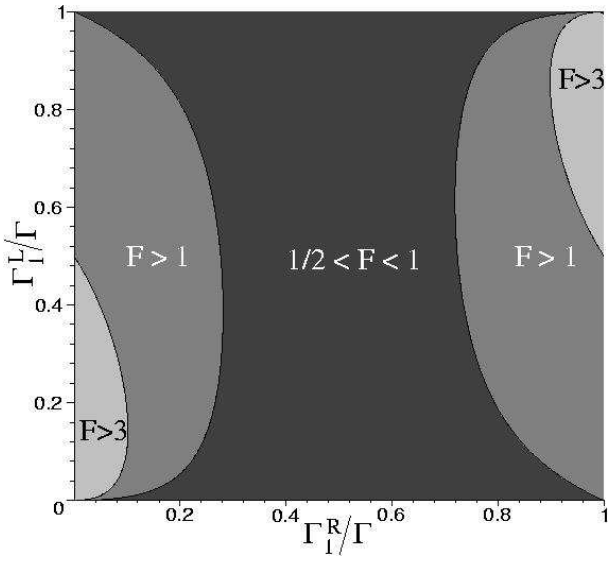

Figure 4.12: *Contour-plot of the Fano factor (plateau F_2) with the choice* $\Gamma_1^{\mathrm{L,R}} = \Gamma - \Gamma_2^{\mathrm{L,R}}$ *and* $\alpha_{\mathrm{ph}} = 0$. *The totally symmetric situation is given for* $\Gamma_1^{\mathrm{L}} = \Gamma_1^{\mathrm{R}} = 0.5\Gamma$. *The Fano factor can become arbitrarily large, if the system is sufficiently asymmetric.*

situation where $\Gamma_1^{\mathrm{L,R}} = \Gamma - \Gamma_2^{\mathrm{L,R}}$ and $\alpha_{\mathrm{ph}} = 0$ the Fano factor F_2 is presented in a contour-plot (see Fig. 4.12). This choice allows the coupling parameters to the left and right reservoir to vary (independently) between 0 and Γ, while having the sum of the couplings to each reservoir fixed. Although not all of the possible coupling situations can be visualized this way, the following features which can be extracted from this plot are valid in general: a super-Poissonian Fano factor $F > 1$ can only be found, if $\Gamma_1^{\mathrm{R}} \neq \Gamma_2^{\mathrm{R}}$ and additionally $\Gamma_1^{\mathrm{L}} \neq 0, \Gamma_2^{\mathrm{L}} \neq 0$. Furthermore a Fano factor $F > 3$ is possible only if $\Gamma_1^{\mathrm{L}} \neq \Gamma_2^{\mathrm{L}}$ besides the above conditions. In the absence of relaxation processes ($\alpha_{\mathrm{ph}} = 0$) we can also find a point symmetry of F_2. This symmetry is broken if $\alpha_{\mathrm{ph}} \neq 0$, as absorption and emission rates of bosons differ due to the boson occupation factors.

Besides the super-Poissonian noise with Fano factors $F > 1$ due to Coulomb correlations and values between $1/2 < F < 1$ in the sub-Poissonian regime, we can also find values of coupling parameters in which the Fano factor drops to values below 1/2. This behavior, however, can only be observed in the presence of relaxation processes, when the coupling strength Γ_1^{L} and Γ_2^{R} are suppressed relative to the other tunnel couplings. If the above couplings are vanishing, there is only one path for the electrons to tunnel through the system, namely from the left electrode to the upper level, then via relaxation onto the lower level until finally the electrons leave the system by tunneling to the right electrode. By choosing specifically $\Gamma_1^{\mathrm{L}} = \Gamma_2^{\mathrm{R}} = 0$ and $\Gamma_1^{\mathrm{R}} = 2\Gamma_2^{\mathrm{L}} = \alpha_{\mathrm{ph}}$ the value of the Fano factor can be minimized and is found to be 1/3. The probabilities to find an unoccupied system or an occupied one with one electron in the lower level

doublet or in upper level doublet are all equal in this case ($P_0 = P_{D_1} = P_{D_2} = 1/3$). This special situation reminds of a system, where a chain of quantum dots are coupled in series, having inter-dot tunnel couplings of the same size than the couplings of the chain ends to the leads. For an infinite chain of such dots (effectively a one-dimensional wire) the Fano factor also reaches 1/3 [157, 158].

To ***summarize*** our discussion of first order transport properties in nanoscopic systems, we found, that excitation energies show up in steps of the current and shot noise voltage characteristics. The effect of the temperature of the reservoirs, to a broadening of the steps only, allows for an extraction of plateau values depending only on the coupling parameters of the system to the leads. The availability of analytic expressions is a big advantage, since free parameters can be fixed successively and even the presence and kind of interaction effects, relaxation effects or coupling asymmetries can be detected. This would not be possible by considering the current only, which provides much more limited information. The observation of super-Poissonian noise, or even a sub-Poissonian Fano factor with values below 1/2, can tell much about transport properties, system parameters, etc. since they are due to characteristic physical mechanisms.

4.3 Co-tunneling

We will focus again on model A as described in chapter 4.1. Elastic and inelastic co-tunneling processes are the additional processes we are including in second order perturbation theory. Elastic processes do not change the energy of the system and have been explained in chapter 3.1.3, whereas inelastic processes modify the energy of the dot (for example into another spin state as shown in Fig. 4.1 or onto another level in the case of a multi-level system). Elastic co-tunneling is therefore present even in equilibrium, but for inelastic processes a finite bias voltage is necessary, which is determined by an energy scale ε_{co} (energy needed for the excitation). For our single level model, this energy is due to the spin-splitting and thus $\varepsilon_{co} = \Delta$. The energy scale, which is relevant for sequential processes to take place (sequential threshold) is defined by $\varepsilon_{seq} = |\varepsilon_\downarrow| = |\varepsilon - \Delta/2|$. As we discussed in some detail in the last section, the model under consideration allows for a description of spin-dependent transport. Furthermore it is possible to find parallels to more complex multi-level systems. However, an exact mapping onto a two level system is not possible anymore for second order processes. In the following we study higher order transport in a quantum dot structure coupled to normal and ferromagnetic leads.

4.3.1 Normal leads

Higher-order transport modifies the current and shot noise in two different ways. First, it introduces an additional broadening of the steps which is effectively given by the sum of Γ and T. Second, it allows for transport in the Coulomb-blockade region at low bias, where sequential tunneling is suppressed. But it may also modify the transport properties at larger bias, when strongly asymmetric coupling situations are present. A discussion of higher order shot noise in the Coulomb-blockade regime has been given by [104, 105], and an extension to the finite bias regime was provided by us [9, 11, 10].

With increasing coupling strength Γ, second- and eventually also higher-order corrections to transport become more and more important. To illustrate the validity range of our second-order perturbation expansion we first consider the non-interacting limit, $U = 0$, since in this case exact results [5] are available for the current and shot noise. The formulas have been discussed at the end of chapter 2.1. In Fig. 4.13 we compare first-order $(I^{(1)}, S^{(1)})$, (first- plus) second-order (I, S), and exact current and noise $(I_{\rm exact}, S_{\rm exact})$ for the parameter set $\varepsilon_\downarrow = -30\Gamma, \varepsilon_\uparrow = 10\Gamma$ (or $\varepsilon = -10\Gamma, \Delta = 40\Gamma$), $k_{\rm B}T = 2\Gamma$, $\Gamma_{\rm L} = \Gamma_{\rm R} = \Gamma/2$ vs. the bias voltage scaled as $eV_b/2\Gamma$. Both current and shot noise are normalized again to the value, the first order contributions reach in the large bias regime and for a coupling $\Gamma_{\rm var} = 1\Gamma$. The normalization factors are $I_{\rm norm} = (e/2\hbar)\Gamma$ and $S_{\rm norm} = (e^2/2\hbar)\Gamma$. (Note that the temperature is fixed, to a value smaller than the $5 - 10\Gamma$ we should usually use in first order. All parameters

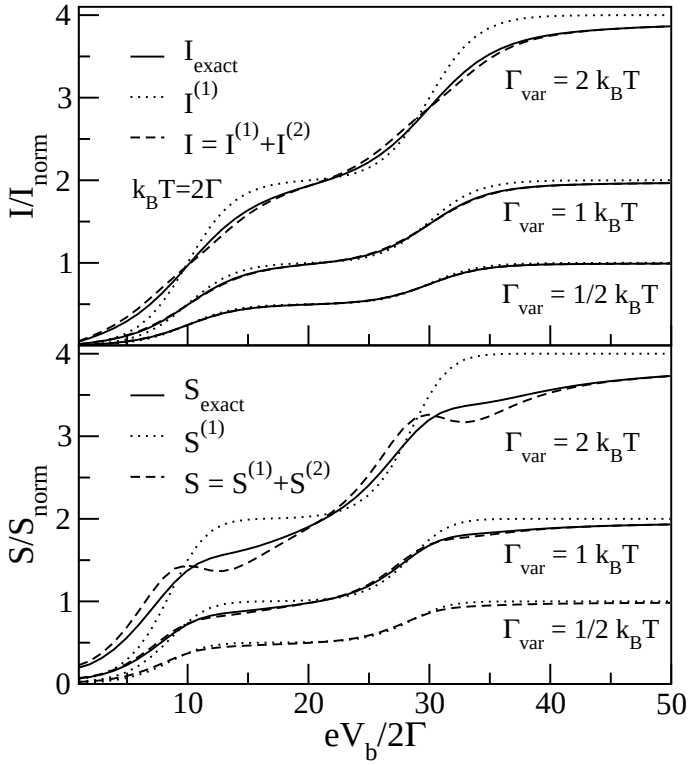

Figure 4.13: *Current I and shot noise S vs bias voltage for $k_{\rm B}T = 2\Gamma, \varepsilon_\downarrow = -30\Gamma, \varepsilon_\uparrow = 10\Gamma, U = 0\Gamma$, and $\Gamma_{\rm L} = \Gamma_{\rm R} = \Gamma/2$. First order (dotted lines) and second order (dashed lines) are compared to the exact results (solid lines) for three coupling parameters $\Gamma_{\rm var} = 1, 2, 4$ times the reference coupling $\Gamma = k_{\rm B}T/2$. Current and shot noise are normalized to $I_{\rm norm} = (e/2\hbar)\Gamma$ and $S_{\rm norm} = (e^2/2\hbar)\Gamma$.*

are expressed in terms of a fixed energy parameter Γ. The coupling strength however is given by a variable parameter $\Gamma_{\rm var}$. This is to tune the coupling between a weak and an intermediate coupling regime and to test, where our theory breaks down. The coupling will be fixed later on.)

Outside the Coulomb-blockade regime, the second-order corrections (dashed lines) to sequential tunneling (dotted lines) start to become important for a coupling of about $\Gamma_{\rm var} \lesssim 0.5 k_{\rm B}T$. As long as the coupling is smaller than $1 k_{\rm B}T$, the exact current and noise (solid lines) are almost perfectly reproduced by second-order perturbation theory, while the first order sequential-tunneling results clearly deviate. For a coupling strength about $\Gamma_{\rm var} \sim 2 k_{\rm B}T$ third-order contributions start to play a role, at least for the noise, where unphysical non-monotonicities arise around the steps. Therefore, we restrict ourselves to $\Gamma_{\rm var} \leq k_{\rm B}T$ for the following discussion.

The elastic co-tunneling processes (which do not change the dot state or its energy) allow for an electron exchange with the reservoirs via an intermediate virtual state. This leads to a finite linear conductance $G = dI/dV_b|_{V_b=0}$. The noise is also non-

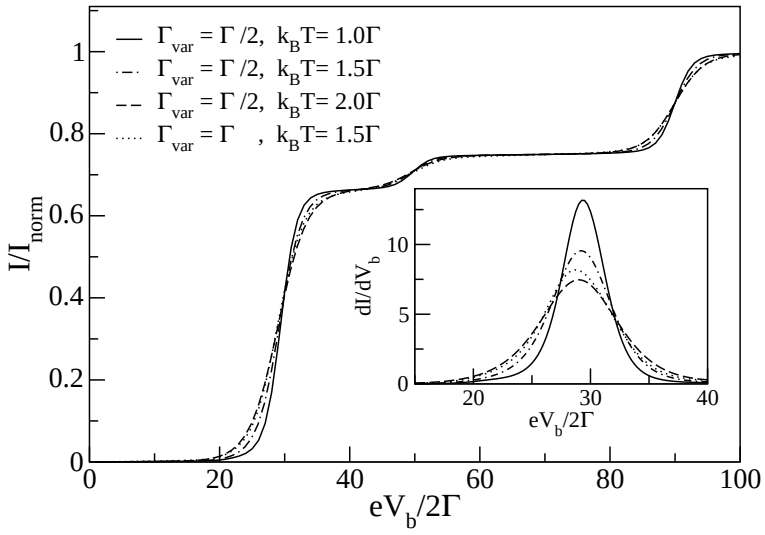

Figure 4.14: *Current I and conductance dI/dV_b (inset) vs bias voltage for $\varepsilon_\downarrow = -30\Gamma, \varepsilon_\uparrow = 10\Gamma, U = 80\Gamma$ and $\Gamma_\mathrm{L} = \Gamma_\mathrm{R} = \Gamma/2$ for various values Γ_var and $k_\mathrm{B}T$. The broadening of the first step due to Γ_var and $k_\mathrm{B}T$ is shown in the inset. The dashed and dotted curves with the same $(\Gamma_\mathrm{var} + k_\mathrm{B}T)$ have about the same width. The current is normalized to $I_\mathrm{norm} = (e/2\hbar)\Gamma_\mathrm{var}$.*

vanishing at zero bias, known from equilibrium fluctuation-dissipation theorem (FDT), $S = 4k_\mathrm{B}TG$. In the Coulomb blockade regime the FDT can be extended to non-equilibrium [104] and takes the form $S^{(2)}(V_b)/2eI^{(2)}(V_b) = \coth(eV_b/2k_\mathrm{B}T)$. Our theory fulfills this relation, however, we stress that it holds only in the regime of purely *elastic* co-tunneling processes. In Fig. 4.14 we show the current I normalized to $I_\mathrm{norm} = (e/2\hbar)\Gamma_\mathrm{var}$. The normalization factor is chosen variable now, to keep the current curves fixed in height. We consider the same set of energy parameters as in Fig. 4.13 but with a finite interaction $U = 80\Gamma$. Since the bias is applied symmetrically, the dot preferably occupies the state with spin $\downarrow$ (Coulomb blockade) until it can be emptied due to first order hopping processes around $eV_b/2\Gamma = \varepsilon_{seq}/\Gamma = 30$ (first step). Further steps arise around $eV_b/2\Gamma = 50$ and 90 due to the double occupied dot state. This parameter set is similar to the experimental situation of Ref. [55] for a quantum dot with occupation $N = 2$. In Fig. 3 of that paper, a conductance feature (step) is observed inside the Coulomb blockade diamond that is attributed to inelastic co-tunneling processes. For our model one expects this inelastic co-tunneling feature in the conductance at a bias of $eV_b/2\Gamma = \varepsilon_{co}/2\Gamma = \Delta/2\Gamma = 20$. This feature is hardly noticeable in the conductance plot of the inset in Fig. 4.14, because our coupling Γ is relatively weak and the energy ε_{co} is fairly close to the sequential tunneling threshold. However, the inelastic co-tunneling processes can clearly be observed in the shot noise and the Fano factor $F = S/2eI$ as discussed below.

We note that the dashed and dotted curves in Fig. 4.14 with same total sum $(\Gamma_\mathrm{var}+k_\mathrm{B}T)$

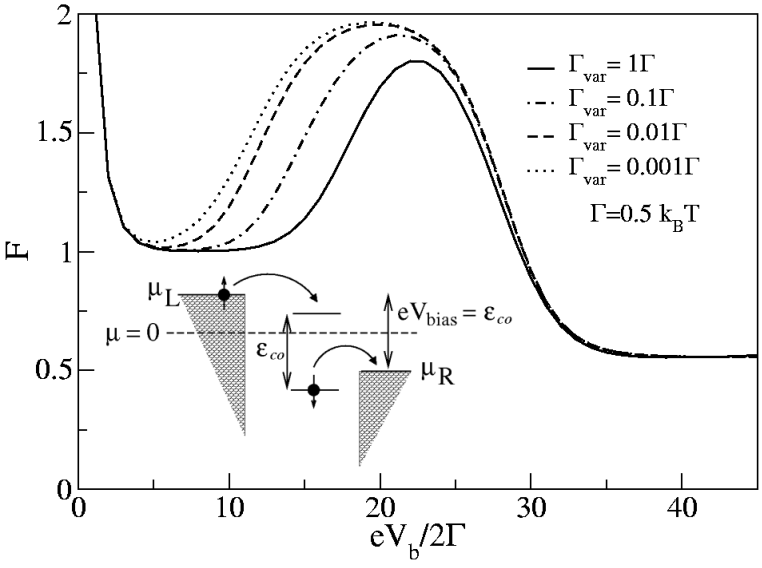

Figure 4.15: *Fano factor $F = S/2eI$ vs bias voltage for the same parameter set as Fig. 4.14 but fixed temperature $k_{\rm B}T = 2\Gamma$ and various coupling strength $\Gamma_{\rm var}$, smaller then the reference coupling Γ. Inelastic co-tunneling leads to a super-Poissonian Fano factor if the bias is larger than $\varepsilon_{co}/2\Gamma = 20$. First order processes may also lead to a super-Poissonian value at a scale $2\varepsilon_\uparrow/2\Gamma = 10$. The crossover between these energy scales runs over three orders of magnitude in the coupling. Outside the Coulomb blockade regime the first order results are recovered already at about $\Gamma_{\rm var}/k_{\rm B}T \sim 0.1$. The inset shows a sketch of the transport situation at $eV_b = \varepsilon_{co}$.*

almost lie on top of each other. The differential conductance plot (inset) shows that the temperature effect is a little stronger: the dashed curve with the highest temperature has the lowest peak. The full width of the conductance peaks is between $(10-16)\Gamma \sim 6(\Gamma_{\rm var}+k_{\rm B}T)$, as compared to 5.44 $k_{\rm B}T$ for pure sequential tunneling [55]. We also note a shift of the peak position from the sequential tunneling value $eV_b/2\Gamma$ to somewhat lower bias voltages, indicating a renormalization of the level positions ε_σ.

The Fano factor $F = S/2eI$ for a fixed temperature and a sequence of coupling ratios $\Gamma_{\rm var}$ is shown in Fig. 4.15. At low bias, the Fano factor varies as [104] $\coth(eV_b/2k_{\rm B}T)$ until it reaches the value 1, as expected for uncorrelated systems. For bias voltages around the spin-flip excitation energy $\varepsilon_{co}/2\Gamma = 20$, the Fano factor becomes super-Poissonian [104], $F > 1$. Once sequential tunneling becomes dominant (at a bias ≥ 30), the Fano factor drops to values between 1 and 1/2.

The super-Poissonian Fano factor appears for bias voltages at which the spin-↑ level acquires some finite occupation probability. This can be either due to inelastic spin-flip co-tunneling, appearing at a bias $\sim \varepsilon_{co}/2\Gamma = 20$, or due to first order tunneling processes [152] at a bias $\sim 2\varepsilon_\uparrow/2\Gamma = 10$. The first order processes are exponentially

suppressed but, for the chosen parameters, still finite [152]. The enhancement of the noise comes from the second and third term of Eq. (3.44), and, physically, is due to bunching of the transfered ↑-electrons during the time when this transport channel is not blocked by the dot being occupied with a ↓-electron. Both the position and the height of the peak in the Fano factor depend on all system parameters. In Fig. 4.15 we study the dependence on the ratio of the coupling strength to the temperature.

With increasing coupling strength, the peak decreases and moves towards higher bias. For $\Gamma_{\rm var} = 0.001\Gamma$ our result (dotted line) coincides with that of a pure first-order calculation, which would show *no* dependence on $\Gamma_{\rm var}/k_{\rm B}T$ in this plot. At larger coupling, though, the second-order processes dominate the first order ones, so that current and noise in the Coulomb blockade regime depend only algebraically and not exponentially on energy. We emphasize that, since the peak is close to the onset of sequential tunneling, an analysis purely based on co-tunneling processes [104] would not be sufficient either. The range of $\Gamma_{\rm var}/k_{\rm B}T$ ratio over which the co-tunneling dominated Fano factor crosses over to sequential tunneling covers three orders of magnitude. For the larger $\Gamma_{\rm var}/k_{\rm B}T$ values the inelastic co-tunneling effects on the shot noise should be experimentally accessible [58]. The importance of co-tunneling processes for the Fano factor at rather weak coupling in the Coulomb blockade regime contrasts with the situation at larger bias where second-order corrections only become noticeable for $\Gamma_{\rm var}/k_{\rm B}T \sim 0.1$.

The extreme sensitivity of the Fano factor to the ratio of the coupling strength over the temperature can be understood even better, when comparing the stationary probabilities of first to second order calculations. For that, we want to keep the parameter set with $\varepsilon = -10\Gamma, \Delta = 40\Gamma, U = 80\Gamma$ and $k_{\rm B}T = 2\Gamma$. We fix the formerly variable coupling parameter $\Gamma_{\rm var}$ to Γ now. A sketch of the situation is given in the inset of Fig. 4.15.

The stationary probabilities are plotted in Fig. 4.16 in dependence of the bias voltage $eV_{\rm b}/2\Gamma$. For the following discussion first order results will always be indicated by thin lines, and second order results by thick lines. If the coupling is sufficiently weak, the two results should become equivalent as co-tunneling contributions can be neglected. In the finite transport regime above the sequential tunneling threshold equivalent curves are obtained already for $\Gamma_{\rm var} \sim 0.1 k_{\rm B}T$ in contrast to the Coulomb blockade regime discussed above. The first order probabilities (thin lines) show equal values (1/3) starting around the sequential threshold $\varepsilon_{seq} = 30\Gamma$ for the states $0, \downarrow, \uparrow$, at 50Γ transitions from $\uparrow \rightarrow d$ become possible which reduce the $p_\uparrow^{\rm st}$ in favor to the $p_\downarrow^{\rm st}$ and at 90Γ transitions from all channels into the others are allowed, leading to all probabilities contributing with 1/4. We find that co-tunneling processes reduce (enhance) probabilities which dominate (are small) in first order.

This can be seen very drastically in the logarithmic plot in the inset of Fig. 4.16. Since

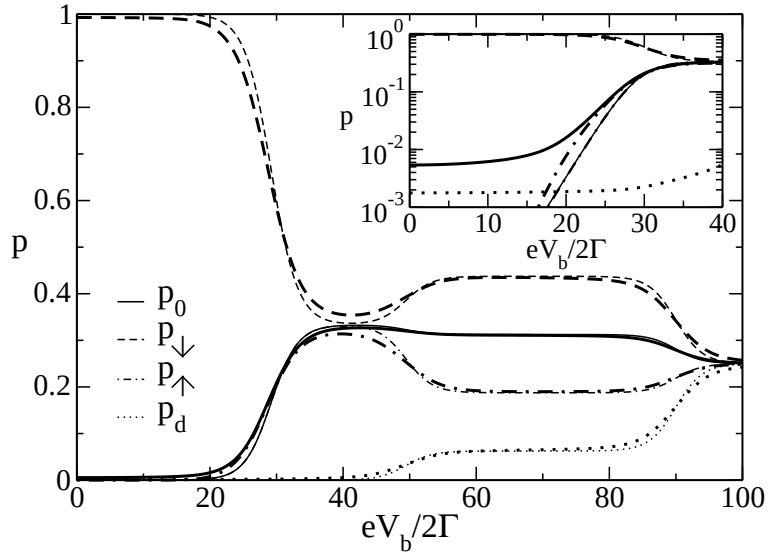

Figure 4.16: *The stationary probabilities for the parameter set as discussed in the text and fixed coupling* Γ *vs. the bias voltage* $eV_\mathrm{b}/2\Gamma$*. With a logarithmic scale plot in the inset, first and second order probabilities in the Coulomb-blockade regime are better resolved. Thinner lines always indicate first order results, thicker lines the complete first plus second order results.*

elastic co-tunneling processes are possible already in equilibrium, the probabilities for the states 0 and d are non-vanishing here in contrast to first order (which are several orders of magnitude smaller). Around $eV_b/2\Gamma = \Delta$ inelastic co-tunneling enhances the probability to be in the state $\uparrow$ which also enhances p_0^{st} since sequential tunneling from $\uparrow \rightarrow 0$ is energetically possible. The first order probabilities of the states 0 and $\uparrow$ are enhanced the same way due to thermal processes leading out of the state with spin $\downarrow$ before the onset of sequential tunneling. They lie on top of each other. It is worth noting, that the excitation energy at $\varepsilon_\uparrow = 10\Gamma$ does not show up in the probabilities (neither in first nor in second order).

The probabilities in Fig. 4.16 show that indeed deviations between first and second order show up mainly around the steps, where big changes of occupations can be observed, and in the Coulomb-blockade regime, where first order contributions are suppressed in general.

The two extreme coupling situations in Fig. 4.15 with $\Gamma_{\mathrm{var}} = 1$ and 0.001 can be considered as first and second order results of our fixed coupling situation. Together with the stationary probabilities in Fig. 4.16 we can better understand the different physical mechanisms in both orders.

To ***summarize*** this section, we discussed the validity of our second order calculations and the additional broadening of the steps in the transport curves due to a stronger coupling to the leads. For the single level coupled to normal leads (model A3), we

found a super-Poissonian Fano factor, at an energy scale ε_{co}, which is different to the scale we would have expected from a first order calculation $[\varepsilon_{co}-\varepsilon_{seq}]$. The situation we discussed here is only one out of several possible parameter sets. Instead of discussing a large number of plots, we refer to other publications [10, 11], and to summarize the possible scenarios for the Fano factor in the Coulomb blockade regime. We restrict ourselves to a large Coulomb interaction U and an energy $\varepsilon < 0$, such that the ground state will be an occupied system. All the cases that we exclude with this choice (e.g. empty ground state) are characterized by a Poissonian behavior of the Fano factor in first as well as second order. For the more interesting regime that we consider here, we can identify three different scenarios:

(I) If $\varepsilon_{co} > 2\varepsilon_{seq}$, Poissonian behavior ($F = 1$) is observed in first as well as second order in the Coulomb-blockade regime. This situation is not discussed here.

(II) For $2\varepsilon_{seq} > \varepsilon_{co} > \varepsilon_{seq}$ a super-Poissonian behavior ($F > 1$) arises at a scale $[\varepsilon_{co}-\varepsilon_{seq}]$ in first and ε_{co} in second order. This is the situation we studied in Fig. 4.15.

(III) When $\varepsilon_{seq} > \varepsilon_{co}$ a super-Poissonian noise is observed in the whole Coulomb-blockade regime in first order, whereas in second order still the scale ε_{co} determines the crossover from Poissonian to super-Poissonian behavior. Here, the difference between first and second order becomes most obvious.

The reason of our choice to discuss situation II here, has been the possibility to compare first and second order scales. It turns out that for large ε_{seq}, when a large bias voltage is required to arrive at the sequential tunneling regime, the first order predictions do not only become strongly modified, but may also give contrary predictions compared to the second order ones.

We want to expand our discussion of the Coulomb-blockade regime by considering the crossover to the finite transport regime as well, where we find the step structures in the shot noise to be modified by second order processes. Interesting behavior can be found for asymmetric coupling situations (as may also be present in a multi-level system) or spin polarized leads (which we introduced with the model A1).

4.3.2 Ferromagnetic leads

In the following we analyze the shot noise and the Fano-factor in the three different configurations AP, P^+ and P^- for the same energy parameters as in the last section. The current turns out to show mostly a monotonic behavior (NDC is found only in very special situations) and will thus not be presented in the following. We discuss the four different situations out of equilibrium, as indicated in Fig. 4.7.

We begin with the discussion of the shot noise in the antiparallel configuration AP with various polarizations ($p = 0.0, p = 0.3, p = 0.5, p = 0.7$) of the leads. In Fig. 4.17

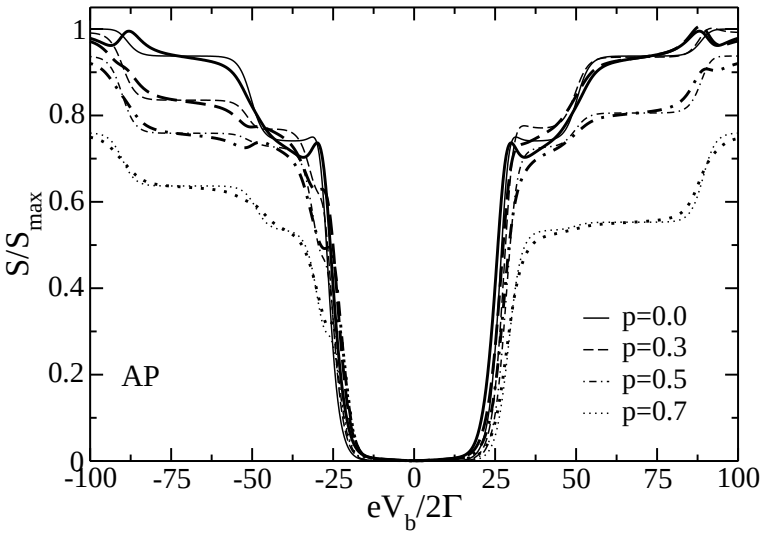

Figure 4.17: *Normalized shot noise in the antiparallel configuration AP for the parameters as in section 4.3.1, but various polarizations of the leads. Correlations of the electron spins for small polarization are destroyed by a stronger polarization. Thin lines correspond to first order results and thick lines correspond to first plus second order results.*

we plot the shot noise normalized to $S_{\rm norm} = (e^2/2\hbar)\Gamma$ vs. the bias voltage $eV_b/2\Gamma$. The thin lines, indicating first order results show a monotonic behaviour for increasing bias voltage, whereas the thick lines (due to first plus second order results) have a ***peak-dip structure*** at the first and the last steps. For stronger polarization of the leads a reduction of this structure as well as a reduction of the noise plateau values is observed. The latter behavior is predicted from Tab. 4.3 in first order.

A qualitative new feature we observe in Fig. 4.17 is a ***thermally broadened step*** in the negative bias region (in first order), which is due to a ***spin inversion***. This is better resolved in Fig. 4.18. The broadened step forms a plateau like structure in first order and may develop into a peak-dip structure when additionally considering second order contributions (for stronger polarization). For positive bias no spin inversion is found, since the minority spin state is further suppressed due to the special AP configuration as is seen in Fig. 4.7.

In the following we explain the origin of the broadened steps and the conditions, under which peak-dip structures are observable in more detail. In Fig. 4.18 we present the normalized shot noise in first and first plus second order (upper and lower left plots) for the different polarizations. The probabilities for the spin $\downarrow$ and $\uparrow$ states are shown on the right side and help to understand the underlying mechanism. In first order we find an initially (small) peak at the resonance (at $eV_{\rm b}/2\Gamma = 30$) to change into a plateau for stronger polarization (Fig. 4.18). The special configuration we consider here leads to a spin inversion, i.e. the dot spin of the dot state equilibrium is effectively reversed

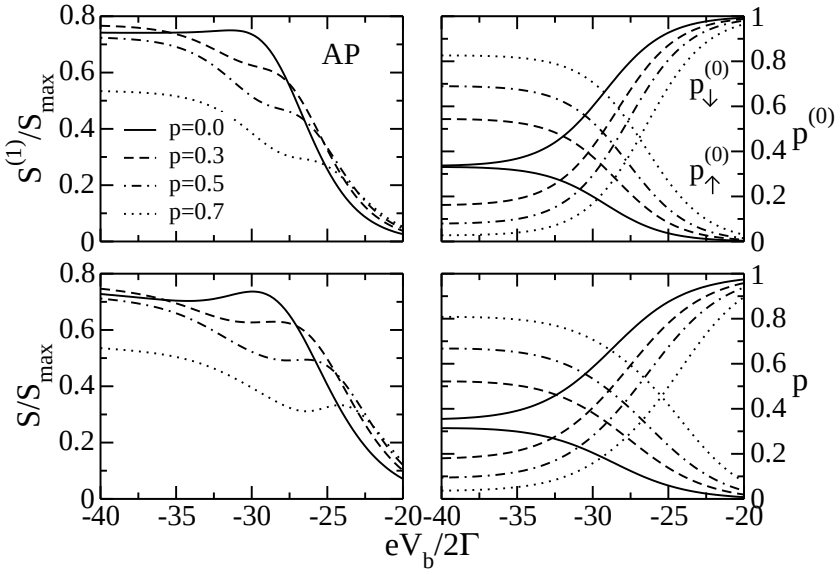

Figure 4.18: *Normalized shot noise in first (upper-left plot) and second (lower-left plot) order and the corresponding probabilities for spin states* $\sigma_1 = \downarrow$ *and* $\sigma_2 = \uparrow$ *in first (upper-right plot) and second (lower-right plot) order, for the antiparallel configuration vs. the bias voltage. Thermally broadened steps show up in first order due to spin inversion. In second order correlation effects slightly modify the steps towards a peak-dip structure.*

once a sufficient bias is applied.

In first order changes in the probabilities are large. The noise increases within a bias region of $eV_b/2\Gamma = -20$ to -40. This increase saturates at a bias, where both spins have about the same probability (within a window defined by the temperature). Here both spins contribute to the transport and have the same importance, leading to a thermally broadened plateau in the noise, when a finite polarization is present. If the bias is increased further, the spin state $\uparrow$ begins to control the transport, i.e. $p^{(0)}_{\uparrow} > p^{(0)}_{\downarrow}$. This effect becomes more pronounced for stronger polarization and leads to an increase of the shot noise again. The crossover points in the probabilities define the middle of the plateaus in the noise.

In second order, inelastic co-tunneling effects lead to a reduction of the probability to be in state $\downarrow$ at lower bias, in favor of the state $\uparrow$. This leads to a shift to lower bias of all features discussed above. Another effect is a stronger pronunciation of the first order effects because of the interplay with co-tunneling processes. Plateaus (at stronger polarization) in weak coupling situations hence may develop into peak-dip structures for stronger coupling situations.

On the other hand we observe in Fig. 4.17 that peak-dip structures (due to a stronger coupling) are destroyed for stronger polarization of the leads, when no such 'temper-

ature plateaus' in first order are present. In these cases, no spin inversion takes place and a stronger polarization only leads to a single dominating spin state. At the same time the transport is reduced, since the system is stuck in this state.
For negative bias the system will be more and more often occupy the state with spin $\uparrow$ if the polarization is increased. It is difficult to empty the dot but also the doubly occupied state or the state with spin $\downarrow$ can hardly be realized. This is why the noise is reduced for any finite bias situation. If once the state $\uparrow$ is emptied, it will be filled again with the same spin, if the state d is realized the state with spin $\uparrow$ follows again, as well. The state with spin $\uparrow$ is the bottleneck of the transport and dominates such that the state with spin $\downarrow$ gets unimportant.
For positive bias and large polarization the system will be stuck in the state with spin $\downarrow$. Since the probability to be in this state is relatively large even for low bias, the polarization needs to be large enough to reduce the transport, with the spin $\downarrow$ state as the bottleneck of the transport.

If we consider the unpolarized situation $p = 0$ again, it might surprise that there are peak-dip structures at the first and last steps in the shot noise, but not at the middle step. We found a competition between the spin states to be crucial for the observation of a peak-dip structure. A peak arises, when the change in the probabilities is maximal and a dip, when the probabilities begin to be in a stable distribution. In Fig. 4.17 at the middle step ($eV_\mathrm{b}/2\Gamma = 50$) the transitions between $\uparrow$ and d come into play, whereas transitions $\downarrow \leftrightarrow d$ are still forbidden. This destroys the spin competition.

These structures are absent for smaller spin-splitting as well as vanishing Coulomb-interaction. Since for $\Delta \to 0$ the probabilities to be in state $\downarrow$ or $\uparrow$ are the same, we can say that the system is 'blind' to the spin and only sees electrons in general tunneling through it. If the system treats both spins equally, none of the two states dominates the other and thus there is no competition between these, which would correlate the electrons. The system is not interested in which spin contributes to the processes.
For vanishing Coulomb-interaction U on the other hand, a competition between singly occupied states is destroyed, since either only one spin state or already the doubly occupied state are dominating the transport. Here, spin $\downarrow$ or $\uparrow$ may have totally different probabilities, such that the system detects very well the state contributing to the transport. But again the situation is somehow simple. The system knows how to treat the different spins, since one is allowed to contribute and the other not. The role of the spins is determined very well, there is no competition.

The competition of spin states is the underlying mechanism to super-Poissonian noise also in the case of dynamical bunching and blocking effects. It should be noted that the absolute values of the probabilities (which may be very different for the two effects) are not necessarily sufficient to decide about the absence or presnce of correlation effects.

We close the discussion of the antiparallel configuration with the Fano factor as shown

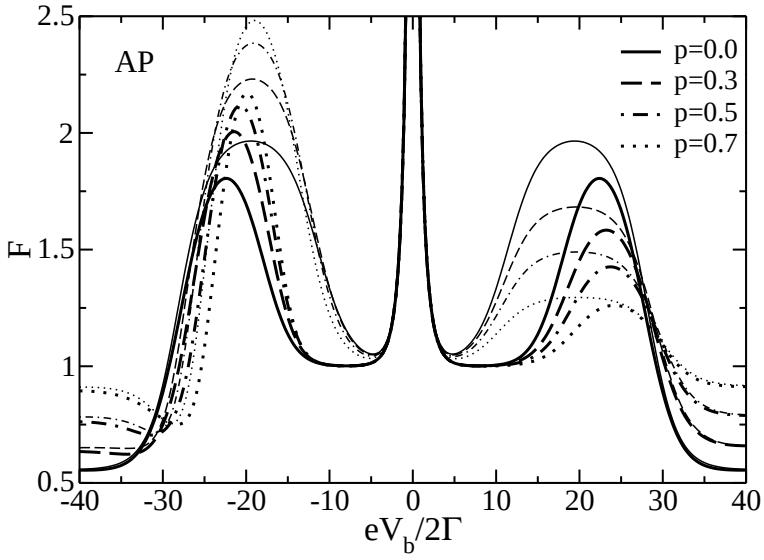

Figure 4.19: *Fano factor vs. bias voltage in the antiparallel configuration for different polarization of the leads. An increase of the spin ↑ for negative bias leads to stronger positive correlations in the Fano-factor, whereas a decrease of the same for positive bias reduces the Fano-factor towards a Poissonian value.*

in Fig. 4.19. Compared to the unpolarized situation (black lines) no significant change between first and second order can be observed. Poissonian and super-Poissonian behavior of the Fano-factor is still determined by the energy scales $\varepsilon_{co} - \varepsilon_{seq}$ in first and ε_{co} in second order. For polarized leads, the super-Poissonian Fano factor is enhanced further in the negative bias region, but suppressed towards a Poissonian value in the positive bias region. This is consistent with our findings that an enhancement of the spin ↑ leads to stronger correlations at negative bias and the suppression of the same to weaker correlations at positive bias. Additionally, in-elastic co-tunneling processes are stronger pronounced at negative bias (compare configuration AP at negative bias in Fig. 4.7), which results in a shift of the peak in the Fano factor towards the co-tunneling scale. For positive bias these processes are blocked and lose their importance (AP at positive bias in Fig. 4.7). Hence the decreasing peaks shift towards the sequential threshold.

In the following we consider the parallel configurations P^+ and P^- (see Fig. 4.7). In agreement with earlier works (e.g. [155, 153, 154]) we find that a bunching of electrons may lead to a super-Poissonian behavior in the Fano-factor also in the finite transport regime (analytical expressions in first order have been presented in section 4.2). However, since this behavior arises from a finite polarization, a suppression of first order processes may give more importance also to second order processes that provide another channel for the transport. This can invalidate first order results, if the polarization (asymmetry of the couplings) becomes so large that second order processes

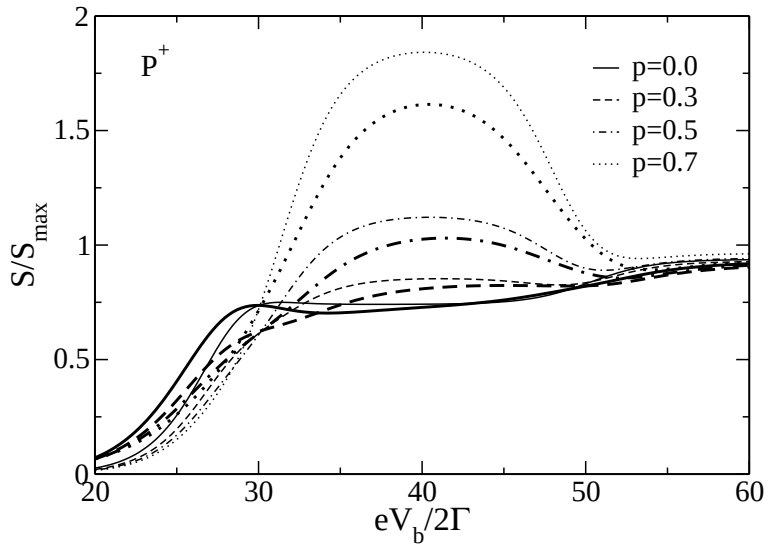

Figure 4.20: *Normalized shot noise in the configuration P^+ for different polarizations of the leads. First order processes may be suppressed even at finite transport below second order contributions resulting in stronger deviations there.*

dominate, as we can see in Fig. 4.20. We want to stress here that the probabilities compared to the unpolarized case (see Fig. 4.16) are almost unchanged even for stronger polarization in the overall bias region.

Below $eV_\mathrm{b}/2\Gamma = 30$ in Fig. 4.20, the probability to be in state $\downarrow$ is practically unity and stronger polarization will reduce the importance of the state with spin $\uparrow$ further. The vanishing of a transport channel consequently leads to a reduction of the noise. Above $eV_\mathrm{b}/2\Gamma = 30$ however, the noise is significantly enhanced due to correlation effects (dynamical bunching [153, 154]). In section 4.2, we discussed this effect within a first order picture. In second order however, there will be a non-vanishing contribution of co-tunneling processes in which the doubly occupied state is realized. This will reduce the probability of the spin $\uparrow$ state, pushing more weight on the dominating spin $\downarrow$ state, thus reducing the correlations. Indeed, this effect is considerably large, since we find a deviation of about 10 percent between first and second order, which is an effect 20 times larger, as we would expect in the unpolarized case for the overall coupling $\Gamma/k_\mathrm{B}T = 1/2$ under consideration. In other words, first order calculations would give the correct results only, if the coupling were about 20 times smaller. The correlations in Fig. 4.20 break down at $eV_\mathrm{b}/2\Gamma = 50$, where the doubly occupied state is available via sequential processes. Both spins have the same role now, since transitions between $\downarrow \leftrightarrow 0$ and $\uparrow \leftrightarrow d$ are possible and the empty and doubly occupied states gain importance.

The situation for the P^- configuration is somehow different. In Fig. 4.21 we find the shot noise to be strongly enhanced even before the sequential threshold. Here

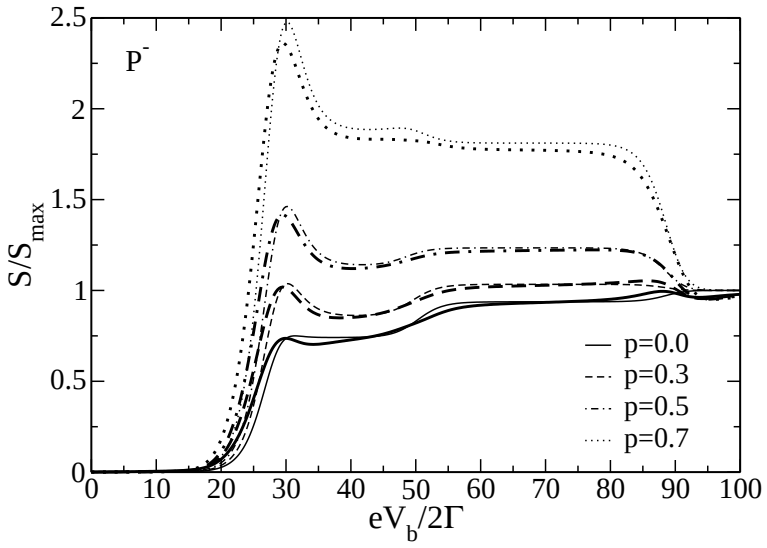

Figure 4.21: *Normalized shot noise in the configuration P^- for different polarizations of the leads. Correlations leading to an enhanced noise may persist over almost the whole bias regime, if corresponding processes are suppressed.*

the state with spin $\uparrow$ (with small probability) is occupied easily when spin $\downarrow$ state is once depleted (via the propagator $\mathbf{P}$ or co-tunneling processes). This gives the state $\uparrow$ more importance. At the threshold, this effect reaches a maximum, broadened by the temperature (in first order $\sim 5k_{\mathrm{B}}T = 10\Gamma$). Above the threshold the role of the spins is reversed compared to the P^+ configuration in the same bias regime. In first order, the noise therefore shows the same behavior as before, whereas co-tunneling processes involving the doubly occupied state are suppressed such that second order corrections are much smaller here. Due the suppression of transitions $\uparrow \rightarrow d$ even above $eV_{\mathrm{b}}/2\Gamma = 50$ the noise remains strongly enhanced. A symmetric role of the spins is reached only in the large bias regime, where all channels are available for transport and probabilities are equilibrated again.

If the correlation effects we discussed for the to parallel configurations are strong enough, this results in a super- Poissonian noise behavior in the Fano-factor, as can be seen in Figs. 4.22 and 4.23. For the configuration P^+ the Fano-factor is reduced towards a Poissonian value in the Coulomb-blockade regime, both in first and second order as the polarization is increased. Above the sequential threshold the correlation effects as discussed for the noise enhance the Fano-factor, which gets super-Poissonian for polarizations between $p = 0.5$ and $p = 0.7$. Second order processes reduce these effects, such that the Fano-factor will have sub-Poissonian values, where first order calculations would already predict super-Poissonian behavior. Again second order effects are relevant unless Γ is reduced more than one order of magnitude further than considered here. The contributing first order processes are suppressed below second order contributions due to strong polarization here.

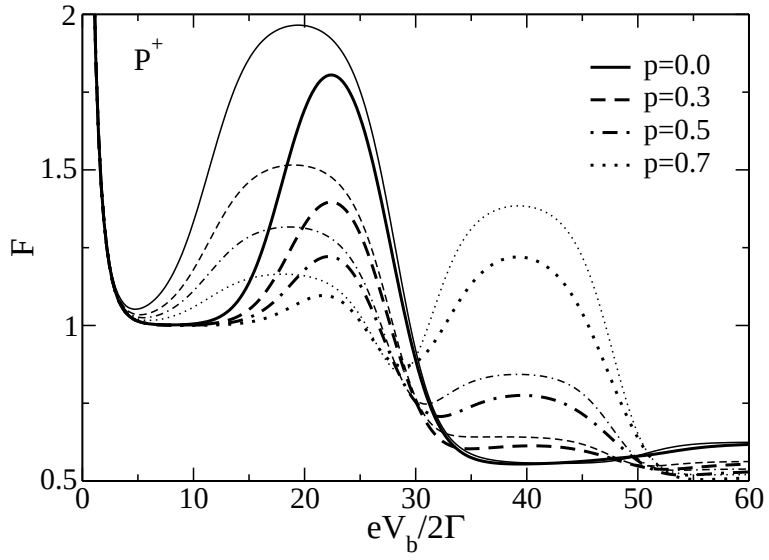

Figure 4.22: *Fano-factor vs. bias voltage in the configuration P^+ for different polarization of the leads. Suppression of correlations in the Coulomb-blockade regime reduce the Fano-factor, an enhancement of correlations above the sequential threshold may lead to super-Poissonian noise. Second order co-tunneling processes may avoid this.*

In the P^- configuration (Fig. 4.23) the Fano-factor turns out to have super-Poissonian behavior in the overall bias regime (for polarizations stronger than $p = 0.5$), up to the last excitation energy at $eV_\mathrm{b}/2\Gamma = 90$. This is due correlations of the two spin states, which vanish only at large bias, where all states contribute the same way to transport.

In summary, we have found that the inclusion of co-tunneling effects besides sequential processes is of relevance in the *Coulomb-blockade* regime, even in a an assumed *weak coupling* situation. New energy scales show up in the Coulomb-blockade regime, which are due to possible inelastic second order excitations. Non-monotonicities in the Fano factor allow for access to further information about electronic structure, interaction or charging effects, probability distributions (and hence indirectly relevant transport channels) and coupling parameters. The current alone could not yield such an amount of information. First order results turn out to be of questionable use in the Coulomb-blockade to describe the relevant physics, since even at very small coupling, higher order contributions change the physical picture significantly.

For *intermediate coupling* situations second order effects change the structure around excitation energies which define the position of *steps in the noise* at finite bias voltage. These steps are due to correlation effects arising from competing spin states (or localized states in a multi-level structure) and should be measurable in an experiment.

For finite polarization of the leads an enhanced shot noise can be observed in the parallel configuration, which may result in a super-Poissonian behavior of the Fano

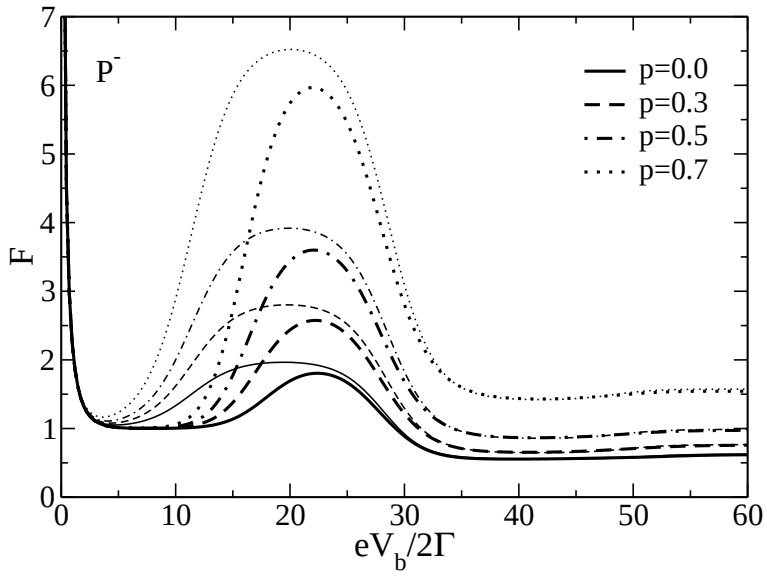

Figure 4.23: *Fano-factor vs. bias voltage in the configuration P^- for different polarization of the leads. Strong correlations in the Coulomb-blockade regime lead to a further growing super-Poissonian noise, which gets Poissonian (for strong polarization) only in the large bias regime. Second order co-tunneling processes are less relevant here.*

factor. Deviations between first and second order stress the importance of higher order contributions even in the finite transport regime. Generally speaking, whenever first order processes are suppressed below second order ones in the transport regime, a combined picture of both orders becomes important. This is obviously the case for strongly asymmetric coupling parameters.

We encountered thermally broadened steps and peaks, non-monotonic peak-dip structures, enhanced shot noise, sub- and super-Poissonian noise, all being features understandable only in a combined picture of first and higher order transport. By explaining the physical mechanisms behind these effects, the shot noise thus can be used as a spectroscopic tool to identify important transport parameters.

4.4 Towards a description of molecules

The model systems we discussed so far describe, strictly speaking, rather localized quantum dot systems than realistic molecules. However, we showed in chapter 2 the possibility to explain a number of experimental features of molecular transport (an even better understanding can be expected with additional shot noise measurements). Furthermore we showed in chapter 3 the possibility to do calculations for more complex systems approaching realistic molecular transport situations. This involves calculations for systems with a complex electronic structure, interaction effects, relaxation (photon), vibration (phonon) or even geometric effects. The molecule specific parameters need to be determined within quantum chemical calculations to reduce the number of free parameters (orbitals). Higher order calculations assure that the finite transport current and shot noise describe the intermediate coupling situation adequately and capture the relevant physics in each transport regime.

However, one point we did not consider so far is the *spatially delocalized* nature of molecular orbitals. This feature can be modeled by considering a number of levels (or quantum dots) coupled in series (often called 'artificial molecules'). In the present section we therefore study the current and shot noise for a chain of three coupled quantum dots or single levels (model C in chapter 4.1). This is to show on the one hand that a description of delocalized molecular orbitals poses no problem, and on the other that new transport mechanisms are possible that only exist in spatially extended systems.

We focus on the weak coupling regime again and choose the energies of the three levels to be equal with $\varepsilon = -2000\Gamma$, with an inter-dot hopping $t = 400\Gamma$. Furthermore, we set $U = 2400\Gamma$ (intra-dot Coulomb-repulsion), $U_{nn} = 1000\Gamma$ (inter-dot Coulomb-repulsion) and consider the temperature to be $k_{\mathrm{B}}T = 5\Gamma$. The bias voltage is chosen symmetric with coupling parameters $\Gamma_1^{\mathrm{L}} = \Gamma_3^{\mathrm{R}} = \Gamma/2$. From our former findings, we know that for a symmetric coupling a monotonic growth of current and shot noise is expected, resulting in a Fano factor with values between 1/2 and 1. However, as we see in Fig. 4.24 this does not necessarily have to be the case. We plot the current and shot noise $(I^{(1)}, S^{(1)})$ normalized to $I_{\mathrm{norm}} = (e/2\hbar)\Gamma$ and $S_{\mathrm{norm}} = (e^2/2\hbar)\Gamma$ vs. the bias voltage $eV_b/2\Gamma$ in the left panel of Fig. 4.24 and the Fano factor $F^{(1)}$ in the right panel. We find not only a non-monotonic behavior of the shot noise, but even a strong enhancement, resulting in a super-Poissonian Fano factor.

The current shows generic behavior, i.e. stepwise increase and only a tiny NDC around $eV_b/2\Gamma = 850$. The noise, however, is tremendously enhanced, with the Fano factor $F > 1$ indicating its super-Poissonian nature over a large bias range, before recovering "normal" behavior beyond a bias of $eV_b/2\Gamma = 1000$. Note the similar behavior as compared to the single level system coupled to ferromagnetic leads. There, 'dynamical

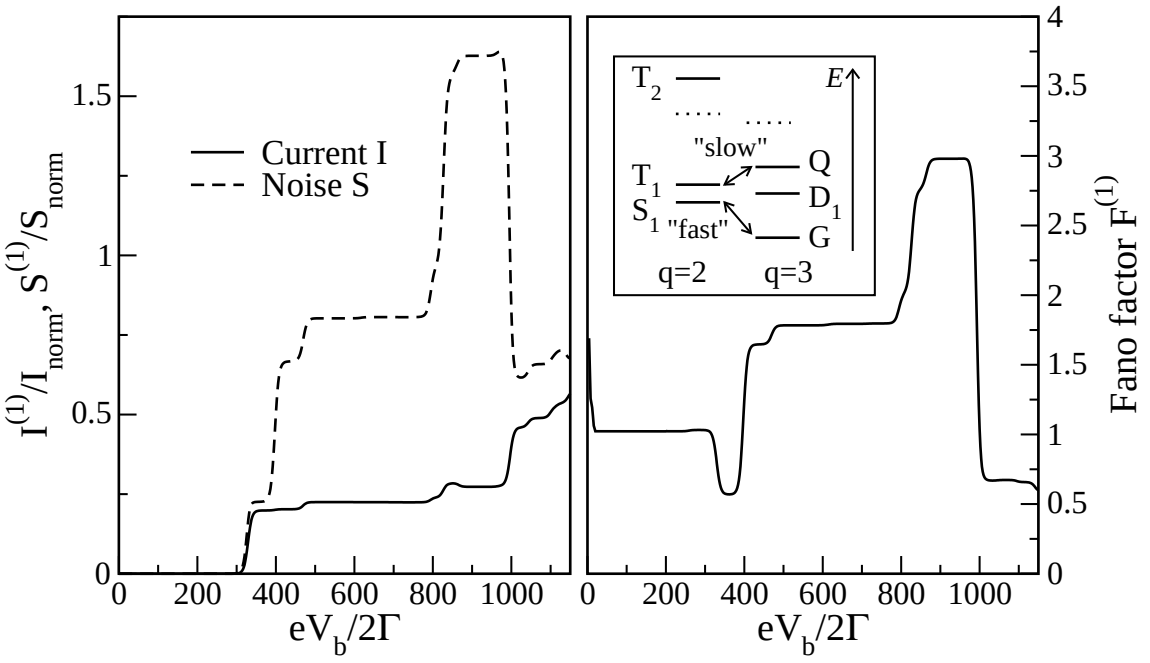

Figure 4.24: *Current I and shot noise S vs. voltage for three coupled dots with $k_BT = 5\Gamma$, $t = 400\Gamma$, $\varepsilon = -2000\Gamma$, $U = 2400\Gamma$, $U_{nn} = 1000\Gamma$. The noise is strongly enhanced in absolute magnitude above $eV_b/2\Gamma \sim 400$, while the current only slightly increases, leading to a Fano factor $F > 1$. This is due to a competition of "fast" and "slow" transport channels. The noise scales like $(U_{nn}/t)^2$ in this regime, while the current saturates as t is lowered. Above $eV_b/2\Gamma \sim 1000$ "normal" behavior resumes, as the "slow" channel of transport is "cut short" (see text).*

bunching' due to competing spin states with large and small probabilities has been due to a finite polarization and hence an asymmetric coupling situation. The physical mechanism leading to the behavior we observe here is different.

As before, we need strong electron interactions ($U, U_{nn} \gg k_BT$) to have the various states compete in transport. The outcome of this competition is determined by the wave functions of the competing states that effectively generate state dependent tunneling transition rates. Finally, the total spin of the states in question can differ by more than the electron spin 1/2 , so some energetically and spatially possible transition rates vanish due to spin selection rules. The dominance of the non-local interaction U_{nn} over the hopping t, leads to a strong modification in the spatial distribution of the relevant many-body wave functions compared to a case of vanishing U_{nn}. Considering the 9 states with total spin 1 in the $q = 2$ charge sector (these split into three triplets), we find if $U_{nn} < t$, the triplet with lowest energy (T_1) will prefer to have electrons on the middle dot, to maximize the kinetic energy. On the other hand, if $U_{nn} > t$ the lowest triplet prefers to have one electron each on the leftmost and the rightmost dot, thus minimizing both intra-dot and inter-dot Coulomb repulsion. This change in

the nature of the lowest triplet wave function is crucial for the "noisy" transport. An equally fundamental role plays the total spin 3/2 quadruplet, the second excited state in the $q = 3$ charge sector. Due to spin selection rules these quadruplet states can only have tunneling transitions to the triplet states of the $q = 2$ (or $q = 4$) charge sectors. It turns out that the transitions between the lowest triplet and the quadruplet form a "slow" channel of transport. The transition rate between them is suppressed by a factor $\sim (t/U_{nn})^2$, as the tunneling can happen only at the interface dots, but the wave functions of the triplet and quadruplet mainly differ by an electron in the middle dot. The current effectively alternates between "fast" tunneling sequences between the well connected doublet and singlet states, and the "slow" sequences between the lowest triplet and quadruplet states, leading to the super-Poissonian noise in the corresponding bias regime. A more detailed discussion is given in Ref. [12].

As the enhancement of the noise is based on spin quantum numbers we expect it to be robust to standard relaxation processes involving phonon and photon emission. A strong magnetic field will modify the details, but not the generic behavior of the transport.

The discussion of the present chapter showed that higher order transport calculations as well as more complex model systems drastically complicate the study of transport properties in molecules or quantum dots. However, characteristic features showing up in the shot noise and/or the Fano factor, but not in the current, allow for a much better understanding of transport and for a determination of unknown system parameters in comparison to experiment.

5 Conclusions

In the following we summarize the main ideas and achievements of this thesis. We stress the novelties compared to existing works and provide an outlook and suggestions for further efforts in this field.
In this thesis we have presented a ***theory of current and shot noise*** in systems like quantum dots or molecules that allows us to push towards an intermediate coupling regime in the molecule-electrode coupling. We have encountered non-Markovian memory effects that manifest themselves in the higher order shot noise in the finite transport regime. Our theory takes into account arbitrary two-particle interaction effects and is valid for arbitrary bias situations. The main constraint of the theory is given by the ratio of the coupling strength Γ over the temperature $k_{\mathrm{B}}T$, which should not exceed unity.

Our theory was applied to a shot noise measurement on self-assembled InAs ***quantum dots*** which we have discussed in *chapter 2*. We find an agreement of experiment and theory, since a predicted Fano factor with values between 1/2 and 1 in a situation of weak coupling is observed and allows to self-consistently determine the absolute strength and asymmetry of the coupling parameters.
The special relevance to study the co-tunneling current and shot noise in ***molecules*** has been illustrated for an experiment on a terphenyl-type molecule. In this case only a current measurement has been realized. Data on shot noise are not yet available. We have modeled the experiment by a single-level system and find a finite Coulomb-interaction as well as asymmetric coupling parameters to explain the current and conductance curves in an intermediate coupling regime. A definite determination of the underlying transport parameters would be possible with additional shot noise data. We furthermore find that more than a single level (molecular orbital) is needed to quantitatively describe the experimental data. An extension of our calculation to describe multi-level systems in an intermediate coupling regime is straightforward within our theoretical approach.

This approach relies on a diagrammatic technique on the Keldysh contour following a microscopic many-body description of the transport problem. Our theory as presented in *chapter 3* expresses the current and shot noise in terms of transition rates (or irreducible self-energy diagrams denoted by us as $\mathbf{W}$). These rates contain the full information about the whole transport properties, as do the Green functions in non-equilibrium Green function techniques (NEGF) or the scattering matrix in a scattering approach. In all existing theories an access to those functions is needed in order to address the transport problem. In our case, this access is provided by self-energy diagrams, which we expand up to first order in the coupling (***sequential tunneling***), and then up to second order (***co-tunneling***), where we find that ***non-Markovian memory effects*** start to play a role in the shot noise (not in the current).

For the case of ***finite frequency noise***, we have shown the equivalence to our zero-frequency noise formula in the limit $\omega \to 0$. This gives our theory a better footing and additionally allows for a better physical understanding of the non-Markovian memory effects in higher orders. The calculation of frequency dependent noise poses no problem within our diagrammatic technique and may be interesting as a future project. However, it is not of our concern, since we want to study molecules and quantum dots in a frequency regime, where the shot noise behaves as white noise (frequency independent).

Our theory can also include ***coherence effects*** when taking into account additionally non-diagonal elements of the density matrix. This modifies the equations which determine the probabilities $\mathbf{p^{st}}$ and 'propagator' $\mathbf{P}$ but still allows a description in terms of transition rates. Indeed, this would be an interesting extension of our theory, since for molecules, described in general by delocalized orbitals (similar to several quantum dots coupled in series), coherence effects may play a role. Transport through delocalized levels can be described within the present theory only in a regime, where the coupling to the reservoirs is small compared to an inter-dot coupling.

Higher order correlators of the current operator can be expressed in terms of transition rates as well. They are non-trivially related to higher derivatives of a so called cumulant generating function (CGF) with respect to a counting field in full counting statistics (FCS). A theoretical description of higher correlators and a study of the relation to the CGF is at first a technical challenge. This is especially relevant with respect to forthcoming experiments on skewness (third correlator), where however at the moment it is not clear at all whether a higher correlator or a higher cumulant is measured. A theory of higher correlators will gain importance in the future, since compared to the shot noise additional information about transport processes can be extracted from them. An advantage of our approach to the FCS is the relatively simple handling of arbitrary complex nanoscale systems, as calculation of current and shot noise is reduced to the task of computing a certain number of transition rates. Although the number of rates grows rapidly with the number of system states, the calculation is effectively reduced to a question of bookkeeping only. A translation of the diagrammatic rules into a computer code is straightforward and facilitates the tedious work of doing the calculations of the rates by hand. Parts of this work has been implemented already. The availability of a program code would be a real advantage since many states of the system can be included immediately and a description of multi-level quantum dots or molecules is made possible in an easy way. Considering different geometries, including arbitrary interaction effects and allowing vibrational (phonons) or relaxation (photons) effects, will enable a realistic description of transport through mesoscopic systems within a microscopic theory.

Our discussion of many possible extensions shows that this theory by no means is restricted to only describe current and zero frequency shot noise in zero dimensional quantum dots in the weak coupling limit.

But of course, a natural way to understand the physics of transport is to start with the simplest system and complicate matters afterwards. As we have seen in the discussion of the experiments summarized above, even with simple models we were able to explain the observed features to some extent.

This is why we have studied current and shot noise in the weak coupling for a single-level system in detail in *chapter 4*. The extension to a multi-level system with a variety of effects which may occur in realistic nanoscopic systems (e.g. molecules) has been discussed afterwards. ***Co-tunneling processes*** in the shot noise play an important role, even in the weak coupling limit, when studying the Coulomb-blockade regime. Both, current and noise are strongly suppressed in this regime and the consideration of their ratio in terms of the Fano factor may be technically possible and provide some informations even within orthodox theory. But dividing a zero by zero may lead to any result, which makes a higher-order calculation necessary to prove or disprove the findings. With our co-tunneling results we show that first order predictions are sometimes physical, sometimes un-physical, but are usually modified, even in typical weak coupling situations. This is the first time that shot noise in the Coulomb-blockade regime has been discussed consistently, including the crossover to the sequential transport regime. In the case of ferromagnetic leads, we have found even stronger modifications of the shot noise in second order compared to the sequential tunneling limit. Interaction effects and an external magnetic field exhibit much stronger signature in the noise (for certain system configurations and polarizations) which allows us to make predictions or to analyze electronic and transport properties of future experiments.

We may ***summarize the results*** on current and shot noise in molecules and quantum dots within a combined picture of sequential and co-tunneling transport as follows:

1) From *first order* calculations, plateau values depending on the coupling parameters of the system can be determined for current, shot noise and Fano factor for all finite transport regimes and complex electronic structures of the system. Here, the self-consistent determination of coupling parameters, being most relevant for the transport, is possible when comparing sequences of plateaus as additional transport channels open up when increasing the bias voltage. Besides the typical values of the Fano factor between 1 and 1/2, a super-Poissonian noise with $F > 1$ can be observed, when the symmetry of the system is broken due to asymmetric couplings (for localized systems) or strong interaction effects being responsible for a special non-local electronic structure (for delocalized systems). The main mechanisms are dynamical bunching or blocking effects, leading to competition among transport channels involving states with different total spins, levels, etc. Often a negative differential conductance (NDC) combined with suppressed shot noise can be observed as consequence, but also a strongly enhanced shot noise is possible. Such behavior may be destroyed due to relaxation effects or higher order tunneling processes, but this must not be so in general.

Even values of the Fano factor below 1/2 are possible, when transport channels do not contribute independently, but condition each other to enable transport through the system. Such a behavior is found in multi-level systems in the presence of relaxation effects in situations similar to diffusive wires.

2) *Second order* calculations are most important in the Coulomb-blockade regime, where a new energy scale due to inelastic co-tunneling processes shows up. We find elastic co-tunneling processes to destroy any super-Poissonian behavior that would result from a pure first order calculation, whereas inelastic co-tunneling processes can enhance the noise to super-Poissonian values again. Inelastic co-tunneling processes give rise to characteristic transport behavior especially for magnetically polarized leads, where spin accumulation or spin inversion may be observed for stronger polarization. A finite spin-splitting due to a magnetic field and a finite Coulomb interaction lead to complex non-monotonic behavior of the Fano factor in the Coulomb-blockade regime. Information about the internal electronic level structure of the system, interaction effects, asymmetric coupling parameters, etc. is thus extractable from experiments on shot noise. The inclusion of co-tunneling processes is necessary, even for weak coupling situations (as typically observed in experiments with quantum dots) since current and shot noise are only algebraically suppressed, in contrast to the exponential suppression in first order. This makes the Fano factor a sensitive measure of transport in a large range of the coupling strength.

3) Whereas the sequential tunneling picture holds mostly on the plateaus, and the co-tunneling picture is dominant in the Coulomb-blockade regime, both processes are relevant in the crossover between different transport regimes, i.e. around the step structures, where new excitations of the system become possible. Here, the shot noise shows complex peak and dip structures due to the interplay of both types of processes. Large peaks in the shot noise may be due to strong polarizations of the leads (in spin-dependent transport) or suppressed couplings (in multi-level systems) and often appear in connection with dynamical electron bunching. Thermally broadened plateaus appear together with spin inversion (or inversion of level occupations in multi-level systems) and may result in a peak-dip structure for stronger coupling situations (when co-tunneling processes start to dominate). The fact that the variety and strength of these step structures does not appear at every excitation step allows for further extraction of information about channels involved in transport.

In conclusion, the use of shot noise as a spectroscopic tool will help to understand mesoscopic systems in much more detail, making a controlled manipulation of nanofabricated devices for technological applications a distinct possibility in the near future.

A Appendix: Diagrammatic Rules

We present the diagrammatic rules for a calculation of the irreducible blocks $\mathbf{W}$, as discussed in chapter 3. In Ref. [129] such rules have been given for blocks denoted by $\mathbf{\Sigma}$ being trivially related to our objects $\mathbf{\Sigma}_{\chi\chi'} = i\mathbf{W}_{\chi'\chi}$. In Ref. [6], we presented the rules for $\mathbf{W}$, expanded to also include bosonic degrees of freedom in Ref. [7].

A.1 Time space

In time space, the rules for calculating the irreducible blocks $\mathbf{W}$ describing electron tunneling and relaxation are as follows:

1) For a given order k draw all topologically different diagrams with $2k$ vertices connected by k tunneling (electron) lines or boson (photon) lines (for orders $k \geq 2$ both kinds of lines might be contained in a diagram). Assign a reservoir index r and a spin index σ to each of the tunneling lines and an index q for the boson lines. Assign states χ and energies E_χ to the propagators.

2) The propagation from t' to t with $t' < t$ on the Keldysh contour implies a factor $\exp[-iE_\chi(t-t')]$.

3) Each vertex containing dot operators B_n (with n different operator structures) gives rise to a matrix element $\langle\chi'|B_n|\chi\rangle$, where $\chi\,(\chi')$ is the dot state entering (leaving) the vertex with respect to the Keldysh contour (for the general Hamiltonian as introduced in chapter 3 we find: $B_1 = c^\dagger_{i\sigma}, B_2 = c_{i\sigma}, B_3 = c^\dagger_{i\sigma}c_{j\sigma}$).

4) Each directed tunneling line with index r running from t' to t implies $\gamma^\pm_{ri\sigma}(t-t') = \Gamma^{i\sigma}_r/2\pi \int_{-\infty}^{\infty} d\omega_l \; f^\pm(\omega_l - \mu_r) \; e^{-i\omega_l(t-t')}$ (with $f^+(x) = f(x)$ for $t < t'$ and $f^-(x) = 1 - f(x)$ for $t > t'$ and $f(x) = 1/[\exp(x/k_\mathrm{B}T) + 1]$ being the Fermi function). In the same way, contributions of a boson line with index q running from t' to t imply $b^\pm(t-t') = \int_{-\infty}^{\infty} d\omega_l \; sign(\omega_l) \; \alpha_\mathrm{ph}(\omega_l) \; n_\mathrm{b}(\pm\omega_l) \; e^{-i\omega_l(t-t')}$ (with $n_b(+x)$ for $t < t'$ and $n_b(-x)$ for $t > t'$ and $n_b(x) = 1/[\exp(x/k_\mathrm{B}T) - 1]$ being the Bose function.

5) There is an overall prefactor $(-i)^m(-1)^c$, where m is the total number of internal vertices and c the number of crossings of tunneling lines (no bosonic lines) plus the number of vertices connecting the state d with $\uparrow$.

6) Integrate over the internal times along the Keldysh contour without changing their ordering and sum over the reservoir, spin and level indices.

A.2 Energy space

In energy representation the rules for calculating the irreducible blocks $\mathbf{W}$, describing electron tunneling and relaxation are as follows:

1) For a given order k draw all topologically different diagrams with $2k$ vertices connected by k tunneling (electron) lines or boson (photon) lines (for orders $k \geq 2$ both kinds of lines might be contained in a diagram). Assign the energies E_χ to the propagators, and energies ω_l $(l = 1, ..., k)$ to each one of these lines.

2) For each of the $(2k-1)$ segments enclosed by two adjacent vertices there is a resolvent $1/(\Delta E_m + i0^+)$ with $m = 1, ..., 2k-1$, where ΔE_m is the difference of the left-going minus the right-going energies.

3) Each vertex containing dot operators B_n (with n different operator structures) gives rise to a matrix element $\langle\chi'|B_n|\chi\rangle$, where $\chi\,(\chi')$ is the dot state entering (leaving) the vertex with respect to the Keldysh contour (for the general Hamiltonian as introduced in chapter 3 we find: $B_1 = c^\dagger_{i\sigma}, B_2 = c_{i\sigma}, B_3 = c^\dagger_{i\sigma}c_{j\sigma}$).

4) The contribution of a tunneling line of reservoir r is $\gamma^{\pm}_{ri\sigma}(\omega_l) = \Gamma^{i\sigma}_r/2\pi\ f^{\pm}(\omega_l - \mu_r)$, taking the plus-sign if the line is going backward with respect to the closed time path, and the minus-sign if it is going forward. The same way the contribution of a bosonic line is given by $b(\pm\omega_l) = sign(\omega_l)\ \alpha_{\rm ph}(\omega_l)\ n_{\rm b}(\pm\omega_l)$.

5) There is an overall pre-factor $(-i)(-1)^c$, where c is the total number of vertices on the backward propagator plus the number of crossings of tunneling lines (no bosonic lines) plus the number of vertices connecting the state d with $\uparrow$.

6) Integrate over the energies ω_l of the tunneling and boson lines and sum over all reservoir and spin indices.

We additionally introduce the rules to determine diagrams with external current vertices in energy representation as we need to calculate the current and shot noise contributions. The blocks $\mathbf{W}^I$ and $\mathbf{W}^{II}$ are determined in a similar way to $\mathbf{W}$. The only difference to $\mathbf{W}$ is that in $\mathbf{W}^I$ ($\mathbf{W}^{II}$) one (two) internal vertices are replaced by external ones representing $\hat{I}\hbar/e$. This amounts to multiplying an overall pre-factor, which arises due to the definition of the current operator and since the number of internal vertices on the backward propagator may have changed. The additional rules therfore read:

7) Assign a factor $+1/2$ for each external vertex on the upper (lower) branch of the Keldysh contour which describes tunneling of an electron into the right (left) or out of the left (right) lead, and $-1/2$ in the other four cases.

8) Sum up all the factors for each possibility to replace one (two) internal vertices by external ones.

Remarks:

a) For a description of frequency dependent noise, there is an additional frequency line ω besides the energies E_χ and ω_l running in a fixed direction and spanned between two external current vertices for $\mathbf{W}^{II}$, or entering (leaving) a diagram to (from) a current vertex for $\mathbf{W}^{I}$, or running through the whole diagram for $\mathbf{W}$.

b) In order to compute higher correlators, rules 7) and 8) remain unchanged, but there may appear more than two external vertices.

c) When taking into account off-diagonal elements of the density matrix to describe coherence effects, there are diagrams with contributions $t_q t_{q'}$ (q, q' being different quantum numbers) instead of $|t_q|^2 \sim \Gamma_q$, leading to modified rules.

d) First and second order rates calculated due to the rules defined here, are presented in appendices B and C. In lowest (first) order, diagrams containing one tunneling or boson line have to be calculated.

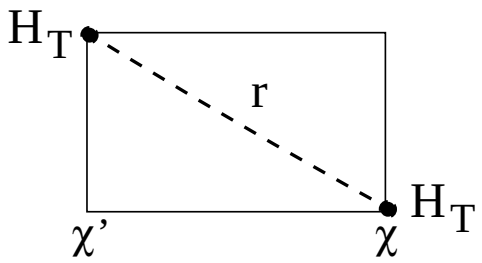

Figure A.1: *An example of a first order diagram used to calculate the stationary probabilities and the object* $\mathbf{P}$ *for the shot noise.*

An example for a diagram describing the coupling to the electronic reservoirs is shown in Fig. A.1. The coupling to a bosonic bath is illustrated by a diagram containing a wiggly line (Fig A.2).

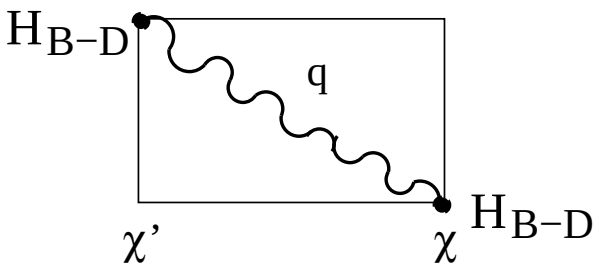

Figure A.2: *An example of a first order diagram describing the coupling to a bosonic bath.*

It is obvious, that in lowest order fermionic and bosonic processes occur independently (due to their incoherent, sequential nature). For higher order processes however, there may be also diagrams containing both kinds of lines, fermionic (tunneling) and bosonic ones at the same time. Such diagrams are also relevant for processes contributing to the rates $\mathbf{W}^I$ and $\mathbf{W}^{II}$. A schematic example for relevant second order diagrams is given in Fig. A.3. All three kinds of diagrams contribute to rates $\mathbf{W}$. However only

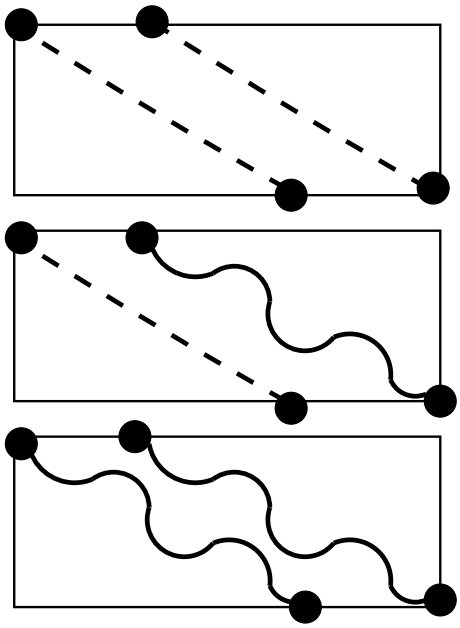

Figure A.3: *In second order there may be diagrams containing two tunneling lines (upper figure), one tunneling and one boson line (middle figure) or two boson lines (lower figure).*

the tunneling lines (dashed lines) can contain an external current vertex. Therefore diagrams like the lower one in Fig A.3 can not contribute to rates $\mathbf{W}^I$ or $\mathbf{W}^{II}$, but those like the middle can.

B Appendix: Sequential tunneling rates

We present the first order matrix elements of transition rates $\mathbf{W}^{(1)}$, $\mathbf{W}^{(1)I}$ and $\mathbf{W}^{(1)II}$ calculated by application of the rules from appendix A, needed to compute the current and shot noise as derived in chapter 3. The rates allow for a description of a multi-level system (N with $i,j = 1 \cdots N$) with spin σ under inclusion of bosonic degrees of freedom.

B.1 Transition rates W

The total transition rates $W^{(1)}_{\chi,\chi'}$ (in the absence of relaxation) are the sum of transition rates associated with electron tunneling through either the left or the right barrier, $W^{(1)}_{\chi,\chi'} = W^{(1)\mathrm{R}}_{\chi,\chi'} + W^{(1)\mathrm{L}}_{\chi,\chi'}$. The inclusion of bosonic degrees of freedom, e.g. to describe relaxation processes as discussed in chapter 4, we have to consider additional rates $W^{(1)\mathrm{ph}}_{\chi,\chi'}$. Assuming weak coupling to the bosonic bath (in addition to weak tunneling), we only keep contributions to either first order in α_{ph} or to first order in Γ. The total transition rates are, thus, given by $W^{(1)}_{\chi,\chi'} = W^{(1)\mathrm{L}}_{\chi,\chi'} + W^{(1)\mathrm{R}}_{\chi,\chi'} + W^{(1)\mathrm{ph}}_{\chi,\chi'}$, where $W^{(1)\mathrm{ph}}_{\chi,\chi'}$ describe pure relaxation while $W^{(1)\mathrm{L}}_{\chi,\chi'}$ and $W^{(1)\mathrm{R}}_{\chi,\chi'}$ models pure tunneling. The additivity of pure tunneling or boson rates is given only in lowest order, where only single lines are present in diagrams. Together with $\Gamma^{i\sigma}_r = 2\pi|t^r_{i\sigma}|^2\rho_e$ we find

$$W^{(1)r}_{\chi',\chi} = 2\pi\rho_e \sum_\sigma \left[f^+_r(E_{\chi',\chi}) \left| \sum_i t^r_{i\sigma} \langle\chi'|c^\dagger_{i\sigma}|\chi\rangle \right|^2 + f^-_r(-E_{\chi',\chi}) \left| \sum_i t^r_{i\sigma} \langle\chi'|c_{i\sigma}|\chi\rangle \right|^2 \right] \tag{B.1}$$

for $\chi' \neq \chi$, together with $W^{(1)r}_{\chi,\chi} = -\sum_{\chi'\neq\chi} W^{(1)r}_{\chi',\chi}$ (sum rule). $E_{\chi',\chi} = E_{\chi'} - E_\chi$ is the energy difference between the many-body states χ and χ'. Here, $f(x) = 1/(\exp(x/k_{\mathrm{B}}T) + 1)$ is the Fermi function, $f^+(x) = f(x)$ and $f^-(x) = 1 - f(x)$, and $f^\pm_r(x) = f^\pm(x - \mu_r)$. The bosonic rates are

$$W^{(1)\mathrm{ph}}_{\chi',\chi} = \sum_\sigma b(E_{\chi',\chi}) \left| \sum_{i\neq j} \langle\chi'|c^\dagger_{i\sigma} c^-_{j\sigma}|\chi\rangle \right|^2 \tag{B.2}$$

for $\chi' \neq \chi$, and $W^{(1)\mathrm{ph}}_{\chi,\chi} = -\sum_{\chi'\neq\chi} W^{(1)\mathrm{ph}}_{\chi',\chi}$, where $b(x) = sign(x)\ \alpha_{\mathrm{ph}}(x)\ n_{\mathrm{b}}(x)$, with the Bose function $n_{\mathrm{b}}(x) = 1/(\exp(x/k_{\mathrm{B}}T) - 1)$. This allows to build the matrix blocks $\mathbf{W}^{(1)}$ to calculate the objects $\mathbf{p}^{(0)\mathrm{st}}$ and $\mathbf{P}^{(-1)}$. The presence of relaxation therefore leads to a modification of the probabilities and propagators $\mathbf{P}^{(-1)}$, whereas the matrices $\mathbf{W}^{(1)I}$ and $\mathbf{W}^{(1)II}$ are not affected (due to only one tunneling line). The results obtained here could be calculated within a golden rule approximation as well. Diagrams associated with the rates Eqs. B.1 and B.2 have been shown in appendix A.

B.2 Current rates $\mathbf{W}^I$

The matrix elements of $\mathbf{W}^{(1)I}$ are given by

$$W^{(1)I}_{\chi,\chi'} = (W^{(1)\mathrm{R}}_{\chi,\chi'} - W^{(1)\mathrm{L}}_{\chi,\chi'})(\Theta(N_\chi - N_{\chi'}) - \Theta(N_{\chi'} - N_\chi)) \tag{B.3}$$

with the Heaviside θ-function, where N_χ is the total number of electrons on the dot within the state χ. This permits the computation of the first order current $I^{(1)}$. An example of a corresponding diagram including one tunneling line is shown in Fig. B.1.

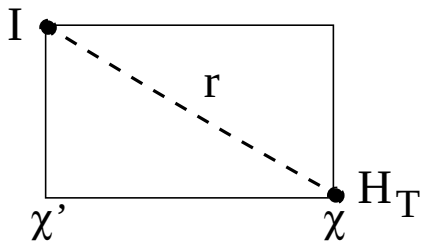

Figure B.1: *An example of a first order diagram contributing to the current.*

B.3 Shot noise rates $\mathbf{W}^{II}$

Correspondingly we find for the matrix elements of $\mathbf{W}^{(1)II}$

$$W^{(1)II}_{\chi,\chi'} = \frac{1}{4}(W^{(1)\mathrm{R}}_{\chi,\chi'} + W^{(1)\mathrm{L}}_{\chi,\chi'})(1 - 2\ \delta_{\chi\chi'}) \tag{B.4}$$

with the Kronecker δ. This is the last missing object to compute the shot noise in first order $S^{(1)}$. In first order there is only one possibility to place the two current vertices, as shown in Fig. B.2.

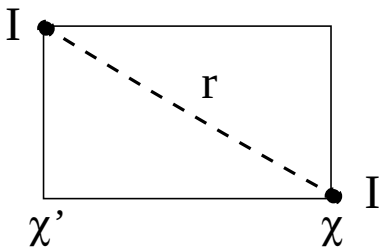

Figure B.2: *An example of a first order diagram contributing to the shot noise.*

C Appendix: Co-tunneling rates

For the calculation of the second order current and shot noise contributions we need to determine additional objects compared to the ones evaluated in appendix B (see current and noise formulas in chapter 3). The remaining objects are $\partial\mathbf{W}^{(1)}, \partial\mathbf{W}^{(1)I}, \mathbf{W}^{(2)}, \mathbf{W}^{(2)I}$ and $\mathbf{W}^{(2)II}$. With these objects, we can immediately compute $\mathbf{p}^{(1)\mathrm{st}}, \mathbf{P}^{(0)}, I^{(2)}, S^{(2)}$ and thus $I = I^{(1)} + I^{(2)}$ and $S = S^{(1)} + S^{(2)}$. Again the objects containing one or two current vertices are calculated by applying the rules specified in appendix A. For the rates $\mathbf{W}^{(2)I}$ ($\mathbf{W}^{(2)II}$) up to four (six) combinations of placing these vertices are possible now, each of them giving rise to a certain prefactor. In contrast to the first order diagrams, a compact expression in terms of rates $\mathbf{W}$ without any current vertices is not possible anymore for second order diagrams. This emphasizes the advantage of the diagrammatic technique, which now facilitates the handling of a large number of irreducible contributions by reducing the problem to a task of book keeping. We thus want to restrict ourselves to a mathematical discussion of the main structure of diagrammatical contributions to $\mathbf{W}^{(2)}$. The rates $\partial\mathbf{W}^{(1)}$, although being first order contributions, turn out to have the same structure as second order rates because of the derivative.

Whereas in first order we had to evaluate a single integral over contributions which took a rather simple form (since the application of the mirror rule allowed to identify a Dirac δ-function), we now have to deal with a double integral. A first integral can always be done due to the δ-function, but a second integral remains and leads to expressions

$$F^{\pm}_{ri\sigma}(\varepsilon) = \int_{-\infty}^{\infty} d\omega \frac{\gamma^{\pm}_{ri\sigma}(\omega)}{(\varepsilon - \omega + i\eta)} \tag{C.1}$$

and

$$B^{\pm}(\varepsilon) = \int_{-\infty}^{\infty} d\omega \frac{b(\pm\omega)}{(\varepsilon - \omega + i\eta)} \tag{C.2}$$

for diagrams coupling to fermionic or bosonic reservoirs. The functions $\gamma^{\pm}_{ri\sigma}(\omega)$ and $b(\pm\omega)$ are related to the Fermi and Bose functions $(f(x), n_b(x))$ as defined in the appendices A and B, the energy ε is composed of energies E_χ in general and η denotes the convergence factor (or factor from the Laplace transformation), which is taken in the limit $\eta = 0^+$ at the end. [For the rates $\partial\mathbf{W}^{(1)}$ only expressions of the kind $\partial_\eta F^{\pm}_{ri\sigma}(\varepsilon)$ and $\partial_\eta B^{\pm}(\varepsilon)$ are relevant.] Since $\alpha_{\mathrm{ph}}(\pm\omega)$ in $b(\pm\omega)$ may include a more complex form, we choose the simplest form here and consider all factors to be constant ($b(\pm\omega) = \alpha_{\mathrm{ph}} n_b(\pm\omega)$). In the following we thus show how to calculate integrals of the type as given in Eqs. C.1 and C.2.

C.1 Calculation of Integral $F^{\pm}$

The integral C.1 diverges, since the integrand does not decay fast enough for $|\omega| \to \infty$ to close the integration contour in the upper or lower complex half plane. In order to make the integral convergent, we introduce a Lorentzian cutoff

$$D_r(\omega) = \frac{X_C^2}{(\omega - \mu_r)^2 + X_C^2} \tag{C.3}$$

with X_C being the cutoff energy, which might be related to the Coulomb interaction for a model with large $U = 2X_C$. In general, results have to be independent of such a parameter. We apply Cauchy's Theorem by collecting all residua. This is done easily, when considering the sum and difference of $F^+_{ri\sigma}(\varepsilon)$ and $F^-_{ri\sigma}(\varepsilon)$. The sum can be immediately evaluated by closing the integration contour in the lower half plane, since there is only one pole at $\omega = \mu_r - iX_C$ leading to

$$F^+_{ri\sigma}(\varepsilon) + F^-_{ri\sigma}(\varepsilon) = \frac{\Gamma_r^{i\sigma}}{2\pi} \int_{-\infty}^{\infty} d\omega D_r(\omega) \frac{1}{\varepsilon - \omega + i\eta} = \frac{\Gamma_r^{i\sigma}}{2\pi} D_r(\varepsilon) \left(\frac{(\varepsilon - \mu_r)\pi}{X_C} - i\pi \right). \tag{C.4}$$

For the difference, we find

$$F^+_{ri\sigma}(\varepsilon) - F^-_{ri\sigma}(\varepsilon) = -\frac{\Gamma_r^{i\sigma}}{2\pi} \int_{-\infty}^{\infty} d\omega D_r(\omega) \frac{\tanh[\frac{\beta}{2}(\omega - \mu_r)]}{\varepsilon - \omega + i\eta} \tag{C.5}$$

with poles at $\omega = \mu_r \pm iX_C$, $\omega = \varepsilon + i\eta$ and $\omega = \omega_m = i\pi(2m+1)/\beta + \mu_r$ for $m = 0, \pm 1, \pm 2, ...$ We close the integration contour in the upper and lower half plane and take the average of these two terms leading to

$$\begin{aligned} F^+_{ri\sigma}(\varepsilon) - F^-_{ri\sigma}(\varepsilon) = \frac{i\Gamma_r^{i\sigma}}{2} \{ D_r(\varepsilon) \left[\tanh\left(\frac{\beta}{2}(\varepsilon - \mu_r) \right) - \tanh\left(\frac{i\beta X_C}{2} \right) \right] \\ - \frac{2}{\beta} \sum_{m=0}^{\infty} \left[\frac{D_r(\omega_m)}{\varepsilon - \omega_m} - \frac{D_r(\omega_{-m-1})}{\varepsilon - \omega_{-m-1}} \right] \} \end{aligned} \tag{C.6}$$

Now we use the digamma function $\psi(z) = d[\ln\Gamma(z)]/dz$ and its representation

$$\psi(x) - \psi(y) = \sum_{m=0}^{\infty} \left(-\frac{1}{m+x} + \frac{1}{m+y} \right), \tag{C.7}$$

and $\psi(z^*) = [\psi(z)]^*$, as well as $\psi(\frac{1}{2} - z) = \psi(\frac{1}{2} + z) + i\pi\tanh(i\pi z)$, to arrive at

$$\begin{aligned} F^+_{ri\sigma}(\varepsilon) - F^-_{ri\sigma}(\varepsilon) = \frac{\Gamma_r^{i\sigma}}{2\pi} D_r(\varepsilon) \{ 2\psi\left(\frac{1}{2} + \frac{\beta X_C}{2\pi} \right) - 2\mathrm{Re}\psi\left(\frac{1}{2} + \frac{i\beta(\varepsilon - \mu_r)}{2\pi} \right) \\ + i\pi \tanh\left(\frac{\beta}{2}(\varepsilon - \mu_r) \right) \}. \end{aligned} \tag{C.8}$$

The sum and the difference of Eqs. C.4 and C.8 lead to the result

$$F^{\pm}_{ri\sigma}(\varepsilon) = \frac{\Gamma^{i\sigma}_r}{2\pi} D_r(\varepsilon)\{\pm\psi\left(\frac{1}{2}+\frac{\beta X_C}{2\pi}\right) \mp \mathrm{Re}\psi\left(\frac{1}{2}+\frac{i\beta(\varepsilon-\mu_r)}{2\pi}\right) + \pi\frac{\varepsilon-\mu_r}{2X_C} - i\pi f^{\pm}_r(\varepsilon)\}. \tag{C.9}$$

Since $X_C >> \max\{\varepsilon, k_{\mathrm{B}}T, eV_b\}$ (where $k_{\mathrm{B}}T = 1/\beta$ and $eV_b = \frac{\mu_{\mathrm{L}}-\mu_{\mathrm{R}}}{2}$), we can further simplify the result and split into real and imaginary parts leading to

$$\mathrm{Re}F^{\pm}_{ri\sigma}(\varepsilon) = \frac{\Gamma^{i\sigma}_r}{2\pi}\left[\pm\ln\left(\frac{\beta X_C}{2\pi}\right) \mp \mathrm{Re}\psi\left(\frac{1}{2}+\frac{i\beta}{2\pi}(\varepsilon-\mu_r)\right)\right] \tag{C.10}$$

and

$$\mathrm{Im}F^{\pm}_{ri\sigma}(\varepsilon) = \frac{\Gamma^{i\sigma}_r}{2\pi}\left[-\pi f^{\pm}_r(\varepsilon)\right] = -\pi\gamma^{\pm}_{ri\sigma}(\varepsilon) \tag{C.11}$$

The part with the logarithmic divergence in C.10 provides an universal factor (besides the temperature dependence), and, when appearing in diagrams, cancels against other diagrams, contributing with the opposite sign. Often contributions of the form $\partial_\omega \mathrm{Re}F^{\pm}_{ri\sigma}(\omega)|_{\omega=\varepsilon}$ are required which are independent of X_C.

C.2 Calculation of Integral $B^{\pm}$

The integral C.2 is calculated in an analoguous way, with the cutoff

$$D(\omega) = \frac{X_C^2}{\omega^2 + X_C^2}, \tag{C.12}$$

where the sum of $B^+(\varepsilon)$ and $B^-(\varepsilon)$ leads to

$$B^+(\varepsilon) + B^-(\varepsilon) = -\alpha_{\mathrm{ph}} D(\varepsilon)\left[\frac{\varepsilon\pi}{X_C} - i\pi\right]. \tag{C.13}$$

For the difference, we find

$$B^+(\varepsilon) - B^-(\varepsilon) = \alpha_{\mathrm{ph}} \int_{-\infty}^{\infty} d\omega D(\omega)\frac{\coth(\frac{\beta\omega}{2})}{\varepsilon-\omega+i\eta} \tag{C.14}$$

with poles at $\omega = \pm iX_C, \omega = \varepsilon + i\eta$ and $\omega = \omega_m = \frac{2i\pi m}{\beta}$ for $m = 0, \pm1, \pm2, ...$ The analoguous calculation to the one for integral C.1 leads to

$$B^+(\varepsilon) - B^-(\varepsilon) = i\pi\alpha_{\mathrm{ph}} D(\varepsilon)\left[\frac{2}{\beta\varepsilon} + \coth\left(i\pi\frac{\beta X_C}{2\pi}\right) - \coth\left(\frac{\beta\varepsilon}{2}\right)\right] + \frac{2i\pi\alpha_{\mathrm{ph}}}{\beta}\sum_{m=0}^{\infty} D(\omega_{m+1})\left[\frac{1}{\varepsilon-\omega_{m+1}} - \frac{1}{\varepsilon-\omega_{-m-1}}\right], \tag{C.15}$$

that we can simplify to

$$B^+(\varepsilon) - B^-(\varepsilon) = 2\alpha_{\rm ph} D(\varepsilon) \left[-\frac{\pi}{\beta X_C} - \psi\left(\frac{\beta X_C}{2\pi}\right) + {\rm Re}\psi\left(1 + \frac{i\beta\varepsilon}{2\pi}\right)\right] + i\pi\alpha_{\rm ph} D(\varepsilon)\left[\frac{2}{\beta\varepsilon} - \coth\left(\frac{\beta\varepsilon}{2}\right)\right] \quad \text{(C.16)}$$

by using $\psi(1+z) = \psi(z) + \frac{1}{z}$ and $\psi(1-z) = \psi(z) + i\pi\coth(i\pi z)$ additionally. Again for $X_C >> \max\{\varepsilon, k_{\rm B}T, eV_b\}$, we find from C.13 and C.16

$$B^{\pm}(\varepsilon) = \pm\frac{i\pi\alpha_{\rm ph}}{\beta\varepsilon} - i\pi\alpha_{\rm ph} n^{\pm}(\varepsilon) \mp 2\alpha_{\rm ph}\ln\left(\frac{\beta X_C}{2\pi}\right) \pm \alpha_{\rm ph}{\rm Re}\psi\left(1 + \frac{i\beta\varepsilon}{2\pi}\right), \quad \text{(C.17)}$$

what we split again into

$${\rm Re}B^{\pm}(\varepsilon) = \mp 2\alpha_{\rm ph}\ln\left(\frac{\beta X_C}{2\pi}\right) \pm \alpha_{\rm ph}{\rm Re}\psi\left(1 + \frac{i\beta\varepsilon}{2\pi}\right), \quad \text{(C.18)}$$

$${\rm Im}B^{\pm}(\varepsilon) = \pm\frac{i\pi\alpha_{\rm ph}}{\beta\varepsilon} - i\pi\alpha_{\rm ph} n^{\pm}(\varepsilon). \quad \text{(C.19)}$$

Again the part with the logarithmic divergence due to X_C has to cancel among the various diagrams, when doing a perturbation expansion up to second order.

Bibliography

[1] U. Meirav and E. B. Foxman, Semicond. Sci. Technol. **11**, 255 (1996).

[2] G. Schön, in *Mesoscopic Electron Transport*, eds. L. L. Sohn, L. P. Kouwenhoven, and G. Schön, NATO ASI Series E, Kluwer, Dordrecht **345**, 1 (1997).

[3] *Molecular Electronics: Science and Technology*, eds. A. Aviram and M. Ratner, Ann. N.Y. Acad. Sci. **852** (1998).

[4] *Molecular Electronics II*, eds. A. Aviram, M. Ratner, and V. Mujica, Ann. N.Y. Acad. Sci. **960** (2002).

[5] Y. M. Blanter and M. Büttiker, Phys. Rep. **336**, 1 (2000).

[6] A. Thielmann, M. H. Hettler, J. König, and G. Schön, Phys. Rev. B **68**, 115105 (2003).

[7] A. Thielmann, M. H. Hettler, J. König, and G. Schön, Phys. Rev. B **71**, 045341 (2005).

[8] M. R. Wegewijs, M. H. Hettler, K. Nowack, C. Romeike, A. Thielmann, and J. König, in *Introducing Molecular Electronics*, to appear in Lecture Notes in Physics (2005).

[9] A. Thielmann, M. H. Hettler, J. König, and G. Schön, cond-mat/0501534 (2005).

[10] A. Thielmann, M. H. Hettler, J. König, and G. Schön, in preparation (2005).

[11] A. Thielmann, M. H. Hettler, J. König, and G. Schön, in preparation (2005).

[12] J. Aghassi, A. Thielmann, M. H. Hettler, and G. Schön, cond-mat/0505345 (2005).

[13] J. Aghassi, A. Thielmann, M. H. Hettler, and G. Schön, in preparation (2005).

[14] V. d. Ziel, *Fluctuation phenomena in semiconductors*, Butterworths Scientific Pub., London (1959).

[15] A. Nauen, *Rauschmessungen an mikroskopischen Tunnelsystemen*, Ph.D Thesis, Hannover, Germany (2003).

[16] Y. Imry, *Introduction to mesoscopic physics, chapter 8*, Oxford University Press (2002).

[17] S. Kogan, *Electronic Noise and Fluctuations in Solids*, Cambridge University Press (1996).

[18] W. Schottky, Ann. Phys. (Leipzig) **57**, 541 (1918).

[19] J. H. Davies, P. Hyldgaard, S. Hershfield, and J. W. Wilkins, Phys. Rev. B **46**, 9620 (1992).

[20] M. Büttiker, in *Quantum Noise in Mesoscopic Physics*, ed. Yu. V. Nazarov, NATO Science Series II: Mathematics, Physics and Chemistry **97**, 3 (2003).

[21] M. Büttiker, Phys. Rev. B **46**, 12485 (1992).

[22] Y. Meir and N. S. Wingreen, Phys. Rev. Lett. **68**, 2512 (1992).

[23] V. A. Khlus, Zh. Eksp. Teor. Fiz. **93**, 2179 [Sov. Phys. JETP **66**, 1243] (1987).

[24] G. B. Lesovik, Pis'ma Zh. Eksp. Teor. Fiz. **49**, 513 [JETP Lett. **49**, 592] (1989).

[25] S. R. E. Yang, Solid State Commun. **81**, 375 (1992).

[26] A. N. Korotkov, Phys. Rev. B **49**, 10381 (1993).

[27] S. Hershfield, J. H. Davies, P. Hyldgaard, C. J. Stanton, and J. W. Wilkins, Phys. Rev. B **47**, 1967 (1993).

[28] Y. V. Nazarov and J. J. R. Struben, Phys. Rev. B **53**, 15466 (1996).

[29] S. Hershfield, Phys. Rev. B **46**, 7046 (1992).

[30] S. Hershfield, Phys. Rev. B **46**, 7061 (1992).

[31] R. C. Liu, B. Odom, Y. Yamamoto, and S. Tarucha, Nature **391**, 263 (1998).

[32] W. D. Oliver, J. Kim, R. C. Liu, and Y. Yamamoto, Sience **284**, 299 (1999).

[33] M. Henny, S. Oberholzer, C. Strunk, T. Heinzel, K. Ensslin, M. Holland, and C. Schönenberger, Sience **284**, 296 (1999).

[34] H. Birk, M. J. M. de Jong, and C. Schönenberger, Phys. Rev. Lett. **75**, 1610 (1995).

[35] Y. P. Li, A. Zaslavsky, D. C. Tsui, M. Santos, and M. Shayegan, Phys. Rev. B **41**, 8388 (1990).

[36] V. V. Kuznetsov, E. E. Mendez, X. Zuo, G. L. Snider, and E. T. Croke, Phys. Rev. Lett. **85**, 397 (2000).

[37] A. Kumar, L. Saminadayar, D. C. Glattli, Y. Jin, and B. Etienne, Phys. Rev. Lett. **76**, 2778 (1996).

[38] M. Reznikov, M. Heiblum, H. Shtrikman, and D. Mahalu, Phys. Rev. Lett. **75**, 3340 (1995).

[39] M. Henny, S. Oberholzer, C. Strunk, and C. Schönenberger, Phys. Rev. B **59**, 2871 (1999).

[40] F. Liefrink, J. I. Dijkhuis, M. J. M. de Jong, L. W. Molenkamp, and H. van Houten, Phys. Rev. B **49**, 14066 (1994).

[41] A. H. Steinbach, J. M. Martinis, and M. H. Devoret, Phys. Rev. Lett. **76**, 3806 (1996).

[42] G. Iannaccone, G. Lombardi, M. Macucci, and B. Pellegrini, Phys. Rev. Lett. **80**, 1054 (1998).

[43] V. V. Kuznetsov, E. E. Mendez, J. D. Bruno, and J. T. Pham, Phys. Rev. B **58**, 10159 (1998).

[44] W. Song, E. E. Mendez, V. Kuznetsov, and B. Nielsen, Appl. Phys. Lett. **82**, 1568 (2003).

[45] S. S. Safonov, A. K. Savchenko, D. A. Bagrets, O. N. Jouravlev, Y. V. Nazarov, E. H. Linfield, and D. A. Ritchie, Phys. Rev. Lett. **91**, 136801 (2003).

[46] N. Y. Kim, W. D. Oliver, Y. Yamamoto, J. Kong, and H. Dai, cond-mat/0311434 (2003).

[47] P. E. Roche, M. Kociak, S. Gueron, A. Kasumov, B. Reulet, and H. Bouchiat, Eur. Phys. J. B **28**, 217 (2002).

[48] P. Jarillo-Herrero, S. Sapmaz, C. Dekker, L. P. Kouwenhoven, and H. S. J. van der Zant, Nature **429**, 389 (2004).

[49] J. Nygard, D. H. Cobden, and P. E. Lindelof, Nature **408**, 342 (2000).

[50] M. R. Buitelaar, T. Nussbaumer, and C. Schönenberger, Phys. Rev. Lett. **89**, 256801 (2002).

[51] G. Schön, in *Quantum Transport and Dissipation, chapter 3*, eds. T. Dittrich, P. Hänggi, G.- L. Ingold, B. Kramer, G. Schön, and W. Zwerger, Wiley-VCH Verlag (1998).

[52] J. Weis, R. J. Haug, K. v. Klitzing, and K. Ploog, Phys. Rev. Lett. **71**, 4019 (1993).

[53] D. Sarkar, U. Zeitler, I. Hapke-Wurst, R. J. Haug, and K. Pierz, IOP Conference Series **171**, 233 (2003).

[54] D. M. Zumbühl, C. M. Marcus, M. P. Hanson, and A. C. Gossard, Phys. Rev. Lett. **93**, 256801 (2004).

[55] S. De Franceschi, S. Sasaki, J. M. Elzerman, W. G. van der Wiel, S. Tarucha, and L. P. Kouwenhoven, Phys. Rev. Lett. **86**, 878 (2001).

[56] D. Goldhaber-Gordon, H. Shtrikman, D. Mahalu, D. Abusch-Magder, U. Meirav, and M. A. Kastner, Nature (London) **391**, 156 (1998).

[57] D. Goldhaber-Gordon, J. Göres, M. A. Kastner, H. Shtrikman, D. Mahalu, and U. Meirav, Phys. Rev. Lett. **81**, 5225 (1998).

[58] A. Nauen, F. Hohls, J. Könemann, and R. J. Haug, Phys. Rev. B **69**, 113316 (2004).

[59] A. Nauen, F. Hohls, N. Maire, K. Pierz, and R. J. Haug, Phys. Rev. B **70**, 033305 (2004).

[60] A. Nauen, I. Hapke-Wurst, F. Hohls, U. Zeitler, R. J. Haug, and K. Pierz, Phys. Rev. B **66**, 161303 (2002).

[61] S. W. Jung, T. Fujisawa, Y. Hirayama, and Y. H. Jeong, Appl. Phys. Lett. **85**, 768 (2004).

[62] M. Pioro-Ladriere, J. H. Davies, A. R. Long, A. S. Sachrajda, L. Gaudreau, P. Zawadzki, J. Lapointe, J. Gupta, Z. Wasilewski, and S. A. Studenikin, cond-mat/0503602 (2005).

[63] G. Kiesslich, A. Wacker, E. Schoell, A. Nauen, F. Hohls, and R. J. Haug, Phys. Stat. Sol. C **0**, 1293 (2003).

[64] G. Kiesslich, A. Wacker, and E. Schoell, Phys. Rev. B **68**, 125320 (2003).

[65] M. Mayor and H. Weber, Chimia **56**, 494 (2002).

[66] M. Mayor, Nachrichten aus der Chemie **50**, 1212 (2002).

[67] C. J. Muller, B. J. Vleeming, J. J. S. Reed, M. A. Lamba, R. Hara, L. Jones II, and J. M. Tour, Nanotechnology **7**, 409 (1996).

[68] T. Böhler, J. Grebing, A. Mayer-Gindner, H. v. Löhneysen, and E. Scheer, Nanotechnology **15**, 465 (2004).

[69] M. A. Reed, C. Zhou, C. J. Muller, T. P. Burgin, and J. M. Tour, Science **278**, 252 (1997).

[70] C. Kergueris, J. P. Bourgoin, S. Palacin, D. Esteve, C. Urbina, M. Magoga, and C. Joachim, Phys. Rev. B **59**, 12505 (1999).

[71] J. Reichert, R. Ochs, D. Beckmann, H. B. Weber, M. Mayor, and H. v. Löhneysen, Phys. Rev. Lett. **88**, 176804 (2002).

[72] M. Mayor, C. v. Hänisch, H. B. Weber, J. Reichert, and D. Beckmann, Angew. Chem. **114**, 1228 (2002).

[73] M. Mayor, H. Weber, J. Reichert, M. Elbing, C. von Hänisch, D. Beckmann, and M. Fischer, Angew. Chem. Int. Ed. **42**, 5834 (2003).

[74] R. M. Metzger, B. Chen, U. Hopfner, M. V. Lakshmikantham, D. Vuillaume, T. Kawai, X. Wu, H. Tachibana, T. V. Hughes, H. Sakurai, J. W. Baldwin, C. Hosch, M. Cava, L. Brehmer, and G. J. Ashwell, J. Am. Chem. Soc. **119**, 10455 (1997).

[75] A. Vilan, A. Shanzer, and D. Cahen, Nature **404**, 166 (2000).

[76] J. Chen and M. A. Reed, Chem. Phys. **281**, 127 (2002).

[77] J. Chen, M. A. Reed, A. M. Rawlett, and J. M. Tour, Science **286**, 1550 (1999).

[78] H. Park, J. Park, A. K. L. Lim, E. H. Anderson, A. P. Alivisatos, and P. L. McEuen, Nature **407**, 57 (2000).

[79] J. Park, A. N. Pasupathy, J. I. Goldsmith, C. Chang, Y. Yaish, J. R. Petta, M. Rinkoski, J. P. Sethna, H. D. Abruna, P. L. McEuen, and D. C. Ralph, Nature **417**, 722 (2002).

[80] J. Reichert, H. B. Weber, M. Mayor, and H. v. Löhneysen, Appl. Phys. Lett. **82**, 4137 (2003).

[81] L. A. Bumm, J. J. Arnold, M. T. Cygan, T. D. Dunbar, T. P. Burgin, L. Jones II, D. L. Allara, J. M. Tour, and P. S. Weiss, Science **271**, 1705 (1996).

[82] U. Banin, Y. Cao, D. Katz, and O. Millo, Nature **400**, 542 (1999).

[83] B. Alperson, I. Rubinstein, G. Hodes, D. Porath, and O. Millo, Appl. Phys. Lett. **75**, 1751 (1999).

[84] D. Porath, Y. Levi, M. Tarabiah, and O. Millo, Phys. Rev. B **56**, 9829 (1999).

[85] R. Möller, A. Esslinger, and B. Koslowski, J. Vac. Sci. Technol. A **8**, 590 (1990).

[86] J. Reichert, *Leitfähigkeitsmessungen an einzelnen organischen Molekülen*, Wissenschaftliche Berichte, FZKA-6851, Ph.D Thesis, Universität Karlsruhe, Germany (2003).

[87] M. Elbing, *Functional molecular building blocks*, Wissenschaftliche Berichte, FZKA-7102, Ph.D Thesis, Universität Karlsruhe, Germany (2005).

[88] S. Yaliraki, A. E. Roitberg, and C. Gonzalez, J. Chem. Phys. **111**, 6997 (1999).

[89] M. Di Ventra, S. Pantelides, and N. Lang, Phys. Rev. Lett. **84**, 979 (2000).

[90] S. Datta, *Electronic Transport in Mesoscopic Systems*, Cambridge University Press, (1995).

[91] R. Landauer, IBM J. Res. Dev. **1**, 233 (1957).

[92] M. Büttiker, Phys. Rev. Lett. **57**, 1761 (1986).

[93] M. Büttiker, Y. Imry, R. Landauer, and S. Pinhas, Phys. Rev. B **31**, 6207 (1985).

[94] Y. D. Wei, B. G. Wang, J. Wang, and H. Guo, Phys. Rev. B **60**, 16900 (1999).

[95] F. M. Souza, J. C. Egues, and A. P. Jauho, in *Physics of Semiconductors 2002*, Proc. of the 26th Int. Conf., Edinburgh **171** (2002).

[96] B. Dong and X. L. Lei, J. Phys.: Condens. Matter **14**, 4963 (2002).

[97] D. Sanchez and R. Lopez, Phys. Rev. B **71**, 035315 (2005).

[98] D. Sanchez, R. Lopez, and M. S. Choi, J. Supercond. **18**, 251 (2005).

[99] J. X. Zhu and A. V. Balatsky, Phys. Rev. B **67**, 165326 (2003).

[100] J. Rammer and H. Smith, Rev. Mod. Phys. **58**, 323 (1986).

[101] A. P. Jauho, N. S. Wingreen, and Y. Meir, Phys. Rev. B **50**, 5528 (1994).

[102] S. Hershfield, J. H. Davies, and J. W. Wilkins, Phys. Rev. Lett. **67**, 3720 (1991).

[103] M. Hamasaki, Phys. Rev. B **69**, 115313 (2004).

[104] E. V. Sukhorukov, G. Burkard, and D. Loss, Phys. Rev. B **63**, 125315 (2001).

[105] D. V. Averin, in *Macroscopic Quantum Coherence and Quantum Computing*, eds. Averin, D. V. and Ruggiero, B. and Silvestrini, P., Springer (2001).

[106] S. A. Gurvitz and Y. S. Prager, Phys. Rev. B **53**, 15932 (1996).

[107] S. A. Gurvitz, Phys. Rev. B **57**, 6602 (1998).

[108] B. Elattari and S. A. Gurvitz, Phys. Lett. A **292**, 289 (2002).

[109] S. A. Gurvitz, IEEE Transactions on Nanotechnology **4**, 45 (2005).

[110] B. Dong, H. L. Cui, and X. L. Lei, Phys. Rev. B **69**, 035324 (2004).

[111] X.-Q. Li, J.-Y. Luo, Y.-G. Yang, P. Cui, and Y. Yan, Phys. Rev. B **71**, 205304 (2005).

[112] M. Magoga and C. Joachim, Phys. Rev. B **56**, 4722 (1997).

[113] J. Lagerqvist, Y.-C. Chen, and M. Di Ventra, Nanotechnology **15**, 459 (2004).

[114] Y. Meir, N. S. Wingreen, and P. A. Lee, Phys. Rev. Lett. **66**, 3048 (1991).

[115] G. H. Ding and T. K. Ng, Phys. Rev. B **56**, 15521 (1997).

[116] F. Evers, F. Weigend, and M. Koentopp, Physica E **18**, 255 (2003).

[117] J. Heurich, J. Cuevas, W. Wenzel, and G. Schön, Phys. Rev. Lett. **88**, 256803 (2002).

[118] M. Brandbyge, J.-L. Mozos, P. Ordejon, J. Taylor, and K. Stokbro, Phys. Rev. B **65**, 165401 (2002).

[119] Y. Xue, S. Datta, and M. Ratner, Chem. Phys. **281**, 151 (2002).

[120] M. H. Hettler, H. Schoeller, and W. Wenzel, in *Nano-Physics and Bio-Electronics: A New Odyssey, chapter 11*, eds. T. Chakraborty, F. Peeters, and U. Sivan, Elsevier (2002).

[121] M. H. Hettler, W. Wenzel, M. R. Wegewijs, and H. Schoeller, Phys. Rev. Lett. **90**, 076805 (2003).

[122] M. A. Kastner, Rev. Mod. Phys. **64**, 849 (1992).

[123] V. N. Golovach and D. Loss, Phys. Rev. B **69**, 245327 (2004).

[124] M. R. Wegewijs, *Electronic Transport in Quantum Dots*, Ph.D Thesis, Delft, Netherlands (2001).

[125] M. Turek and K. A. Matveev, Phys. Rev. B **65**, 115332 (2002).

[126] I. L. Aleiner and L. I. Glazman, Phys. Rev. Lett. **77**, 2057 (1996).

[127] D. Boese and H. Schoeller, Europhys. Lett. **54**, 668 (2001).

[128] A. Mitra, I. Aleiner, and A. J. Millis, Phys. Rev. B **69**, 245302 (2004).

[129] J. König, H. Schoeller, and G. Schön, Phys. Rev. Lett. **76**, 1715 (1996).

[130] J. König, J. Schmid, H. Schoeller, and G. Schön, Phys. Rev. B **54**, 16820 (1996).

[131] H. Schoeller, in *Mesoscopic Electron Transport*, eds. L. L. Sohn, L. P. Kouwenhoven, and G. Schön, NATO ASI Series E, Kluwer, Dordrecht **345**, 291 (1997).

[132] J. König, *Quantum Fluctuations in the Single-Electron Transistor*, Shaker, Aachen (1999).

[133] G. Mahan, *Many Particle Physics*, Plenum Publishing Corporation, (2000).

[134] A. Braggio, J. König, and R. Fazio, cond-mat/0507527 (2005).

[135] G. Johansson, P. Delsing, K. Bladh, D. Gunnarsson, T. Duty, A. Käck, G. G. Wendin, and A. Aassime, in *Quantum Noise in Mesoscopic Physics*, ed. Yu. V. Nazarov, NATO Science Series II: Mathematics, Physics and Chemistry **97**, 337 (2003).

[136] H. A. Engel and D. Loss, Phys. Rev. Lett., **93**, 136602 (2004).

[137] L. S. Levitov and G. B. Lesovik, JETP Lett. **58**, 225 (1993).

[138] L. S. Levitov, H. Lee, and G. B. Lesovik, J Math. Phys. **37**, 4845 (1996).

[139] L. S. Levitov, in *Quantum Noise in Mesoscopic Physics*, ed. Yu. V. Nazarov, NATO Science Series II: Mathematics, Physics and Chemistry **97** (2003).

[140] Y. V. Nazarov, Ann. Phys. (Leipzig) **8**, 507 (1999).

[141] W. Belzig and Y. V. Nazarov, Phys. Rev. Lett. **87**, 067006 (2001).

[142] W. Belzig and Y. V. Nazarov, Phys. Rev. Lett. **87**, 197006 (2001).

[143] M. Kindermann and Y. V. Nazarov, Phys. Rev. Lett. **91**, 136802 (2003).

[144] W. Belzig, Phys. Rev. B **71**, 161301 (2005).

[145] G. Johansson, P. Samuelsson, and A. Ingerman, Phys. Rev. Lett. **91**, 187002 (2003).

[146] D. A. Bagrets and Y. V. Nazarov, Phys. Rev. B **67**, 085316 (2003).

[147] B. Reulet, J. Senzier, and D. E. Prober, Phys. Rev. Lett. **91**, 196601 (2003).

[148] L. S. Levitov and Chtchelkatchev, JETP Letters **77**, 393 [Pisma Zh. Eksp. Teor. Fiz. **77**, 464] (2003).

[149] H. Sprekeler, G. Kiesslich, A. Wacker, and E. Schoell, Semicond. Sci. Technol. **19**, 37 (2004).

[150] F. Cavaliere, A. Braggio, J. T. Stockburger, M. Sassetti, and B. Kramer, Phys. Rev. Lett. **93**, 036803 (2004).

[151] G. Michalek and B. R. Bulka, Eur. Phys. J. B **28**, 121 (2002).

[152] A. Cottet and W. Belzig, Europhys. Lett. **66**, 405 (2004).

[153] A. Cottet, W. Belzig, and C. Bruder, Phys. Rev. Lett. **92**, 206901 (2004).

[154] A. Cottet, W. Belzig, and C. Bruder, Phys. Rev. B **70**, 115315 (2004).

[155] B. R. Bulka, J. Martinek, and G. Michalek, Phys. Rev. B **60**, 12246 (1999).

[156] B. R. Bulka, Phys. Rev. B **62**, 1186 (2000).

[157] C. W. Beenakker and M. Büttiker, Phys. Rev. B **46**, 1889 (1992).

[158] K. E. Nagaev, Phys. Lett. A **169**, 103 (1992).

[159] I. Djuric, B. Dong, and H. L. Cui, IEEE transactions on Nanotechnology **4**, 71 (2005).

[160] I. Djuric, B. Dong, and H. L. Cui, cond-mat/0411091 (2004).

[161] E. G. Mishchenko, Phys. Rev. B **68**, 100409 (2003).

[162] M. Pioro-Ladriere, M. Ciorga, J. Lapointe, P. Zawadzki, M. Korkusinski, P. Hawrylak, and A. S. Sachrajda, Phys. Rev. Lett. **91**, 026803 (2003).

[163] M. Ciorga, M. Pioro-Ladriere, P. Zawadzki, J. Lapointe, Z. Wasilewski, and A. S. Sachrajda, Phys. Rev. B **70**, 235306 (2004).

[164] M. H. Hettler, H. Schoeller, and W. Wenzel, Europhys. Lett. **57**, 571 (2002).